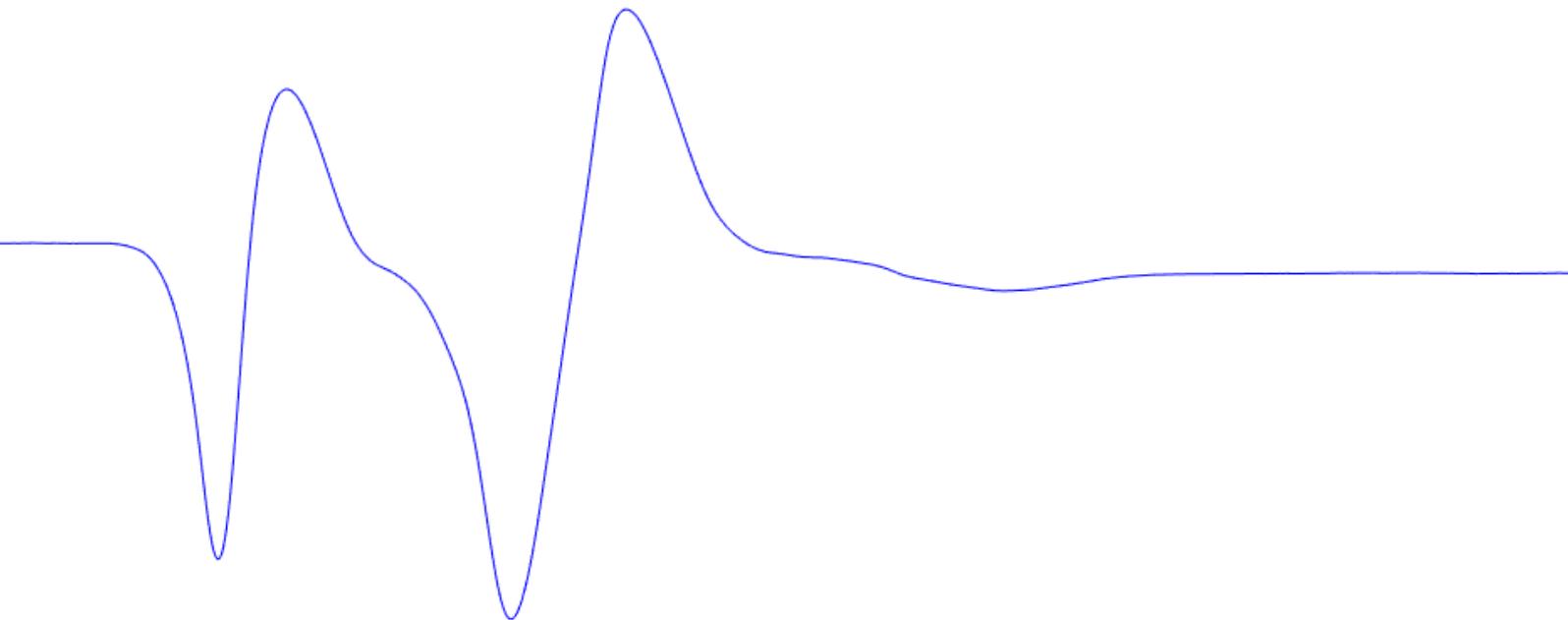# Physics of nerves: Action potentials in Lumbricus Terrestris axons in the presence of anaesthetics, and the collision of pulses

Aske Krogsgaard

Department of physics and astronomy

Univerity of Aarhus

Supervisors: Thomas Heimburg, Niels Bohr Institute, University of Copenhagen
Morten Skovgaard, Department of biomedicine, University of Aarhus
Sune Nørhøj Jespersen, Department of physics and astronomy, University of Aarhus

June 5, 2016

Abstract

This thesis presents and compares two very different models for nerve signal excitation and propagation – the Hodgkin-Huxley model and the soliton model. The models are compared both to each other on a more theoretical basis as well as to data from a series of experiments performed on the medial giant axon and lateral giant axons of the large earthworm – lumbricus terrestris. Experiments with colliding pulses were carried out, and annihilation of pulses were found in the majority of measurements in agreement with expectations based on the Hodgkin-Huxley model. The temperature dependence of the excitation threshold was investigated and found to be in apparent qualitative agreement with the Hodgkin-Huxley model, though this was conclusively proven. The results are on the other hand in direct disagreement with the soliton model. Lastly the dependence of the excitation threshold on the concentration of added anaesthetics was investigated. Two anaesthetic drugs were used – lidocaine and pentobarbital. The results show a linear increase in threshold as a function of anaesthetic concentration as predicted by the soliton model. Futhermore the local anaesthetic lidocaine and the general anaesthetic pentobarbital show similar behaviour, which is also predicted by the soliton model. The similarities are however not in disagreement with the Hodgkin-Huxley model, and in total the results, though not very conclusive, have to be said are in better agreement with the Hodgkin-Huxley model than the soliton model.

Dansk abstract

Denne afhandling præsenterer og sammenligner to grundlæggende forskellige modeller for eksitation of propagation af nerve signaler – Hodgkin-Huxley modellen og soliton modellen. Modellerne sammenlignes både med hinanden på et mere overordnet, teoretisk plan men også mere specifikt på baggrund af resultater fra en række eksperimenter udført på den medial gigant axon og laterale gigant axoner i store regnorm – lumbricus terrestris. Eksperimenter med kolliderende pulser blev udført, og annihilation blev observeret i de fleste tilfælde i overensstemmelse med forudsigelser fra Hodgkin-Huxley modellen. Temperaturafhængigheden af tærskelniveauet for eksitation af aktionspotentialer blev undersøgt, og resultaterne er i umiddelbar kvalitativ overensstemmelse med forudsigelser fra Hodgkin-Huxley modellen. Denne overensstemmels var dog ikke endegyldigt vist. Resultaterne er dog i direkte modstrid med soliton modellen. Til sidst blev tærskelværdiens afhængighed af koncentrationen af anæstetika undersøgt. To forskellige anæstetika blev brugt – lidokain og pentobarbital. Resultater viser en lineær sammenhæng mellem koncentration af anæstetika og tærskelværdien som forudsagt af soliton modellen. Yderligere viser det lokale anæstetikum lidokain og det generelle anæstetikum pentobarbital ens påvirkning af nerven, hvilket også er i overensstemmelse med soliton modellen. Denne lighed er dog ikke i modstrid med Hodgkin-Huxley modellen, og alt i alt må resultaterne siges at stemme bedre overens med Hodgkin-Huxley modellen end med soliton modellen.

Acknoledgements

I would like to extend my gratitude first of all towards all of my supervisors. Thomas Heimburg for all his guidance and supervision throughout the course of the project, Morten Skovgaard for welcoming me in his lab, his guidance during the experiments and for his patience with someone from a non-medical background having taken on a biomedical project, and last not but least Sune Nørhøj Jespersen. I would also like to thank Rima Budvytyte for help with experiments performed in Copenhagen, Majken Sand for help with histological images and Tove, Ebbe and my parents for reading and commenting on the thesis.

Contents

Abbreviations

AP	Action potential
DOPC	1,2-Dioleoyl-sn-glycero-3-phosphocholine
DPPC	1,2-Dipalmitoyl-sn-glycero-3-phosphocholine
DPPG	1,2-Dipalmitoyl-sn-glycero-3-phosphoglycerol
GABA	Gamma-Aminobutyric acid
HH	Hodgkin-Huxley
LGF	Lateral Giant Fibre
MAC	Minimum Alveolar Concentration
MGF	Medial Giant Fibre
TEA	Tetraethylammonium
TTX	Tetrodotoxin

1 INTRODUCTION

The map of the world of neuroscience is one still full of blank spots. It is somewhat paradoxical that we know as little as we do about the nervous system and particularly the brain, since we have used just that – our brains – to figure out everything else we know about the universe. The field of neuroscience is one of great interest to scientists of all different backgrounds around the world and also to me personally. There are lots of very exciting perspectives in neuroscience research in terms of clinical applications and disease treatment in addition to it just being intrinsically interesting. All academia strives to achieve a better understanding of ourselves in relation to the world around us. Ralph Waldo Emerson writes thus in his essay *Nature* [15]

"Every man's condition is a solution in hieroglyphic to those inquiries he would put. He acts it as life, before he apprehends it as truth. In like manner, nature is already, in its forms and tendencies, describing its own design. Let us interrogate the great apparition, that shines so peacefully around us. Let us inquire, to what end is nature?

All science has one aim, namely, to find a theory of nature. [...] Whenever a true theory appears, it will be its own evidence. Its test is, that it will explain all phenomena. Now many are thought not only unexplained but inexplicable; as language, sleep, madness, dreams, beasts, sex."

But no scientific discipline attacks this problem more literally and head on than neuroscience. If we can talk about, where *the self lives*, its *home* has got to be the brain. Quite naively we might therefore say, that if we want to understand *ourselves*, we have to understand the brain. The reason why we know so relatively little about the brain is obviously due to the immense and awe-inspiring complexity of the human body. So when asking the brain what it does for a living, it is not likely to give us a simple answer.

The focus of this thesis is not on anything as complex as the brain or intricate neural networks, but however on the underlying more basic phenomena – the propagation of a nerve signal (action potential AP) down the axon of a single nerve cell. In 1952 Alan Hodgkin and Andrew Huxley published their paper describing the later fittingly named Hodgkin-Huxley model (HH-model) for nervous excitation and propagation [38]. This model has been the dominating theory on the subject of nerve signal excitation and propagation since then. In spite of its great explanatory power and agreement with experimental findings there are, however, as we will see later, several problems with the model, and we are still left with a lot of unanswered questions. In 2005 researchers at the Niels Bohr Institute in Copenhagen published a paper describing a fundamentally different perspective on these phenomena [34]. This new model will be referred to as the soliton model. In this thesis these two very different models (along with some other alternatives) are discussed, and their predictions compared with new experimental data. In particular the mechanism of anaesthetics is discussed.

The history of medicine is long. Irj who lived in the Pharaoh's Egypt 1500BC was described in the hieroglyphs on the door of his tomb as being:

"Palace doctor, superintendent of the court physicians, palace eye physician, palace physician of the belly and one who understands the internal fluids and who is guardian of the anus."

Medicine's ancient roots are even still honoured today in the Hippocratic oath that newly trained physicians take when leaving medical school. Even though today we do not swear by

Apollo the physician and *Aesculapius the surgeon* and various other Greek gods, our modern version of the oath is still based on the original words of Hippocrates. Since the days of Irj and Hippocrates medicine has come a long way and has matured out of the superstitions and religious myths that permeated the field in its ancient youth and into a proper scientific field. Due to the vast complexity of the subject matter, however, a lot of modern medicine is still based to a great extend on empirical evidence without solid theoretical foundations, or what we in a slightly less respectful wording might call *trial and error*. Anaesthesiology is a good example of this. Anaesthetics are used every day on hospitals around the world, and anaesthesiologists know exactly what and how much to administer for just the desired effect. *Why* and *how* it works on the other hand is still somewhat of a mystery.

Many anaesthetics were discovered more or less by accident, and many were in fact at first used for recreational purposes before their medical applications were realised. The American physician Crawford W. Long partook, like so many people in his time, in *ether frolics* as a young, aspiring medical student. He noticed that during these frolics, pain from bumps and bruises and the like was dulled somewhat, and in 1842 he performed his first surgery on an *etherised* patient. This operation was the first performed under general anaesthesia. Other early anaesthetics were discovered in similar ways. Today the list of known anaesthetics is long, and we have abandoned use of many such early drugs as ether, chloroform, and cocaine (local anaesthetic). On the list are very diverse substances such as pure noble gases and more complex molecules such as isoflurane or halothane. This chemical diversity has puzzled researches, as it was hard to imagine the effect being down to the drugs binding to some sort of specific receptor in the nervous system in spite of the German physician and Nobel Prize laureate Paul Ehrlich's assertion that this is the only way in which agents work. *Corpora non agunt nisi fixata* (agents only work when they are bound).

In figure 1 the famous Meyer-Overton correlation is seen. Meyer and Overton independently discovered this correlation between the potency of an anaesthetic and its olive oil to gas partition coefficient in 1899 and 1901 respectively. The more soluble in lipids a drug is, the more potent its anaesthetic effect. This correlation along with the chemical diversity indicates that a more general explanation might be required for the mechanism of anaesthetics than the substances binding to membrane proteins. The soliton theory, as will be explained later on, offers an example of such a general explanation. It is therefore interesting to look into the predictions made by this theory as well as more conventional ones on the behaviour of action potentials in the presence of anaesthetics. It is the aim of this thesis to do just that.

2 THEORY

In this chapter the background theory behind the two models of interest – the Hodgkin-Huxley model and the soliton model – will be unfolded. The central phenomena characterising nerve signals will be presented, and the two model's explanations of these will also be presented. First an introduction to basic neuroanatomy and -physiology is given. The Hodgkin-Huxley model is then presented, as it is the generally accepted model for these phenomena and therefore the one a contending model needs to challenge. Thereafter the soliton model will be introduced, and lastly the two models will be compared in a general sense. Later on they will be compared and discussed in relation to the specific experimental results of the present study.
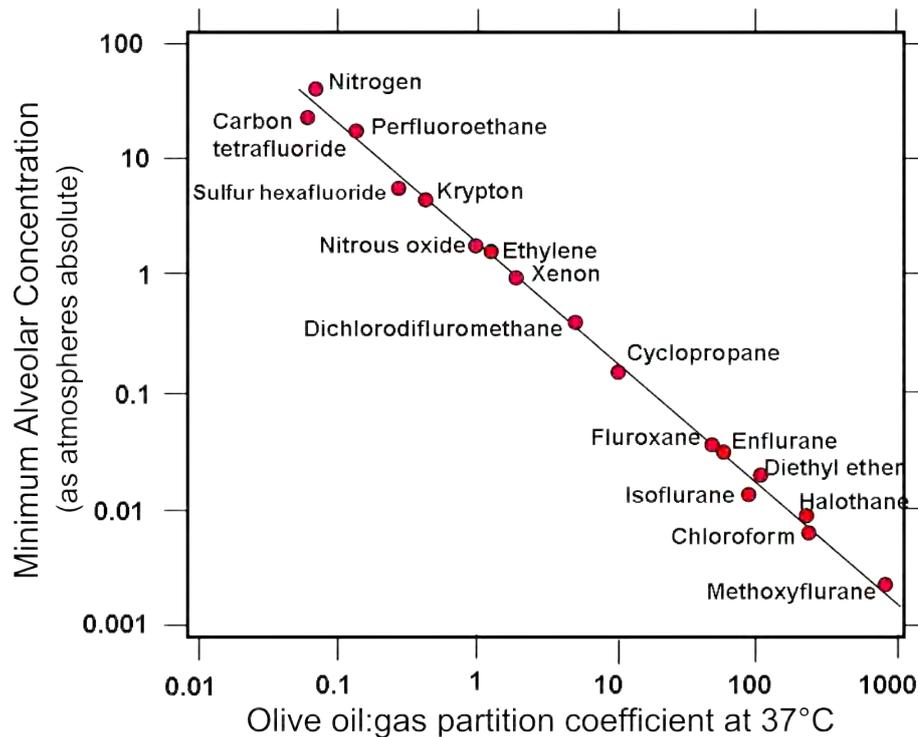
Figure 1: *The minimum alveolar concentration (MAC) of a range of different anaesthetics plotted as a function of their olive oil to gas partition coefficient at 37° celsius. The minimum alveolar concentration indicates the necessary concentration of vapour in the lungs in order to prevent movement in 50% of cases when exposed to pain stimuli as under surgery. The lower MAC the more potent the drug. The graph shows a clear correlation between the potency of a substance and how well it dissolves in olive oil. Figure taken from [72].*

2.1   NERVES

Before delving into the physics of nerve signals some elementary cell biology is necessary. The cell theory was formulated in 1838 by Matthias Schleiden and Theodor Schwann. It states that the cell is the fundamental building block of all life. The term cell is a very wide one. The human body is estimated to be made up of around 35 trillion cells distributed over hundreds of different types. Each type of cell is highly specialised and responsible for a very specific task in the body. We are in this context interested in the nervous system composed of nerve cells – neurons. Again neurons are not just neurons. There is a variety of different types of neurons from the sensory neurons in the tips of your fingers to the pyramidal cells and the star shaped and therefore aptly named astrocytes in your brain. In figure 2 three different types of neurons are shown. Even though different neurons have quite different anatomy and perform very different tasks, they are all still composed of only a handful of different functional regions. We will therefore for simplicity consider a model neuron in order to understand the organization and function of neurons.

THE NEURON

In figure 3 two neurons are seen. A neuron consists of a cell body known as the soma (simply greek for body – $\sigma\tilde{\omega}\mu\alpha$), several branch like projections sprouting out from the soma known
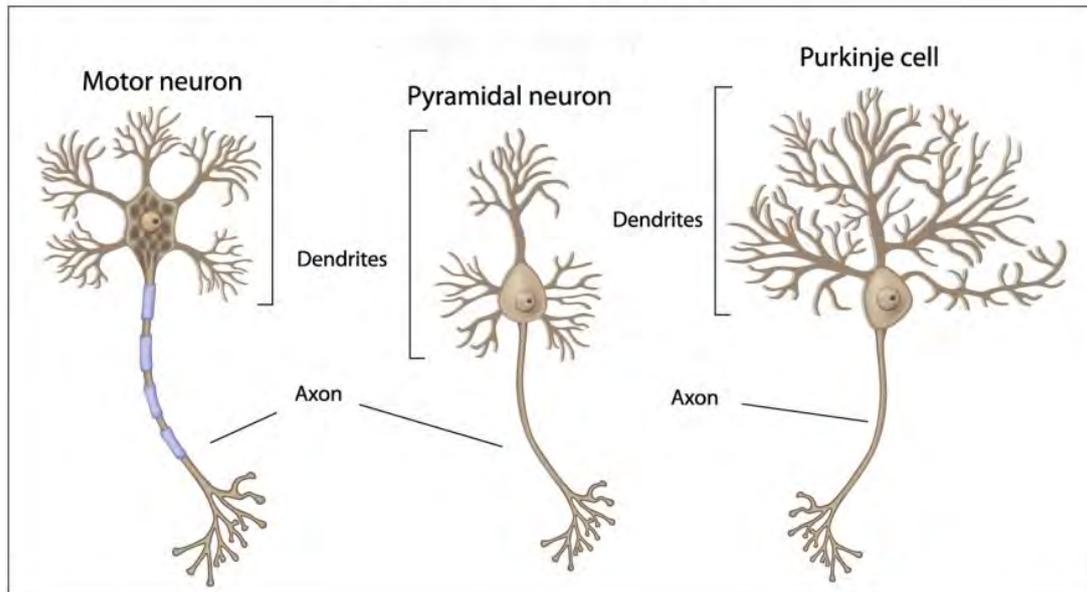
Types of Neurons

Figure 2: *Examples of three different neurons. On the left a motor neuron controlling muscles or glands. In the middle a pyramidal neuron as found in the cortex and other parts of the brain. On the right a Purkinje cell with its vast dendritic web as found in the cerebellum. On the left the myelin is shown as blue wrapping. Figure taken from [69].*

as dendrites, and a long cylindrical projection known as the axon. The soma contains the cell nucleus, storing the cell's genetic material, along with a variety of organelles responsible for metabolism, protein synthesis, and other tasks vital for sustaining the cell. The dendrites collect information from neighbouring neurons and relay it to the soma, where it is integrated, and subsequently signals are sent down the axon at the end of which dendrites from other cells collect the information, relaying the information to their soma, and the process continues. The role of the axon is to transport information integrated in the soma to the next neuron. At the end of the axon it branches out into small projections, which attach on to other neurons. These connections between nerve cells are known as synapses. In most advanced animals (as well as in some more primitive ones) the axon is surrounded by a layer of fatty material known as myelin (see figure 2). The exact chemical composition of myelin varies, but it consists largely of water and lipids. Lipids are a family of molecules comprising fats and waxes. Examples of familiar lipids are cholesterol, stearin, and beeswax. The function of the myelin remains the same though, no matter the composition. It acts as an insulator, and thereby it increases the conduction speeds of the action potentials (in the HH-model that is). This will be discussed later in the sections *Cable theory* and *Strengths and shortcomings*. The myelin sheath is produced by glia cells – Schwann cells in the peripheral nervous system and oligodendrocytes in the central nervous system. There are periodic gaps in the sheath known as the nodes of Ranvier. One section of myelin covering is typically around a millimetre long, where as the nodes are of the order of micrometres. The nodes of Ranvier are thought to be the active sites in relation to signalling due to the high concentration of membrane proteins known as ion channels.

For a thorough introduction to neuroanatomy and physiology see for example [42].
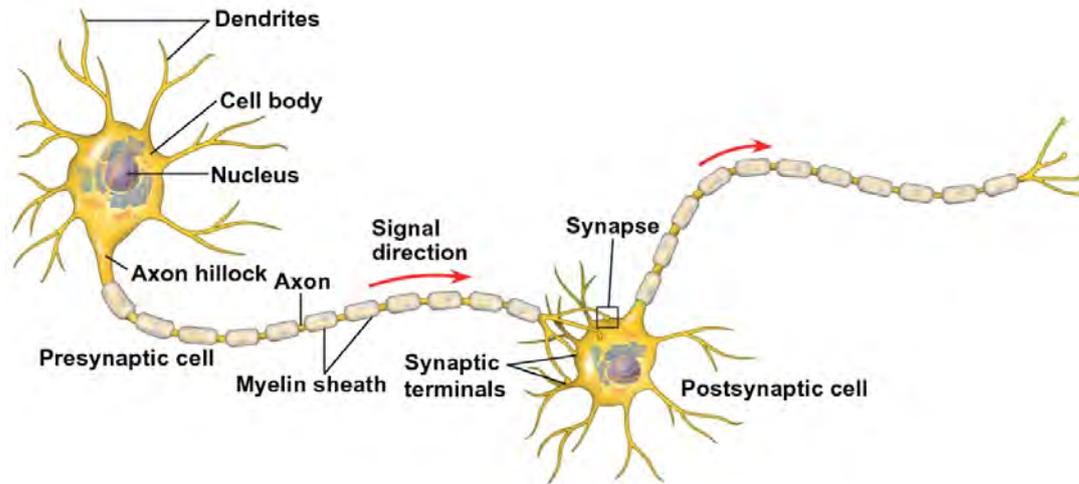
Figure 3: *Sketch of two neurons with synaptic connections. Information delivered to the cell body (soma) from the dendrites is integrated and relayed down the axon towards the synaptic terminals at the end, where the signal is passed on to the postsynaptic cell. Figure taken from [70]*

SIGNALS

Now having introduced some basic neuroanatomy let us turn our attention to the actual nerve signals themselves. Already in ancient Greece the idea existed that the intent behind our movements, in a physiological sense, originated from the brain. This idea was most famously described by the Greek physician Galen of Pergamon [74]. Galen thought that weightless, invisible substances, which he called *animal spirits*, flowed out from the ventricles in the brain and out into the muscles causing them to contract or extend. The spirits also carried sensory input back the other way to the brain. This very spiritual theory dominated for a surprisingly long time. The father of modern philosophy Rene Descartes slightly modified the theory and brought it a little closer to earth. He believed that instead of being mysterious, weightless, invisible substances the animal spirits were actual liquids, and the nervous system was thus a hydraulic system. The spirits were released from the pineal gland, where the soul also lived [74].

"[. . .]it is necessary to believe that the spirits, flowing through the nerves into the muscles, and inflating them sometimes more and sometimes less, now some, now others according to the different ways in which the brain distributes them, cause the movements of all the limbs; and that the little threads of which the internal substance of the nerves is composed serve the senses."

Jan Swammerdam a Dutch biologist showed that muscles could be brought to contract even when separated from the brain thus disproving the theory of animal spirits. The first to discover the connection between nerve signals and electricity was the Italian physician and natural scientist Luigi Galvani.

There are several good stories about just how Galvani came about his discovery of *animal electricity* as he called it [56]. The validity of these stories is probably dubious, but they are quite cute nonetheless. Galvani conducted extensive anatomical research on frogs trying to prove that their testicles resided in their legs. One day he had performed some experiments with static electricity. Later the same day he dissected frogs on the same table, and when he touched the exposed sciatic nerve with a scalpel that had picked up some charge, the leg of the frog twitched.

5

Another story says that he was inspired, when he saw the legs of the frogs, his wife was preparing for dinner, twitched when touched with the knife. Galvani started systematic investigations into the phenomena and reasoned that nerve signals were in fact flowing electricity. Some of Galvanis contemporaries did not agree with his reasoning among them such a prominent name as Alessandro Volta, and the debate was still open the next half a century or so.

In the middle of the 19th century the remarkable work of physiologists Emil du Bois-Reymond and his student Julius Bernstein cemented the relationship between electricity and nerve signals as believed by Galvani. In figure 4 a measurement of what Bernstein called *the negative variation* – what we today would call an action potential – is shown. This graph is from Bernstein's original publication and is presumably the earliest measurement of the action potential. For comparison In figure 29 examples of extracellular measurements from the earthworm medial and lateral giant axons are shown. The quality of Bernstein's measurements is quite impressive. Bernstein also showed that the nerve signals were in fact travelling electric wave pulses.

The action potential, as nerve signals are known today, is a phenomenon with a range of defining characteristics. It is an all-or-none phenomenon, meaning that below some threshold voltage the cells are not excited, and no signals are sent. When this threshold is surpassed, an action potential is initiated. This AP looks exactly the same every time. The shape, duration and amplitude is unaffected by the strength of the stimulus. The strength of the stimulus is instead conveyed by sending more or fewer APs after each other in so called *spike trains*. Nerve signals are thus in a sense digital in their nature. The shape of an action potential is as shown In figure 8. The AP is a travelling self sustaining single wave pulse. In order to create such a pulse a non-linear process is required. We will see different explanations of how this non-linearity enters the picture. After a neuron has fired, there is a small period of time, in which the cell is incapable of firing – the refractory period. Both the action potential and the refractory period are typically on the order of microseconds in duration. The voltage changes involved in these processes are relatively small – on the order of millivolts. All of these defining characteristics need to be explained by any model for nerve signals. Both in the conventional Hodgkin-Huxley model and the proposed soliton model the mechanisms behind action potentials are intimately linked with specific nature of the cell membrane.

The cell membrane

In this section we will take a closer look at the structure of the cell membrane and discuss its function in the HH-model. In the following section the function in the soliton model will be discussed.

The cell membrane is what separates the inside of the cell from the outside, extracellular fluid. It is primarily composed of lipids, which are bound together in a bilayer as can be seen In figure 5. A lipid molecule consists of a hydrophilic head group and a hydrophobic hydrocarbon chain. The lipid bilayer is, due to its non-polar center, impermeable to ions and other molecules dissolved in the extracellular fluid – at least under most circumstances. This will be discussed in the section *Lipid pores*. Embedded into the lipid membrane are different proteins. Some of these proteins are thought to serve different purposes in relation to transport of ions across the membrane. Some of these are passive transporters known as ion channels, others are active transporters. The passive ion channels, though passive, do not let any ion through the gates. They are said to be selective as they allow predominantly sodium, potassium, calcium or some other ion to pass through. Some of these channels are always left open, and others are closed until activated. In the latter case they are said to be gated. The gating mechanism can be electrical, chemical or
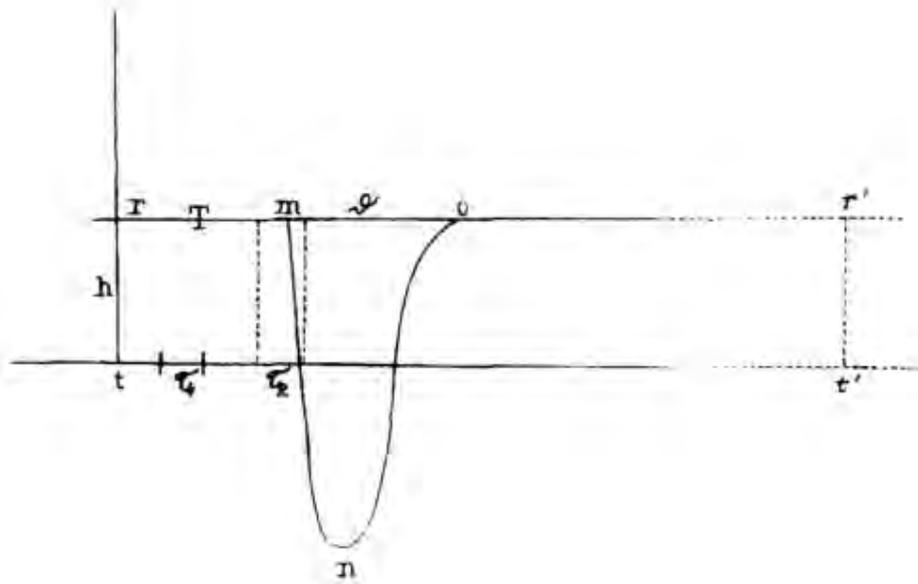
Figure 4: *Recording of the negative variation made by Julius Bernstein in 1871. The negative variation is what we today know as an action potential. Figure taken from [56].*

mechanical. In the case of a voltage gated channel (which are of primary interest in the present context) the activation happens when the membrane is depolarized (or hyperpolarised for some channels) and reaches a certain threshold potential, where another geometrical conformation of the protein is energetically favourable. Some channels are also actively inactivated again once another potential has been reached. An example of this is the sodium channel. This inactivation is the reason for the refractory period mentioned earlier. This refractory period where no action potentials can be initiated will become of interest later on when discussing the collision of two counter-propagating action potentials. In 1957 Jens Christian Skou published his first article describing the famous sodium-potassium pump, which later would earn him the Nobel Prize in chemistry. One of only two Nobel Prizes awarded to a scientist at the University of Aarhus. The sodium-potassium pump is an example of an active transporter. It pumps sodium *out of* the cell and potassium *into* the cell. Due to these active transport membrane proteins the concentrations of ions such as sodium, potassium, and chloride are kept at different levels across the membrane – they maintain chemical gradients across the membrane. Due to the charged nature of ions, these chemical gradients also lead to an electrical gradient across the membrane. The existence of these gradients is what allows us to excite the cell. If the concentrations were just allowed to equilibrate, the cells would not allow for the dynamic behaviour that is observed. We have now reached a point, where we are ready for the first equation of this thesis. The Nernst equation describes the equilibrium membrane potential for a given ion also known as the Nernst potential. At the Nernst potential there is no net flow of ions across the membrane, and we have an equilibrium situation. At membrane potentials different from the Nernst potential ions would flow across the membrane in an attempt to return to equilibrium. The flow of ions changes sign at the Nernst potential, so if there is an influx of ions at potentials above the Nernst potential, there is an efflux of ions at potentials below the Nernst potential. For this reason it is often referred to as the reversal potential.

Were all the ion pumps turned off, the ions would start to diffuse through the open channels across the membrane down their chemical gradient, until the resulting membrane potential
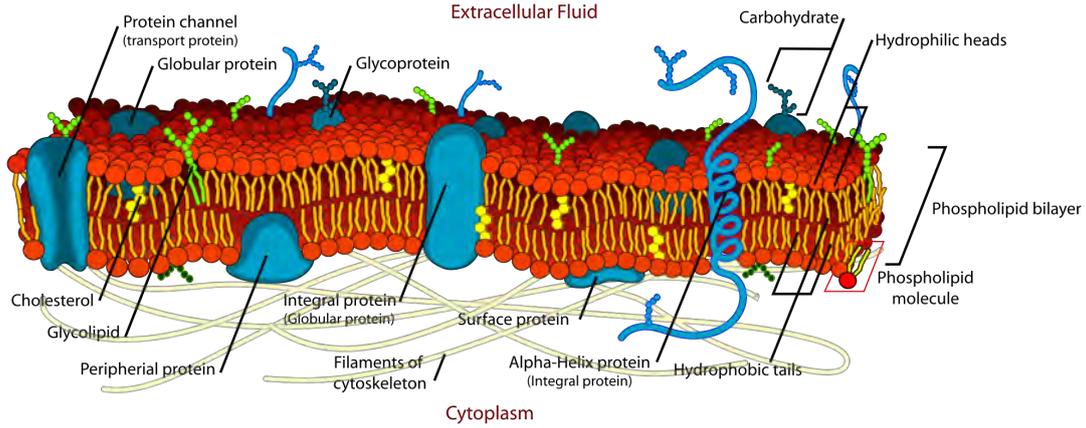
Figure 5: *Sketch of a piece of cell membrane with examples of different types of proteins embedded into the lipid bilayer. Figure taken from [73].*

countered the chemical potential thus reaching some equilibrium state and potential. To begin with we shall consider the case where the membrane is only permeable for *one* type of ion. As biophysicists our jumping off point in the quest for this equilibrium potential is of course the Boltzmann distribution. In this context, however, instead of talking about the probability of finding an ion on one side or the other, we consider concentrations. By simply taking the logarithm and rewriting slightly for a given ion S we then get

$$V_S = V_i - V_o = \frac{RT}{z_S F} \ln \frac{S_o}{S_i}. \tag{2.1}$$

This is the Nernst equation where R is the gas constant, T the temperature, z_S the valence of the ion S, F Faraday's constant and S_o and S_i the concentration of the ion outside and inside respectively. The Nernst equation only considers the case where one single type of ion is able to traverse the membrane. In reality the membrane is permeable to a range of different ions in varying degree. In this case it is necessary to use the Goldman equation

$$V_m = \frac{RT}{F} \ln \left(\frac{P_K[\text{K}^+]_o + P_{Na}[\text{Na}^+]_o + P_{Cl}[\text{Cl}^-]_i}{P_K[\text{K}^+]_i + P_{Na}[\text{Na}^+]i + P_{Cl}[\text{Cl}^-]_o} \right). \tag{2.2}$$

We have for clarity here only considered the three most important ions. The Goldman equation also considers the specific permeability of the different ions P_{Ion}. The Goldman equation is however still fairly rough. The temperature dependence of $1/T$ should for example not be taken too literally, as cells have a tendency to accommodate to temperature changes over time. Effects of temperature will be discussed further later on. The resting potential of most neurons is approximately -70mV. In the conventional HH-theory the thing of primary interest is the flow of ions in and out of the cell and the resulting voltage changes across the membrane. The soliton theory on the other hand considers more mechanical features of the membranes and changes in these.

Again for further details see for example [42] or [37].

Phase transitions

As mentioned the membrane consists primarily of lipids organized in a double layer. We need to consider the lateral organization of the molecules as well as the radial. That is we need to consider the organisation in the plane of the membrane. It turns out that at biological temperatures the
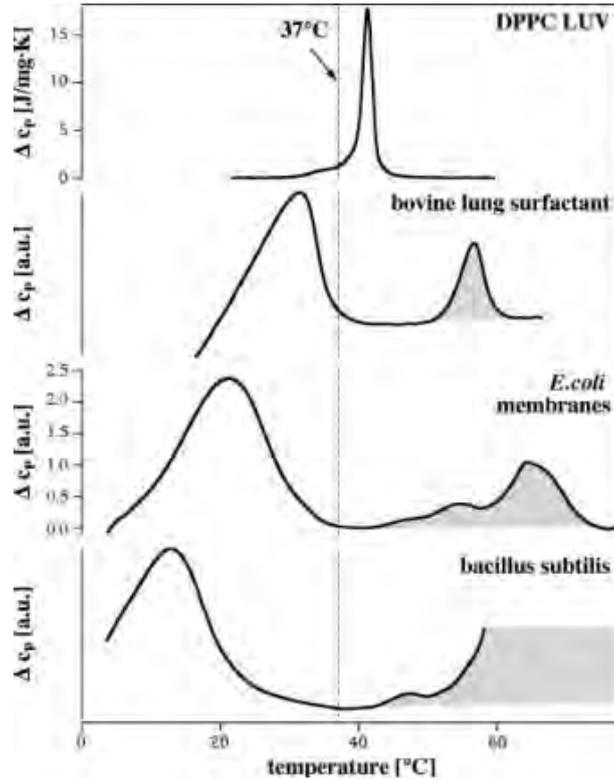
Figure 6: *Heat capacity profile for four different types of biomembrane. From the top artificial unilamellar dipalmitoylphosphatidylcholine (DPPC) vesicles, bovine lung surfactant, E.coli membranes and bacillus substilis membranes. Clear transition peaks are seen in the immediate vecinity of biological temperatures indicated by the dotted line – bovine body temperature of 37°C. The peaks shaded grey are transition peaks associated with protein folding. Figure taken from [34].*

membranes are not organized in a strict lattice structure, but behave more like a liquid crystal, as can be found in many flat screen TVs [34]. The molecules are more or less free to move around among each other in the lateral plane. A few degrees below biological temperatures is found a phase transition in a range of different membranes. When cooled the liquid crystal membrane transitions to another phase state of more ordered and rigid structure. In fact they are seen to be organized laterally in a triangular lattice. This more compact organisation results in a decrease in membrane area. In figure 6 heat capacity profiles for four different types of lipid membranes are shown. All four graphs show clear phase transitions near biological temperatures.

Transversally (or radially) a change is observed as well. The hydrocarbon tails are frozen into a stretched out configuration, where at warmer temperatures they are more free to wiggle about. This means the membrane thickens. In figure 7 this change is sketched out.

These changes result in an increase in membrane thickness of about 16%, an increase of membrane volume of about 4%, and a decrease in membrane area of about 24% [34]. Here we have implicitly assumed a membrane consisting of only one type of lipid. In reality biological membranes are obviously much more complicated comprising different types of lipids in both saturated and unsaturated forms and in addition to that all the different embedded membrane proteins. This obviously complicates the image a bit, but nonetheless structural changes such as thickening of the membrane and shortening of the nerves during pulse propagation have been observed n experiments [63][13][62][29]. A range of other characteristics of the membrane change radically near the phase transition. The membrane is compressed causing a rise in lateral density. This steep rise in density causes a spike in the lateral compressibility. This increase in
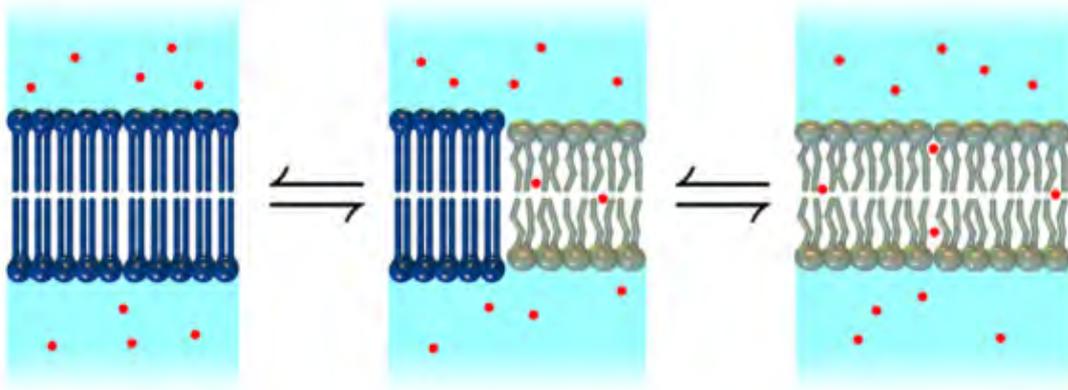
9

Figure 7: *Organisational changes in the lipid bilayer below (left), at the verge (middle) and above the phase transition (right). Figure taken from [25].*

compressibility is what is going to allow the non-linear behaviour we are looking for. This will be further unfolded later.

2.2 The Hodgkin-Huxley model

In the following several sections the theory of the central components of the two models are laid out to give an understanding of the differences in their nature. Some aspects that might not be central to the models but play key roles in relation to the experiments performed for this thesis will be expanded in detail, some here and some further in the experiments chapter.

The ionic hypothesis

The Hodgkin-Huxley model [38] or the ionic hypothesis is on the surface very simple, but at closer look things are not as straight forward, as they seem at first glance. The ionic hypothesis as the name suggests deals with currents of ions flowing into and out of the cell as the primary cause of the electrical signal. It is in nature a purely electrochemical theory. When ion channel proteins embedded in the membrane are opened, electrical and chemical gradients drive the ions through the channels causing the membrane potential to change locally. All these currents of charge can be easily described and understood using an equivalent circuit picture.

The ions travelling through the ion channels, by the virtue of their charge, represent an electric current running through a resistor. As mentioned the ion channels are selective towards specific ions. They thereby have a specific resistance, or equivalently conductance, for a given ion. In Hodgkin and Huxley's original work they discovered the particular importance of precisely the sodium and potassium ions through a series of so called *voltage clamp* experiments. In a voltage clamp experiment the researcher inserts an electrode into the cell and another is kept outside. One can then control the voltage drop across the membrane and measure the resulting current across it. When they had conceived the idea that the transmembrane current could be separated into components carried by different ions, the next step was naturally to determine what these ions were. This could be done by looking at the reversal potential for the measured current and comparing it with those found for various ions using equation 2.1 in combination with removing or substituting ions in the surrounding solution. The two main components of the transmembrane current were identified as being sodium and potassium currents. It was found that the conductances for sodium and potassium change on different time scales and differently
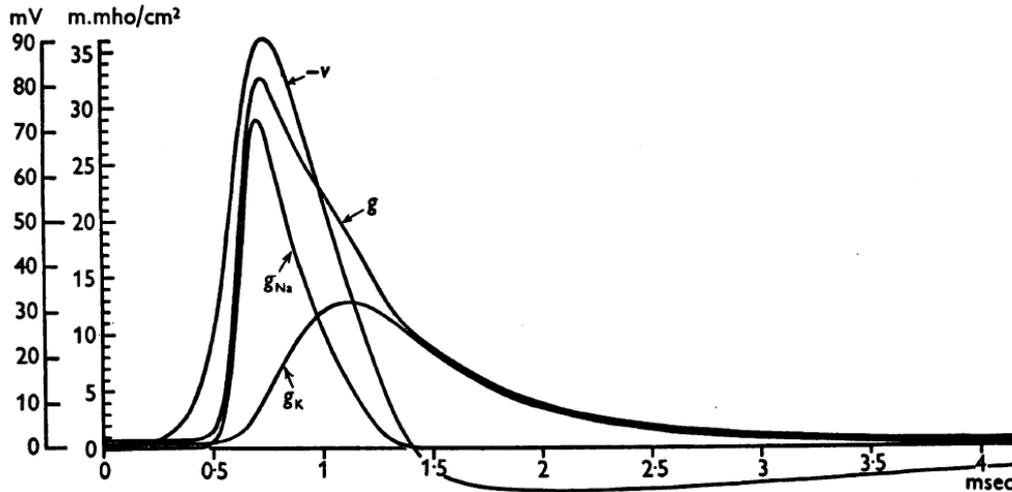
Figure 8: *Ion conductances for sodium g_{Na} and potassium g_K as well as the total membrane conductance g during a propagated action potential V as a function of time. The graphs are numerical solutions to equation 2.19 and are from Hodgkin and Huxley's original paper [38].*

as functions of voltage. This calls for some selective mechanism only letting sodium pass through the membrane at the upstroke of the AP and then later also opening the gates for potassium ions. The time dependence of the conductances can be seen In figure 8. The selectivity for the different ions can be elegantly illustrated by applying certain neurotoxins such as tetrodotoxin (TTX) or tetraethylammonium (TEA) to the surrounding solution. When TTX is applied all negative (inward) currents are in voltage clamp experiments found to disappear. Conversely when TEA is applied all positive (outward) currents disappear. This elegantly shows that the two components of the combined current must happen in different ways. TTX will be making appearances from time to time throughout this thesis

This selectivity has puzzled researchers, and different models for the mechanism of the selectivity have been suggested over the years. Some suggested that the ions did in fact not travel through passive channels but were actively transported by *carrier proteins*. Today researchers have returned to the channel model, as it has been refined over the years. Naively we could suggest that a channel filters out ions depending on their size. Obviously any channel can only let through ions of smaller dimensions than the dimensions of its own pore. An important thing to keep in mind is that an ion in an aqueous solution does not travel alone. Water molecules are polar and they therefore tend to gather round the ions. This means that for instance a sodium ion always travels with an entourage of water – *the waters of hydration*. Sodium and potassium have the same charge, but since sodium is smaller, its charge is more localised and therefore it has a larger *water entourage* than potassium, and effectively it is larger. This is not enough however. This could explain why potassium is preferred over sodium but not the other way around. It was proposed that inside the channel there is a *filter*, which requires the ions to shed their waters of hydration in order to pass. This is only energetically favourable if the chemical bonds that are formed with amino acid residues on the walls of the filter are able to compensate the energy cost of shedding the waters of hydration. As we see the idea of selective ion channels is not a trivial one devoid of problems. It is exactly this selection mechanism that grants the channels their specific conductance and thereby also resistance for specific ions.

That was a small detour. Let us now return to establishing our equivalent circuit picture. The membrane is by default non-permeable for ions. It separates the conducting intracellular
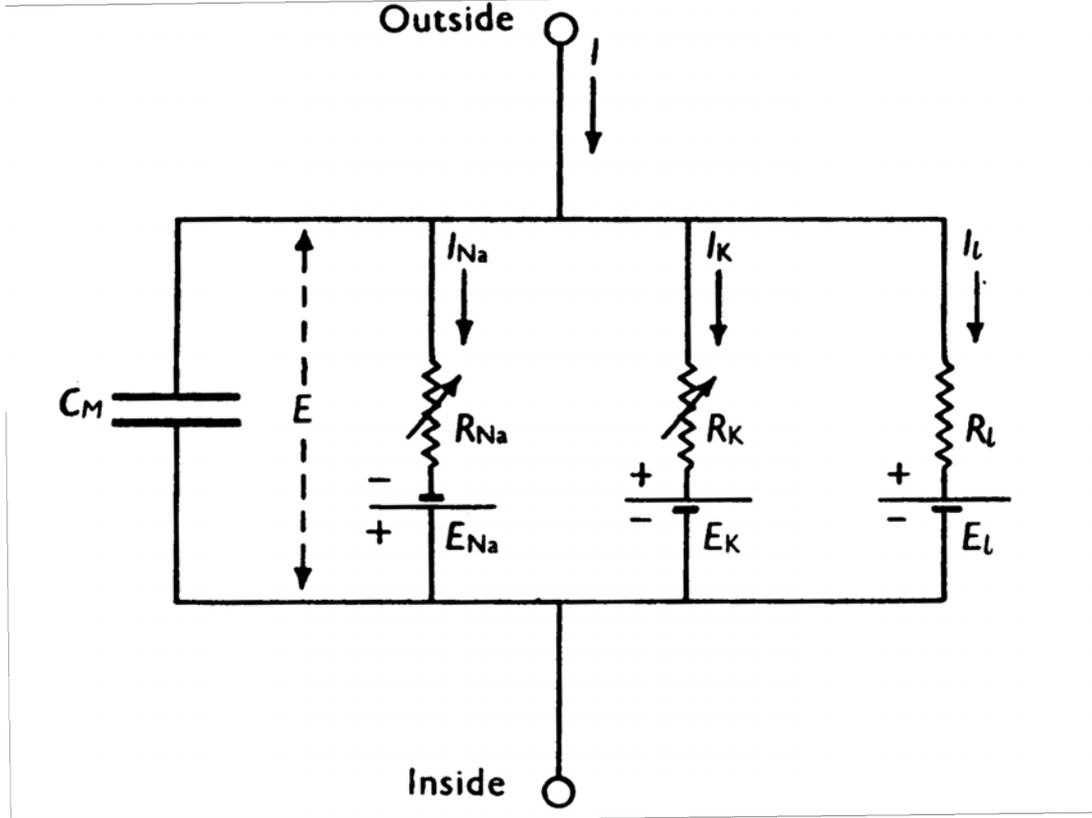
11

Figure 9: *Circuit diagram of the equivalent circuit used to describe the cell membrane and the embedded proteins such as ion channels and pumps in the Hodgkin Huxley model. The membrane represents a capacitor, the ion channels represent resistors with specific resistances for their preferred ions. And the pumps maintain chemical and thereby electrical gradients across the membrane which act as batteries continuously being charged by the pumps. Figure taken from [75].*

and extracellular fluids. It has a non-zero resting potential. It thus acts as a capacitor with some capacitance C_m. The active channels such as the sodium-potassium pump mentioned earlier maintain the potential difference across the membrane. These chemical gradients act as batteries producing an electromotive force, and the active transporters such as the sodium-potassium pump continuously charge the batteries. The membrane with ion channels and ion pumps can therefore be seen as a simple RC-circuit like the one shown In figure 9.

During the upstroke of an action potential charge runs from outside the cell into it. It flows over the capacitor and over the resistors. The current flowing over the capacitor is

$$Q = CV \Rightarrow I_m = C_m \frac{\partial V_m}{\partial t} + \frac{\partial C_m}{\partial t} V_m. \tag{2.3}$$

If we assume the capacitance does not change significantly with time, we can neglect the last term. This might be somewhat problematic, as will be discussed later on, but for now we will discard the last term. The current running through say a sodium channel is given by Ohm's law as

$$I_{Na} = g_{Na} \left(V_m - V_{Na} \right), \tag{2.4}$$

where g_{Na} is the conductance of the sodium channel, and V_{Na} is the reversal potential of the sodium channel given by the Nernst equation (2.1). Likewise we get a similar current contribution

from the other ion channels (potassium and a leakage current), and combining these four currents we get the Hodgkin-Huxley equation in its most generic form

$$I = C_m \frac{dV_m}{dt} + g_{Na}\left(V_m - V_{Na}\right) + g_K\left(V_m - V_K\right) + g_l\left(V_m - V_l\right).\tag{2.5}$$

The subscript l in the conductance and reversal potential in the last term refers to a leakage current of various ions. Though predominantly chloride, other ions contribute as well, and they are all collected under this leakage term.

Equation 2.5 looks simple and elegant, and in a way it is, but partly because we have hidden all the subtleties of the ion channel behaviour in the terms g_{Na}, g_K, and g_l. The next challenge is to find expressions for these functions. They are obviously functions of time, but as the sodium and potassium channels are voltage gated, the conductances are also functions of voltage. They also change with various thermodynamic parameters such as temperature as will be shown later.

The time and voltage dependencies were found simply by fitting experimental data and is not based on a theoretical foundation. The refined equation is given as

$$I = C_m \frac{dV_m}{dt} + \bar{g}_{Na} m^3 h \left(V_m - V_{Na}\right) + \bar{g}_K n^4 \left(V_m - V_K\right) + \bar{g}_l \left(V_m - V_l\right),\tag{2.6}$$

where $\bar{g}_{Ion}$ is the maximal conductance for the given ion, n, m, and h are dimensionless quantities between 0 and 1 indirectly expressing what ratio of channels are open at a given point in time. The fraction of the maximal conductance for a given ion at a given point in time is obviously given by the factors $m^3 h$ and n^4, and not by m, h, and n individually. The values for the exponents of these factors n, m, and h – 4, 3, and 1 respectively – have since been given a physiological interpretation. The idea behind this is that each ion channel protein consists of 4 subunits that all contribute to the opening and/or closing of the channel – all four have to *open* for the channel as a whole to open. It has therefore been put forward that the *four n's* in the equation above each describe the probability of *one* of these subunits opening. Equivalently the *three m's* and *one h* for the sodium channel also correspond to subunits in the sodium channel. This interpretation should not be taken too literally though. The exact values for the exponents have been found simply from fitting to data and could might as well have had another value, and they could even have been non-integer. The time dependence of the conductance is expressed by the time dependence of the gating variables n, m, and h. Due to the binary nature of the ion channels the time dependence can be described by a set of three simple master equations

$$\frac{dm}{dt} = \alpha_m\left(V_m\right)\left(1 - m\right) - \beta_m\left(V_m\right)m$$
$$\frac{dn}{dt} = \alpha_n\left(V_m\right)\left(1 - n\right) - \beta_n\left(V_m\right)n$$
$$\frac{dh}{dt} = \alpha_h\left(V_m\right)\left(1 - h\right) - \beta_h\left(V_m\right)h,\tag{2.7}$$

where the α_{ion}'s and β_{ions}'s are rate constants that depend on voltage but not on time. If we divide the above equations with $\alpha_{ion}\left(V_m\right) + \beta_{ion}\left(V_m\right)$ we can rewrite the above equations thus

$$\tau_m\left(V_m\right)\frac{dm}{dt} = m_\infty\left(V_m\right) - m,\tag{2.8}$$

and likewise for the other two, where τ_m is given by

$$\tau_m\left(V_m\right) = \frac{1}{\alpha_m\left(V_m\right) + \beta_m\left(V_m\right)}.\tag{2.9}$$

m_∞ is given by

$$m_\infty\left(V_m\right) = \frac{\alpha_m\left(V_m\right)}{\alpha_m\left(V_m\right) + \beta_m\left(V_m\right)}. \tag{2.10}$$

When writing the equations on this form we see that for a given value of V_m m changes with time as an exponential function with time constant τ_m and goes towards the value m_∞.

The explicit voltage dependencies found by Hodgkin and Huxley for $\alpha_{n,m,h}$ and $\beta_{n,m,h}$ in the squid giant axon are here included for completeness. They are given by

$$\alpha_n = \frac{0.01\left(V_m + 10\right)}{\exp\left(\frac{V_m+10}{10} - 1\right)}$$
$$\beta_n = 0.125\exp\left(\frac{V_m}{80}\right). \tag{2.11}$$

$$\alpha_m = \frac{0.1\left(V_m + 40\right)}{1 - \exp\left(-0.1(V_m + 40)\right)}$$
$$\beta_m = 4\exp\left(-0.0556(V_m + 65)\right). \tag{2.12}$$

$$\alpha_h = 0.07\exp\left(-0.05(V_m + 65)\right)$$
$$\beta_h = \frac{1}{1 + \exp\left(-0.1(V_m + 35)\right)}. \tag{2.13}$$

Now that we have unpacked equation 2.5 it is apparent that the story is a little more complicated than it would appear at first.

CABLE THEORY

When an action potential is initiated, the transmembrane current behaves as described in the previous section, but that local potential needs to be translated into a longitudinal current running down the axonal *cable*. The appropriate differential equation to describe this – the cable equation – can be derived fairly readily by considering and summing all the currents flowing into and out of a segment of axonal cable of length Δx [9].

We can expand our equivalent circuit picture in order to understand the longitudinal currents. The circuit in figure 9 describes the mechanisms at a single point or small segment on the axon. The axon comprises many such circuits connected to each other side by side in parallel. The circuits are connected by the axoplasm inside the cell and the surrounding extracellular fluid outside the cell. Outside the cell we have a large body of conducting fluid and therefore lots of ions at our disposal, and we can therefore neglect the extracellular resistance. We cannot however neglect the resistance of the axoplasm. The resistance of a segment of cable of length Δx and radius a must be $R_L = r_L \Delta x/\left(\pi a^2\right)$, where r_L is the longitudinal resistivity of the axoplasm. Thus by Ohm's law the current flowing through that segment is $I_L = -\pi a^2 \Delta V/\left(r_L \Delta x\right)$, where ΔV is the voltage drop across the segment. Taking the limit of $\Delta x \to 0$ yields

$$I_L = \frac{-\pi a^2}{r_L}\frac{\partial V}{\partial x}. \tag{2.14}$$

This is the longitudinal current at a given point on the axon. Again considering a piece of axon of length Δx the current running both into and out of the segment at the ends is given by

the above expression, but there are other contributions we need to consider as well. We know that the membrane acts as a capacitor so some current is needed to charge it: $2\pi a \Delta x c_m \partial V/\partial t$, where c_m is the specific membrane capacitance. Current running out of the cell through ion channels is, expressed in terms of a current per unit membrane area i_m, and likewise for current injected into the cell by an electrode i_e, given as $2\pi \Delta x i_m$ and $2\pi \Delta x i_e$ respectively. Summing all of these expressions and again taking the limit of $\Delta x \to 0$ gives us the general cable equation

$$c_m \frac{\partial V}{\partial t} = \frac{1}{2ar_l} \frac{\partial}{\partial x} \left(a^2 \frac{\partial V}{\partial x} \right) - i_m + i_e. \tag{2.15}$$

Assuming that the radius of the axon a does not change significantly with x, we can pull it outside the derivative. If we assume that i_m fulfils Ohm's law, we can simplify equation 2.15 to get the linear cable equation

$$\frac{a}{2r_l} \frac{\partial^2 V}{\partial x^2} = c_m \frac{\partial V}{\partial t} + \frac{V}{r_m} + i_e. \tag{2.16}$$

This can be further rewritten to clarify the interpretation of the equation by introducing the length constant $\lambda = \sqrt{ar_m/2r_l}$ and the time constant $\tau = r_m c_m$

$$\lambda^2 \frac{\partial^2 V}{\partial x^2} = \tau_m \frac{\partial V}{\partial t} + V - r_m i_e. \tag{2.17}$$

The two quantities τ_m and λ set the scales for the time and spatial developments respectively. Note that $\tau_m = r_m c_m$ is just the time scale from elementary circuit analysis of an RC-circuit. It sets the time scale for charging and discharging the membrane capacitor.

If we realise that the right side of equation 2.16 is just the right side of equation 2.6 (plus an injection current which we set to zero), we can combine the two equations to get [38]

$$\frac{a}{2r_l} \frac{\partial^2 V}{\partial x^2} = C_m \frac{dV_m}{dt} + \bar{g}_{Na} m^3 h \left(V_m - V_{Na} \right) + \bar{g}_K n^4 \left(V_m - V_K \right) + \bar{g}_l \left(V_m - V_l \right). \tag{2.18}$$

Hodgkin and Huxley assumed that the propagating AP fulfilled the linear wave equation $\partial^2 V/\partial x^2 = (1/c)^2 \partial^2 V/\partial t^2$, where c is the conduction velocity. This is the same as making the reasonable assumption that $x = ct$. Taking the differential we get $\partial x = c\partial t$, since c is constant. This allows us to remove the spatial derivative in the above equation leaving us an ordinary second order differential equation

$$\frac{a}{2r_l c^2} \frac{\partial^2 V}{\partial t^2} = C_m \frac{dV_m}{dt} + \bar{g}_{Na} m^3 h \left(V_m - V_{Na} \right) + \bar{g}_K n^4 \left(V_m - V_K \right) + \bar{g}_l \left(V_m - V_l \right), \tag{2.19}$$

This equation allows us to calculate the propagating AP in the Hodgkin-Huxley model. We will in the next section find another differential equation describing APs (or solitons) in the soliton model.

Before moving on to the soliton model we need to consider the effects of myelination in the HH-picture. Myelinated axons are basically axons wrapped in extra layers of cell membrane from the surrounding glial cells. This can be seen on figure 19. We can use the rule for capacitors in series to find the inverse of the total capacitance of the myelinated segment by adding the inverse of the capacitance for the individual layers. But instead of adding individual layers of myelin we can integrate over the thickness of the membrane itself and the myelin. If a single layer of cell membrane or myelin has capacitance per unit area c_m and thickness d_m, and the segment has length L and radius a we thus get [9]

15

$$\frac{1}{C_m} = \frac{1}{c_m 2\pi d_m L} \int_{a_i}^{a_o} \frac{da}{a} = \frac{\ln(a_o/a_i)}{c_m 2\pi d_m L}, \tag{2.20}$$

where a_i and a_o are the inner and outer radii of the myelinated segment respectively. A segment of myelinated axon has very low capacitance but very high membrane resistance. We can therefore neglect the last term in equation 2.16, and if we also set $i_e = 0$, we get the diffusion equation

$$\frac{\partial V}{\partial t} = D\frac{\partial^2 V}{\partial x^2}, \tag{2.21}$$

with a diffusion constant of $D = \pi a_i L/C_m r_l$. Note that the denominator in this diffusion constant is the product of a capacitance and a resistance – a time constant for an RC-circuit. The larger the denominator is (the RC-circuit time constant), the smaller the diffusion constant and therefore the slower the propagation velocity. It is now clear that myelination leads to lower membrane capacitance and thereby to a larger diffusion constant for the saltatory conduction and thereby a higher conduction velocity. Another way of understanding the fact, that myelination leads to larger conduction velocities, is that less current, and thereby time, is wasted trying to charge the membrane because of the lower capacitance. Another feature of myelinated nerves is that the conductances differ at different points on the axon. The ion channel proteins are concentrated at the nodes of Ranvier where there is no myelin sheath. The concentration here is significantly larger than in a given patch of equal size on a nonmyelinated axon.

2.3   The soliton model

In 2005 researchers at the Niels Bohr Institute in Copenhagen suggested a new model for nerve signal propagation which is fundamentally different from the HH-model [34]. Where the HH-model is electrochemical, based on ions passing through protein channels in the cell membrane to create voltage spikes, the soliton model is in its nature mechanical (or acoustic) and thermodynamic. It is interested in changes in the mechanical properties of the membrane due to a phase transition as described in the section *Phase transitions*.

It has long been known that nerves contract during firing [63], and the changes in the other spatial dimensions, that are quite naturally related to this contraction, have since been measured [62]. These mechanical changes are completely ignored in the HH-model. For instance in the derivation of the HH-equations we assumed that the capacitance of the membrane does not change with time, and therefore we neglected the last term of equation 2.3. If the membrane changes thickness this is obviously not true. These mechanical changes are at the very heart of the soliton model. It is the propagation of these – as mechanical or acoustic waves – that is in focus.

The soliton model is a younger theory than the HH-model. In the HH-model a phenomenology for the observations, made in particular in the first half of the 20th century, has been found and established as consensus (for most cases) over the years. The model provides a fairly well defined framework for describing a range of different phenomena related to nerve signals, as many researchers over the years have spent considerable effort to refine and extend the theory. The soliton model is very much still work in progress. This is worth keeping in mind when reading the following sections. There are still missing pieces of the puzzle, but more and more pieces are being found and put in place, and the model provides an increasingly complete picture. This also means that we will spend some more time considering the soliton model than we did with the HH-model in the sections above.

Solitons

A soliton is a wave pulse (or packet) that can maintain its shape and speed while travelling as well as after collisions with other solitons. This latter fact will be important when we get to discussing the experimental results. The stability of solutions to the governing equations, we will derive in ths section, has been studied theoretically and it was found that they are stable under head-on collisions. Solitons are known from a range of other fields and have been known for a long time. Solitons were first described by the Scottish engineer John Scott Russell in 1834 [57].

"I was observing the motion of a boat which was rapidly drawn along a narrow channel by a pair of horses, when the boat suddenly stopped—not so the mass of water in the channel which it had put in motion; it accumulated round the prow of the vessel in a state of violent agitation, then suddenly leaving it behind, rolled forward with great velocity, assuming the form of a large solitary elevation, a rounded, smooth and well-defined heap of water, which continued its course along the channel apparently without change of form or diminution of speed. I followed it on horseback, and overtook it still rolling on at a rate of some eight or nine miles an hour, preserving its original figure some thirty feet long and a foot to a foot and a half in height. Its height gradually diminished, and after a chase of one or two miles I lost it in the windings of the channel. Such, in the month of August 1834, was my first chance interview with that singular and beautiful phenomenon which I have called the Wave of Translation."

Solitons can occur when non-linear effects are able to counterbalance the distortive effects of the dispersion in the media. In a dispersive media the speed of sound will depend on frequency. We know from Fourier theory that a solitary wave pulse has to be composed of several frequency components. The shape of such a solitary wave pulse, travelling through a dispersive medium, will therefore be distorted by the dispersion, as not all of the components are travelling equally fast. The isentropic lateral area compressibility of the membrane κ_S^A is found empirically to be a decreasing function of frequency [34], and from fluid mechanics we have the expression for the speed of sound $c^2 = 1/\rho_0 \kappa_S^A$ so the speed of sound in the cell membrane is through κ_S^A an increasing function of frequency.

The speed of sound is known to depend strongly on the density. The density of the membrane changes dramatically in the neighbourhood of the before mentioned phase transitions that have been found at temperatures slightly below biological temperatures. This introduces a non-linearity into the system. As a pulse propagates it changes the mechanical properties of the membrane which then in turn affect the propagation of the pulse. It is this non-linearity which is going to allow solitons to propagate in nerve membranes. Non-linear effects also tend to distort waves but in a different way than dispersion does. In the example of John Scott Russell's *translational wave* non-linear effects would try to break the wave as we see water waves doing at the shores. The interplay between these two distortive effects allows solitons to exist when they exactly counterbalance each other.

The jumping off point for a mechanical (or acoustic) wave description of nerve signals has to be the wave equation

$$\frac{\partial^2 \Delta \rho^A}{\partial t^2} = \frac{\partial}{\partial x} \left(c^2 \frac{\partial \Delta \rho^A}{\partial x} \right). \tag{2.22}$$

Here $\Delta \rho^A$ is the difference in lateral density of the membrane from the equilibrium value ρ_0, and c is the speed of sound. If the speed of sound was constant, the above equation would be

exactly the regular linear wave equation. However we just noted above that the speed of sound depends strongly on the local density. We will deal with this in a moment, but first we will turn our attention to dispersion. Biological membranes show acoustic dispersion so in order to accommodate this phenomenon in the mathematics we must include an extra derivative term in our wave equation

$$\frac{\partial^2 \Delta \rho^A}{\partial t^2} = \frac{\partial}{\partial x}\left(c^2 \frac{\partial \Delta \rho^A}{\partial x}\right) - h\frac{\partial^4 \Delta \rho^A}{\partial x^4}. \tag{2.23}$$

Here h is a constant which exact value has to be determined from experimental data. If we plug in a plane wave solution $\Delta \rho^A = \rho_0 \sin(\omega t - kx)$ with frequency ω, wavenumber k and amplitude ρ_0 into the above equation we get the dispersion relation

$$v^2 = \frac{w^2}{k^2} = c_0^2 + hk^2 \approx c_0^2 + \frac{h\omega^2}{c_0^2}. \tag{2.24}$$

This dispersion relation tells us that the propagation velocity increases with increasing frequency which is what is expected based on experimental findings [34]. It is not given that this dispersion relation describes the actual dispersion as best possible, and further data on the frequency dependence of the compressibility would be required to illuminate this further, but for now this relation more or less behaves in the way we want it to. It also has to be noted that when we introduce the non-linear effects below we will no longer get the dispersion relation above. It only holds for small amplitude waves (when only the first term of the Taylor expansion below is kept).

Now let us turn our attention to the other effect trying to tear our soliton apart. The non-linear effects. As mentioned above the speed of sound depends on the local lateral density of the membrane. This is obviously a function of x, and therefore we cannot pull c outside the derivative. We must use a non-linear wave equation instead. We therefore expand the speed of sound around its equilibrium value in the fluid phase c_0 keeping only terms up to second order

$$c^2 = \frac{1}{\rho^A \kappa_S^A} \approx c_0^2 + p\Delta \rho^A + q\Delta \left(\rho^A\right)^2. \tag{2.25}$$

Here again p and q are constants, which need to be found from fitting to experimental data. If we use this expression for the speed of sound our wave equation looks like this

$$\frac{\partial^2 \Delta \rho^A}{\partial t^2} = \frac{\partial}{\partial x}\left(\left(c_0^2 + p\Delta \rho^A + q\Delta \left(\rho^A\right)^2\right)\frac{\partial \Delta \rho^A}{\partial x}\right) - h\frac{\partial^4 \Delta \rho^A}{\partial x^4}. \tag{2.26}$$

Just as we used the wave equation to get rid of the spatial derivative in equation 2.18, we can rewrite the above equation by introducing the new variable $z = x - vt$

$$v^2\frac{\partial^2 \Delta \rho^A}{\partial z^2} = \frac{\partial}{\partial z}\left(\left(c_0^2 + p\Delta \rho^A + q\Delta \left(\rho^A\right)^2\right)\frac{\partial \Delta \rho^A}{\partial z}\right) - h\frac{\partial^4 \Delta \rho^A}{\partial z^4}. \tag{2.27}$$

This is in the soliton model the equivalent differential equation to equation 2.18.

LIPID PORES

In the last section we derived the governing equations for the mechanical pulses travelling down the axonal membrane during signalling. These can be solved and they allow for solitons just as hoped [45][6], but we will not delve further into the mathematics of solving the equations here. When discussing the HH-model we talked about voltage changes and transmembrane currents.

Our understanding of what nerve signals are has since the days of Galvani or at least since the days of Bernstein been that they are electric pulses. So far while discussing the soliton model we have not talked about voltage or currents or the like at all. Let us now take a look at how electricity enters the picture in the soliton model.

In the HH-picture described earlier we assumed that ions travel through ion channel proteins embedded into the membrane. In the 70s and 80s Erwin Neher and Bert Sakmann developed an experimental technique known as the patch clamp technique [52]. This would later earn them the Nobel Prize. A patch of membrane is isolated inside the tip of a glass micropipette with an electrode inside of it. This allows the researcher to make recordings from a delimited area of membrane. With sufficiently small pipettes one can isolate patches containing just *one or a few* membrane proteins. This elegant technique shed further light on the details of the role of ion channels in signalling. However while one *can* isolate a single membrane protein from the other proteins, one *cannot* isolate it from the surrounding lipid membrane. One will always have large numbers of lipid molecules in ones patch. In a square μm of membrane you would normally find something on the order of 100s or 1000s of protein molecules, depending on whether it is a myelinated nerve or not, but you would find several millions of lipid molecules [4]. From a certain perspective it might be natural to ascribe the observed behaviour of a patch of membrane to the thing that sticks out from the bunch – the proteins. But we cannot just neglect the lipid membrane and assume that it plays no role in the transmembrane currents without testing it. This has been tested. Various researchers have investigated the conductive properties of pure lipid membranes, that is, in the absence of membrane proteins [55][51][20][32]. It has been found that these pure lipid membranes show behaviour remarkably similar to that found in actual biological membranes. In figure 10 is shown a comparison of the transmembrane current in a patch clamp experiment on a biological membrane and on an artificial one devoid of membrane proteins.
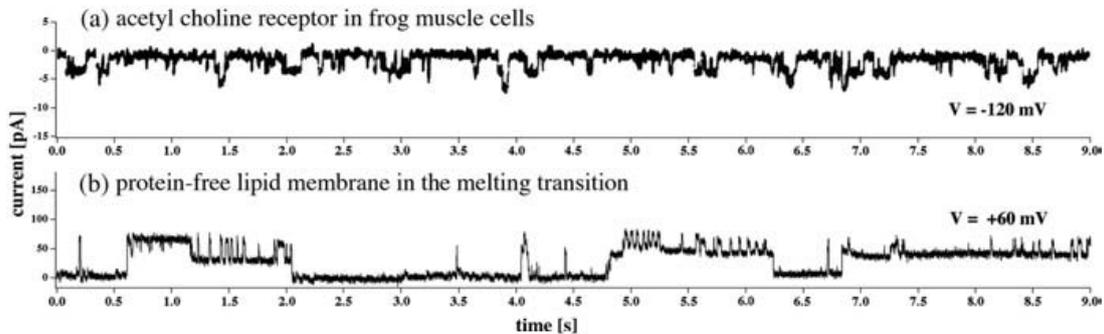

Figure 10: *Comparison of transmembrane current events from patch clamp experiments on a biological membrane (acetyl choline receptor muscles in frog)(top) and DOPC:DPPC artificial pure lipid membrane (bottom). Data are from [52] (top) and [31] (bottom). Figure taken from [32].*

It is known that applying an electric field to a cell can increase the permeability of the cell membrane for various substances. This phenomenon is known as electroporation. In order for these lipid pores, which have been observed, to have any significance for nervous signalling they have to be able to form under biological conditions. There is, as we know, a nonzero electric potential across the membrane of a neuron, but this is not enough to form pores able to explain the voltage changes observed. Furthermore if the pores are to explain part of the electric pulse associated with the action potential they must only form where the AP is. The typical resting potential of nerve membrane is $\tilde{}70mV$. The voltages applied in electroporation are on the order of several hundreds of millivolts. The resting potential is thus not enough to account for these

19

lipid pores. If we take a closer look at the thermodynamics of the situation, however, we find something interesting [32][44].

To create a lipid pore some free energy barrier has to be overcome. In electroporation this is accomplished by applying large voltages (in the context of cell biology). In the situation we are interested in the properties of the membrane alone has to allow for pore formation without application of some external force but simply through thermodynamic fluctuations. It has been found that both the heat capacity, the compressibility and the permeation rates of various ions change radically around the phase transition [34]. In figure 11 is shown graphs of the permeation rate of sodium ions and rhodamine 6G dye molecules, along with heat capacity profiles and profiles for lateral density and compressibility.
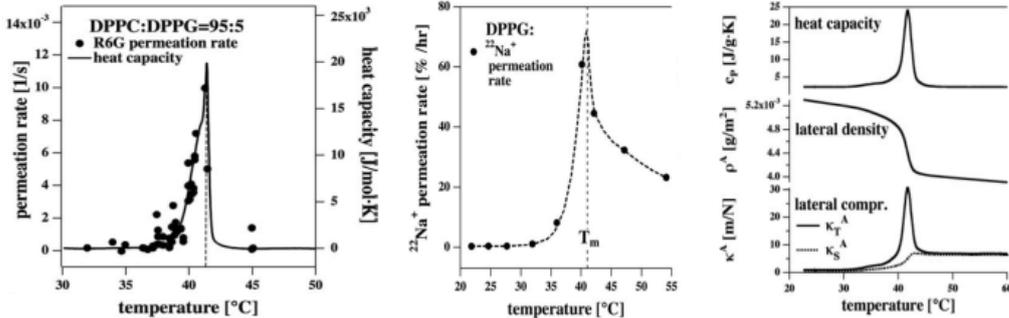

Figure 11: *Left: permeation rate of rhodamine 6G molecules through DPPC:DPPG artificial lipid membrane as a function of temperature (dots) and heat capacity profile for the same membrane (solid line). The dotted line indicates the melting temperature. Middle: permeation rate of sodium ions through a DPPG artificial membrane as a function of temperature (dots). The dotted line is just to illustrate the tendency in the data. Right: heat capacity profile (top), lateral density profile (middle) and lateral compressibility profile for an artificial DPPC membrane. Two first figures found in [32] and the last one in [34]. Data from [55] (left, middle) and [34] (right).*

We will now find relations between these quantities. In equilibrium thermodynamics we just look for the state that maximises the entropy in order to find the actual state of the system. Here we are, however, interested in fluctuations around equilibrium, and therefore we have to look outside of the entropy maximum. For small variations δn_i of variables n_i we can to a good approximation expand the entropy to second order around its equilibrium value S_0, and since S_0 is the entropy maximum, the first derivatives are zero, so we discard the linear terms

$$S \approx S_0 + \frac{1}{2} \sum_{ij} \frac{\partial^2 S}{\partial n_i \partial n_j} \delta n_i \delta n_j = S_0 - \sum_{ij} g_{ij} \delta n_i \delta n_j, \qquad (2.28)$$

where $g_{ij} = -0.5 \left(\partial^2 S / \partial n_i \partial n_j \right)$. For notational clarity the δ before n_i has been dropped in the partial derivatives. This notation will be kept throughout these derivations. Boltzmann tells us that the probability of a given fluctuation δn_i is given by

$$P\left(\delta n_i\right) = P_0 \exp \left(\frac{-S}{k} \right) = P_0 \exp \left(\frac{-g_{ii} \delta n_i^2}{k} \right), \qquad (2.29)$$

where k is the Boltzmann constant and P_0 is a proportionality constant to normalize the probability distribution. For a Gaussian distribution such as the above P_0 is thus $P_0 = \sqrt{g_{ii}/k\pi}$. Taking the second moment as a quantitative measure of the strength of the fluctuation we get

$$\langle \delta n_i^2 \rangle = \int \delta n_i^2 P\left(\delta n_i\right) dn_i = \sqrt{g_{ii}/k\pi} \int \delta n_i^2 \exp\left(\frac{-g_{ii}\delta n_i^2}{k}\right) dn_i = \frac{k}{2g_{ii}}. \qquad (2.30)$$

Here the brackets indicate the expectation value or the thermodynamic average. The above result can also be derived in a similar but stricter way by considering the second moments of the Boltzmann distribution, as we have done above, but without using an expansion of the entropy [23]. We can write this in terms of the corresponding thermodynamic forces X_i.

$$X_i = \frac{\partial S}{\partial n_i} = -\sum_j g_{ij}\delta n_j \Rightarrow \langle \delta n_i^2 \rangle = k\left(\frac{\partial X_i}{\partial n_i}\right)^{-1} = \frac{k}{g_{ii}}. \qquad (2.31)$$

The above result tells us that the strength of the fluctuations are linked to the curvature of the entropy potential through g_{ii} and also to changes in the relevant thermodynamic force. Now let us look at the heat capacities. The heat capacities at constant volume and constant pressure are defined as

$$C_V = \frac{\partial Q}{\partial T} = \frac{\partial E}{\partial T}, \qquad C_P = \frac{\partial H}{\partial T}, \qquad (2.32)$$

respectively, where Q is the heat, T is the temperature, E is the internal energy, and H is the enthalpy. Rewriting the differentials and using the fact that $X_E = 1/T$ plus equation 2.31 we get

$$\partial T = T^2 \partial\left(\frac{1}{T}\right), \quad \partial E = \partial n_E, \quad X_E = \frac{1}{T} \Rightarrow \qquad (2.33)$$

$$C_V = -\frac{1}{T^2}\left(\frac{\partial X_E}{\partial n_E}\right)^{-1} = \frac{\langle \delta n_E^2 \rangle}{kT^2} = \frac{\langle E^2 \rangle - \langle E \rangle^2}{kT^2}. \qquad (2.34)$$

Likewise we get expressions for C_P and the volume and area compressibilities κ_T^V and κ_T^A

$$C_P = \frac{\langle H^2 \rangle - \langle H \rangle^2}{kT^2},$$
$$\kappa_T^V = \frac{\langle V^2 \rangle - \langle V \rangle^2}{VkT^2},$$
$$\kappa_T^A = \frac{\langle A^2 \rangle - \langle A \rangle^2}{AkT^2}, \qquad (2.35)$$

where obviously V and A are the membrane volume and membrane area respectively. The subscript T in κ_T^V and κ_T^A indicate that we are now talking about the *isothermal* compressibilities whereas in the derivation of equation 2.26 we used the *isentropic* compressibility. On experimental grounds it has been proposed that near the phase transition the change in membrane volume is closely and simply related to the change in enthalpy. Similarly the change in membrane area is also related to change in enthalpy [29][13]

$$\Delta V\left(T\right) = \gamma_V \Delta H\left(T\right), \qquad (2.36)$$
$$\Delta A\left(T\right) = \gamma_A \Delta H\left(T\right),$$

where γ_V and γ_A are just proportionality constants. Now we can combine the above expressions with those in equation 2.35

$$\Delta \kappa_V^T = \frac{\gamma_V^2 T}{V} \Delta c_P,$$

$$\Delta \kappa_A^T = \frac{\gamma_A^2 T}{A} \Delta c_P. \tag{2.37}$$

Now we have found relations that link the volume and area compressibilities to the heat capacity at constant pressure. It is very reasonable to assume that the free energy necessary for creating a pore should be closely related to the area compressibility. The membrane that used to be, where the pore now is, obviously has to be pushed out of the way somehow. This has to be easier, and therefore less costly in terms of energy, the larger the area compressibility is. We will now find a relation that describes this intuitive assumption. We consider an area fluctuation of ΔA and expand the free energy as a function of ΔA around its equilibrium value F_0 and keep only terms up to second order. The linear term is neglected as one would expect both positive and negative fluctuations ΔA. The difference in free energy then becomes

$$\Delta F = \frac{1}{2} \frac{\partial^2 F}{\partial A^2} \Delta A^2. \tag{2.38}$$

This can be rewritten in terms of the area compressibility

$$\kappa_A^T = -\frac{1}{A} \frac{\partial A}{\partial \Pi} \Rightarrow \Delta F = \frac{1}{2} \frac{1}{\kappa_A^T A} \Delta A^2, \tag{2.39}$$

where Π is the lateral pressure. This is equivalent to the potential energy derived from Hooke's law with an elastic constant of $1/\kappa_A^T A$. The probability of such a fluctuation is of course again given by the Boltzmann factor, and we note that the probability of fluctuations of different sizes is the same as long as the fraction $\Delta A^2/\kappa_A^T$ is the same. This means that the size of the pores scales as

$$\Delta A^2 \propto \kappa_A^T. \tag{2.40}$$

Finally we want to link this to the permeability of the membrane. We proceed in the same manner as above by expanding the permeability as a function of ΔA around its equilibrium value P_0 up to second order and discard the linear term. It is then just a matter of using equations 2.40 and 2.37 to get

$$P = P_0 + \alpha \Delta c_P, \tag{2.41}$$

where α is just a constant. In the phase transition the heat capacity, the compressibility and the permeability of the membrane are all seen to change dramatically in strikingly similar manners as seen In figure 11. We have now also found mathematical relations that link all of these quantities. In the vicinity of the phase transition the area compressibility rises, and the free energy needed in order to create a pore is lowered thus allowing for more and bigger pores thereby increasing the permeability. The phenomenon that Hodgkin and Huxley measured – currents of ions permeating through the cell membrane – has traditionally been ascribed to ion channel proteins. But pure lipid membranes have shown similar behaviour and quantised currents. In the HH-model the ion channel proteins are highly selective towards a preferred ion. We have not mentioned selectivity yet when discussing lipid ion channels. It has been found that lipid ion channels show selectivity to some extent [5]. In figure 12 current-voltage relations are shown for different ions for a synthetic DPPC membrane.
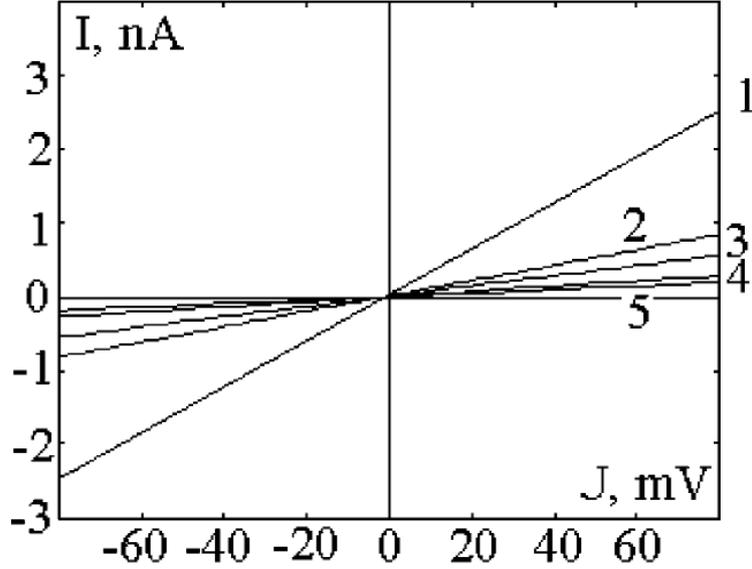
Figure 12: *Transmembrane current as a function of voltage for a DPPC lipid membrane for different monovalent ions – 1: Li, 2: Na, 3: K, 4: Rb and finally 5: Cs. The figure is taken from [5].*

In the discussion of I-V curves it is interesting to take a look at the effects of electrostriction [33][50]. The charges on the two plates of a capacitor attract each other. This attraction causes a mechanical force on the capacitor. This force is given by

$$\mathcal{F} = \frac{1}{2}Eq = \frac{1}{2}\frac{V_m}{D}q = \frac{1}{2}\frac{V_m^2 C_m}{D}, \tag{2.42}$$

where $E = V_m/D$ is the electric field associated with the membrane potential V_m, q is the charge on the capacitor and D is the thickness of the membrane. The quadratic dependence on the voltage tells us that a hyperpolarisation of the membrane leads to a greater mechanical force, and inversely depolarising the membrane leads to a smaller force. A strong force normal to the membrane will suppress the gel phase as the membrane is thinner in the fluid phase. When the electric force causes a change in membrane thickness from D_1 to D_2 the force does work given by

$$\Delta W = \int_{D_1}^{D_2} \mathcal{F}dD \propto V_m^2. \tag{2.43}$$

It is therefore reasonable to assume that the free energy of pore formation is also related to the square of the voltage

$$\Delta F = \Delta F_0 + \alpha V_m^2, \tag{2.44}$$

where ΔF_0 is the free energy of pore formation without any applied voltage. α is merely a proportionality constant. From Boltzmann statistics we have that the probability of finding an open pore is given by

$$P_{open}(V_m) = \frac{K(V_m)}{1 + K(V_m)}, \tag{2.45}$$

where $K(V_m)$ is the equilibrium constant between open and closed pores

23

$$K\left(V_m\right) = \exp\left(-\frac{\Delta F}{kT}\right). \tag{2.46}$$

Through Ohm's law this leads to a current-voltage relation as

$$I_m = g_p P_{open}\left(V_m - E_0\right), \tag{2.47}$$

where g_p is the conductance for a single pore and E_0 is the Nernst potential. In [50] this expression is compared to experimental data. It is found to describe data very well. The I-V profiles found in pure lipid membranes are also compared to I-V curves for a particular family of protein channels. The striking similarity indicates that these I-V curves might as well stem from lipid pores as from protein channels.

It has been suggested that membrane proteins could play a role in catalysing and facilitating pore formation [49]. The presence of proteins expectedly changes the thermodynamic properties of the membrane. Some simple geometrical considerations nicely illustrate the effects of proteins. A protein embedded into a lipid membrane does not necessarily have the same thickness as the surrounding lipid. If it for instance is a little thicker it will tend to stretch the thickness of the lipids in its neighbourhood. The phase transition is linked to geometrical changes of the membrane, thus around the protein the gel phase is slightly favoured. This means around a *gel-favouring* protein one expects to find greater fluctuations of for instance membrane area making pore formation more likely. Lipid pores show several properties similar to those of a protein channel and could potentially, at least in part, explain the voltage pulse accompanying the soliton during signalling. Another phenomenon that might play a role in this is electromechanics.

Before discussing electromechanics we might note something about the nature of these two models that has now become more apparent. The fundamental question in the comparison of these models is which of the two pulses – the mechanical and the electrical – is the one primarily responsible for driving the action potential. In the HH-model the mechanical perturbation of the membrane, which is observed, must be a consequence of the electrical signal. In the soliton model it is the other way around. We will later on discuss some other suggested models that are somewhere in between these two views.

Electromechanics

It is reasonable to assume that the mechanical deformation of the membrane might affect its electrical properties as well. The capacitance is an obvious example of an electrical property which changes with variations in area and thickness of the membrane. In order to get the full picture of the interplay between the electrics and the mechanics of the situation one would need to consider a long series of possible effects. Below we will discuss only a couple of possibilities in this context to illustrate the principles and ideas at work in the soliton model.

As mentioned the cell membrane consist mainly of a lipid bilayer. The exact chemical composition of this lipid bilayer varies from membrane to membrane but the two individual layers in a single membrane are not necessarily identical either [50][30]. They are differently charged for instance. The non-zero resting potential of a neuron results in a charge asymmetry of the two surfaces of the membrane. This asymmetry allows mechanical perturbations to change the membrane potential. The Gouy-Chapman theory describes the interactions of a charged surface with ions in a surrounding solution. The ions create a layer of surface charge on the cell membrane in this case. The Gouy-Chapman theory also takes into account the effects of thermal motion and describes how the potential due to the accumulated charges near the surface decays with distance

from the surface. In [4] and [35] the membrane potential at the inner and outer surfaces of the membrane have been estimated using the Gouy-Chapman theory. This is a first rough estimate of the electromechanical effects at play, and in later publications by the same authors the view of electromechanical phenomena in biomembranes has been refined. We will look at this below, but seeing as the Gouy-Chapman approach was the first attempt to describe these phenomena, we will also start here. The Gouy-Chapman theory yields an expression for the surface charge density σ relating it to the surface potential V_0 [30]

$$\sigma = \sqrt{8\epsilon_0\epsilon c_0 kT}\sinh\left(\frac{eV_0}{2kT}\right), \tag{2.48}$$

where ϵ is the relative permittivity of water, and ϵ_0 is the vacuum permittivity, c_0 is the ionic strength, k the Boltzmann constant, and e the elementary charge. For small potentials $|eV_0| < 2kT \Rightarrow |V_0| < 50mV$ we can expand the hyperbolic sine function to zeroth order and get [4]

$$V_0 = \frac{1}{\epsilon_0\epsilon\kappa}\sigma, \tag{2.49}$$

where κ is the Debye constant. σ is obviously different for the gel and the fluid phases of the membrane. Using the above expression one can calculate an estimate for the voltage change assocated with a propagating density pulse forcing the membrane through the phase transition. This is found to be around $50mV$ [35][4] – roughly on the same order of magnitude as the voltage change measured during an action potential. The membrane potential was predicted to change from $-100mV$ to $-150mV$.

We began this section by noting that the membrane capacitance would change if the spatial dimensions of the membrane were to change. The capacitance of a parallel plate capacitor is given by

$$C = \epsilon\frac{A}{d}, \tag{2.50}$$

where ϵ is the dielectric constant of the material, in our case the cell membrane, A is the area of the capacitor plates and d is the distance between them. As previously mentioned both the area and the thickness of the membrane changes locally during propagation of an action potential. The area of a DPPC artificial membrane is 24.6% larger in the fluid state than in the gel state. The thickness is on the other hand 16.3% smaller in the fluid state [4][33]. If we assume that the dielectric constant of the membrane does not change with the membrane state we can find a numerical relation between the capacitances in the two phases

$$C_f = \epsilon\frac{A_g(1 + 0.246)}{d_g(1 - 0.163)} = 1.49C_g, \tag{2.51}$$

where the subscript f's and $g's$ indicate the fluid and gel phases respectively. We see that the capacitance changes significantly. We have to consider what this means for the membrane potential. Furthermore just as we have various other susceptibilities linked to different thermodynamic variables – heat capacity and temperature, compressibility and pressure etc. – we also have a capacitive susceptibility [33].

$$dq = \frac{\partial q}{\partial V_m}dV_m = \hat{C}_m dV_m, \tag{2.52}$$

where q is the charge, V_m is the membrane potential and $\hat{C}_m$ is the capacitive susceptibility. The capacitive susceptibility tells us how strongly the charge of the membrane reacts to changes

25

in membrane potential, just as the heat capacity tells us how much the internal energy (for constant volume) changes with varying temperature. Just as for the other thermodynamic susceptibilities, we have discussed previously, we can find a similar fluctuation relation for the capacitive susceptibility

$$\hat{C}_m = \frac{\langle q^2 \rangle - \langle q \rangle^2}{kT}. \tag{2.53}$$

And just as for the heat capacity a pronounced maximum is found around the phase transition. This maximum means that at the phase transition even small changes in membrane potential can cause dramatic increases in capacitance leading to large capacitive currents. The capacitive susceptibility is given as

$$\hat{C}_m = \frac{dq}{dV_m} = \frac{q\left(V_m + dV_m, T\right) - q\left(V_m, T\right)}{dV_m}. \tag{2.54}$$

Since $q = C_m V_m$, $q\left(V_m + dV_m, T\right)$ and $q\left(V_m, T\right)$ are related to the area and thickness of the membrane through equation 2.50

$$q\left(V_m + dV_m, T\right) = \epsilon \frac{A_g + \Delta A\left(V_m + dV_m, T\right)}{D_g + \Delta D\left(V_m + dV_m, T\right)}\left(V_m + dV_m\right), \tag{2.55}$$

$$q\left(V_m, T\right) = \epsilon \frac{A_g + \Delta A\left(V_m, T\right)}{D_g + \Delta D\left(V_m, T\right)}\left(V_m\right).$$

In figure 13 a graph of the capacitive susceptibility as a function of voltage is shown along with graphs of the area and density also as functions of voltage.

This peak in capacitive susceptibility around the phase transition will play a role in excitation processes. In [33] the difference in capacitance between the two phases calculated in equation 2.51 has been translated into capacitive currents. If the change in capacitance from equation 2.51 happens over $0.5ms$ (the time scale for the upstroke of an action potential) it will result in capacitive currents of $100\mu A/cm^2$ for $V_m = 100mV$ compared to the ionic currents from the HH-model for the squid giant axon of $100 - 600\mu A/cm^2$.

If we take the differential of the charge accumulated on the membrane, assuming it is a function of voltage V_m and mechanical force normal to the membrane $\mathcal{F}$, we get

$$dq = \left(\frac{\partial q}{\partial V_m}\right)_{\mathcal{F}} dV_m + \left(\frac{\partial q}{\partial \mathcal{F}}\right)_{V_m} d\mathcal{F}, \tag{2.56}$$

As noted earlier on several occasions a change in thickness is associated with a change in area as well. We can therefore rewrite the above expression using the lateral pressure Π

$$dq = \left(\frac{\partial q}{\partial V_m}\right)_{\mathcal{F}} dV_m + \left(\frac{\partial q}{\partial \Pi}\right)_{V_m}\left(\frac{\partial \Pi}{\partial \mathcal{F}}\right)_{V_m} d\mathcal{F} = \left(\frac{\partial q}{\partial V_m}\right)_{\Pi} dV_m + \left(\frac{\partial q}{\partial \Pi}\right)_{V_m} d\Pi. \tag{2.57}$$

When the charge is constant i.e. $dq = 0$ we get

$$dV_m = -\frac{\left(\frac{\partial q}{\partial \Pi}\right)_{V_m}}{\left(\frac{\partial q}{\partial V_m}\right)_{\Pi}} d\Pi = \left(\frac{\partial V_m}{\partial \Pi}\right)_q d\Pi = \beta_q d\Pi. \tag{2.58}$$

Here we have introduced the quantity β_q. This is a kind of piezoelectric susceptibility and describes changes in the membrane voltage V_m as the lateral pressure is varied. This was fairly
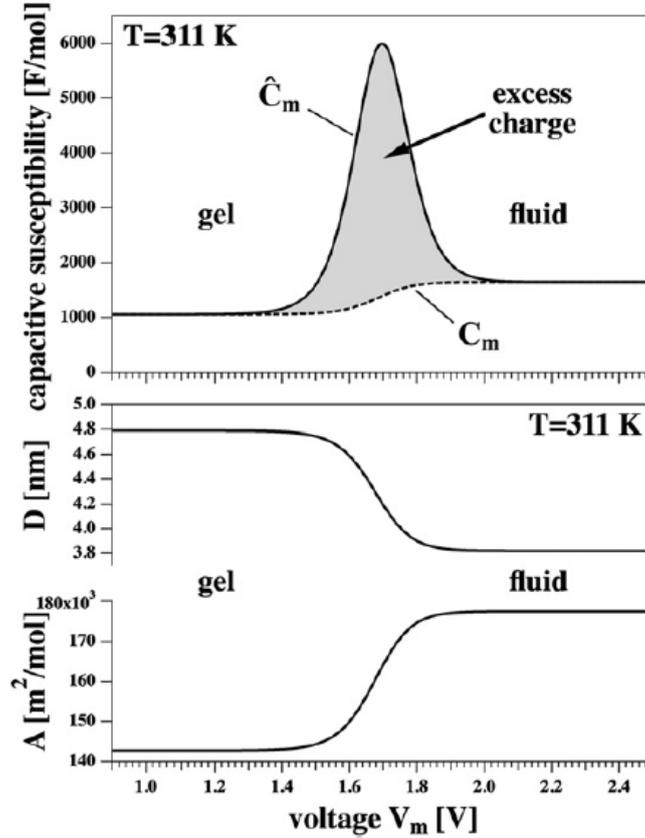
Figure 13: *Top: Capacitive susceptibility as a function of voltage for a DPPC membrane (full drawn line). A pronounced peak is seen right at the transition from the fluid to the gel state. The membrane capacitance is plotted as well (dotted line). The capacitance is seen to change from the fluid to gel state. Bottom: Membrane area and thickness plotted as functions of voltage again for a DPPC membrane. Figure taken from [33].*

readily derived and is just one example of a conceivable electromechanical effect [24]. Another example is what is known as flexoelectricity – electric changes induced by a flexing of the membrane [50].

We ended the section *The ionic hypothesis* on the note that the HH-model is somewhat more complicated than it seems at first glance. The last few pages have shown that the soliton model is rather complex as well. The foundation and underlying idea is simple – everything is linked to the phase transition – but the implications as seen above are somewhat intricate. It seems that nerve signals just are a rather complicated affair, and, as is the case in most natural science investigations, the exact details of how they work are secrets that mother nature is not willing to give up that easily.

2.4 S t r e n g t h s a n d s h o r t c o m i n g s

In the previous several sections we have introduced the HH-model and the alternative soliton model for nerve signals. The two models attack the problem from very different angles and focus on very different aspects of the common phenomenon they are trying to describe and explain. The HH-model is based on the idea of ion channel proteins embedded in the membrane opening and letting ions flow through thus creating an electrical pulse. The soliton model is centered around

the fluid/gel phase transition just below biological temperatures. This allows for propagation of a density pulse which in turn through electromechanical effects and the creation of lipid channels result in a copropagating electrical pulse. Both models answer questions about the nature of nerve signals, but on the other hand both models leave a series of questions unanswered as well. We will now take a look at the pros and cons of both models. In their original article [38] Hodgkin and Huxley write thus

"The agreement must not be taken as evidence that our equations are anything more than an empirical description of the time-course of the changes in permeability to sodium and potassium. An equally satisfactory description of the voltage clamp data could no doubt have been achieved with equations of very different form, which would probably have been equally successful in predicting the electrical behaviour of the membrane. It was pointed out in Part II of this paper that certain features of our equations were capable of a physical interpretation, but the success of the equations is no evidence in favour of the mechanism of permeability change that we tentatively had in mind when formulating them."

While the HH-model provide a mathematical framework that is able to reproduce many of the characteristics of nerve signals there are some phenomenological problems with the model. The equivalent circuit picture introduced earlier treats each component of the axon as an electric component – the lipid membrane as a capacitor, the concetration gradients across the membrane as batteries (the active transporters such as the sodium-potassium pump keep these batteries charged), and the protein channels as resistors. When an AP is initiated current in the form of ion fluxes flow across these resistors. Current flowing through a resistor creates heat independent of the direction of the current. This means that in the HH-model heat is released both at the up- and downstroke of the action potential. When the sodium channels open heat is produced. When the potassium channels open, and the cell is repolarised, and from an electric point of view returns to *normal*, heat is also produced. In total the action potential should be accompanied by a measurable heat release. This is not what has been observed experimentally. At the upstroke of the AP heat is released but that is then followed by a phase of heat absorption [40][1]. This has been studied by various researchers through the years. In 1922 the English physiologist Archibald Hill won the Nobel Prize in Physiology or Medicine for his studies on heat production in muscles. It has been established that the reabsorption of heat is not due to conduction in the aqueous medium. There is no significant net heat produced during an AP – the integral of the heat over the course of the AP is aprroximately zero. It has further been found that the heat exchanges involved in the process of propagation of APs in myelinated fibres is not located at the nodes of Ranvier, which would be expected if it was due to the ionic currents running across resistors. Since $dQ = TdS$ for a reversible process no net heat release $dQ = 0$ also means no net change in entropy $dS = 0$. When a protein channel opens, ions glide down their electrochemical gradient in attempt to equilibrate the outside and inside concentrations. This is clearly an irreversible process which increases the entropy of the system. The HH-model cannot explain this and in fact it does not try to or even considers thermodynamics. It has to be noted in this context that the permeation of ions through lipid pores obviously also is an irreversible process, which increases the entropy. Hodgkin himself writes in his book [30]

"In thinking about the physical basis of the action potential perhaps the most important thing to do at the present moment is to consider whether there are any unexplained observations which have been neglected in an attempt to make the experiments fit into a tidy pattern. [...] perhaps the

most puzzling observation is one made by A.V. Hill and his collaborators Abbott and Howarth (1958). [...] Hill and his colleagues found that it was diphasic and that an initial phase of heat liberation was followed by one of heat absorption. [...] a net cooling on open-circui was totally unexpected and has so far received no satisfactory explanation."

This should naturally lead to investigations into a thermodynamic framework for understanding nerve signals. Various researchers have looked into the phenomena from a thermodynamic perspective, and fifty years after Hodgkin and Huxley published their original paper a thermodynamic alternative model was proposed. We have discussed the soliton model in the previous sections. The soliton model is a thermodynamic model, and it is based on reversible processes. It solves the problems regarding heat, as heat is first released when the membrane is forced through the phase transition and *freezes*. Heat is subsequently absorbed when the membrane *melts* and returns to its natural fluid state. It has several other challenges however. But one neuroscience model at a time.

Something we have already pointed out is the fact that changes in the mechanical properties of the membrane are ignored in the HH-model. Changes in thickness has been observed experimentally [63]. These would cause a change in the capacitance of the membrane. This is assumed to be constant in the HH-model. We noted earlier that if the membrane (DPPC membrane – other membranes would behave differently) is forced all the way through the phase transition the thickness would change by 16%. We calculated that this leads to a difference in capacitance between the two phases of 50% (equation 2.51). This is clearly a quite significant change. In biomembranes the difference will naturally be different due to the presence of proteins, inhomogeneity in lipid composition and so on. The membrane is not necessarily forced all the way through the transition either.

The HH-model has enjoyed great success since it was proposed around 60 years ago. Its great predictive power and simple phenomenology is very compelling. Due to the extensive work laid in furthering the theory over the years the burden of proof weighing on proponents of alternative theories is significant. Given the above unresolved problems and the lack of a thermodynamic aspect to the theory it is however important that investigations into these phenomena are made.

The soliton model leaves several central questions unanswered as well. It should be noted that the model is work in progress and cannot be expected to have answers ready for all aspects of nerve signals from the get-go, but there are several problems with the model. In the section *Signals* we stated some defining characteristics of nerve signals. A central one is the all-or-none behaviour of action potentials. In the HH-model this fits neatly with a threshold potential necessary for conformational change of the protein ion channels and is reproduced nicely by the math. In the soliton model this is unexplained. As the peaks in the various susceptibilities of the membrane, pronounced as they are, are not delta functions one would expect threshold for the onset of an action potential that is somewhat *smeared out* and not all-or-none. Analogue signalling has been observed in some experiments in some situations [60][3], but the defining all-or-none behaviour is observed every day in laboratories around the world and in all different nerves. Recently results have been published regarding solitary elastic waves in membranes that show a sharp excitation threshold. Though akin to the solitons of the soliton model the waves described in [59] are not solitons as they do not survive collisions for instance.

The refractory period is another routinely observed phenomenon which is somewhat unclear in the soliton model. Periodic solutions to the governing differential equation (2.26) showing a refractory period have been found under the condition that the total length of the nerve be held constant [65]. It has been found that there is a minimum distance between such peeriodic pulses

corresponding to a refractory period. If the length is constant a positive change in lateral density (a contraction) of the membrane must be accompanied by a section of membrane with a negative lateral density change (an expansion). Because of pulse propagation this length of membrane with negative density change also translates into a period of time where excitation is not possible. Another feature of this negative density change is an undershoot – a hyperpolarisaton. This follows from the exact same arguments presented in the section *Electromechanics*. The assumption that nerves are kept at constant length in biological circumstances is not completely obvious though.

Other problems are related to the effect of neurotoxins such as tetrodotoxin (TTX), which take effect already at very small concentrations (orders of magnitude smaller than for local anaesthetics) and signal propagation in non-myelinated axons. Tetrodotoxin is among other places found in pufferfish. In Japan *fugu* (Japanese for pufferfish) is a delicacy. Because the fish contains tetrodotoxin careless preparation of the fish can be fatal, and from time to time it is. In the HH-model nerve poisons such as TTX find a natural explanation in binding to the channel proteins thus inhibiting signals. In the soliton model an explanation has to be linked to the substance altering the general state of the membrane.

The soliton model does not include a clear explanation for signal propagation in non-myelinated axons and the significantly lower conduction velocity found in such axons. The conduction velocity found for the solitonic solutions to the equation 2.26 resembles that found experimentally in myelinated nerves. This is thought to be because transverse modes are locked out by the myelin sheath. Transverse waves are known to be slower than longitudinal waves.

ANAESTHESIA

Before discussing the mechanism of action of anaesthesia both general and local in the two models we should probably mention the differences between the two concepts. Anaesthesiology is an interesting field both for the natural scientist as well as for the philosopher. The question of how anaesthesia works is of course a question of how the body works, but it is also a question of what conciousness is. Local anaesthesia is the medically induced local absence of sensation. When at the dentist you are given a local anaesthetic drug to not feel pain from the drill. The nerves in your teeth may not be susceptible to pain input, but the nerves in the rest of your body works just fine as normal. General anaesthesia is the medically induced total loss of consciousness. When under general anaesthesia you are not aware and you do not feel pain anywhere on your body. The understanding of general anaesthesia would therefore tell us a great deal about what the evasive concept of conciousness is. This phenomenological difference might hint at a possible difference in underlying mechanism, but as we will see, neither local nor general anaesthesia is completely if mostly understood.

A strength of the soliton model is that an explanation for the effect of both general and local anaesthetics is readily obtained. The mechanisms behind general anaesthesia is still unclear in the HH-picture. In figure 1 the Meyer-Overton relation is shown. It states that the anaesthetic potency of a substance is related to its oil to water partition coefficient. This naturally leads to the suspicion that the underlying mechanism is related to the lipid membrane rather than the membrane proteins. There have been several lipid theories of general anaesthetic action within the HH framework and there still are. In the soliton model the Meyer Overton relation has a natural explanation through what is known as the freezing point depression law.

We consider an anaesthetic drug dissolved in a lipid membrane [25]. Suppose the drug is perfectly soluble in the fluid phase of the lipid but not soluble in the gel phase. This is obviously

an idealised situation, but for simplicity let us stick to this. The drug is dissolved in the membrane, which is in the fluid phase, so a transition to the gel phase is unfavourable as the drugs has to be disposed of in order to make the transition, since it is not soluble in the gel state. This causes a shift in the phase transition towards lower temperatures. This phenomenon is something we are familiar with from our everyday lives. We salt the roads when there is snow on them in winter, and we add antifreeze to our windshield washer fluid and coolant for our cars. This works because of the freezing point depression law. Returning to our anaesthetic in the membrane. The chemical potentials of the lipid membrane in the fluid and the gel phase are given by

$$\mu_f = \mu_{f0} + RT \ln (x_f),\tag{2.59}$$
$$\mu_g = \mu_{g0},$$

respectively where R is the gas constant, μ_{f0} is the chemical potential of the fluid phase in the absence of anaesthetic, and μ_{g0} for the gel phase. x_f is the molar fraction of the lipid. We have $x_f = 1 - x_A$, where x_A is the molar fraction of the anaesthetic in the fluid phase. In equilibrium we have $\mu_f = \mu_g = \mu_{g0}$. This along with the above equation gives us

$$\Delta\mu = \mu_{f0} - \mu_{g0} = -RT \ln (x_f).\tag{2.60}$$

Since the change in Gibbs free energy is zero at equilibrium we have

$$\Delta\mu = -RT \ln (x_f) = \Delta H - T\Delta S,\tag{2.61}$$

where ΔH is the change in molar enthalpy during melting, ΔS is the change in molar entropy during melting. During melting we have $T_m = \Delta H/\Delta S$ since the change in Gibbs free energy is zero. Using this on the above equation we get

$$\ln (x_f) = \ln (1 - x_A) = -\frac{\Delta H}{R} \left(\frac{1}{T} - \frac{1}{T_m} \right).\tag{2.62}$$

If we now use a couple of approximations we arrive at the freezing point depression law. For small x_A we can approximate $\ln (1 - x_A)$ by its first order Taylor polynomium $-x_A$. If we are close to the melting temperature we can also make the approximation $T_m T \approx T_m^2$. Inserting these two approximations above we get

$$\Delta T = T - T_m = -\frac{T_m^2 R}{\Delta H} x_A.\tag{2.63}$$

The above equation is exactly the freezing point depression law. It tells us that the freezing temperature is shifted down linearly with anaesthetic concentration. Since the phase transition is what facilitates signals in the soliton model this immediately explains the linear Meyer-Overton relation, as the threshold is shifted. Note that this also means that the threshold for excitation should increase linearly as a function of anaesthetic concentration. In addition it should in principle always be possible to initiate a signal no matter how high the concentration. The phase transition is merely shifted. It does not disappear. The shape of the transition is also altered, which naturally also affects the ability to elicit APs. We will return to this when discussing the experimental data.

Hypotheses for general anaesthetic action based on anaesthetics being dissolved in the lipid membrane have also been proposed in the HH-picture, and in fact for a very long time the majority of theories were lipid theories [66][18]. Arguments against such hypotheses include the

existence of a *cutoff* in the effect of long chain alcohols. When you reach a certain legth the anaesthetic effect vanishes and the substances cease to follow the Meyer-Overton relation. This is puzzling as longer chain alcohols are more soluble in lipids and should therefore be more and more potent anaesthetics with increasing chain length. In the soliton model this cutoff effect neatly finds a natural explanation. Another way of understanding the freezing point depression law is by looking at the freezing points of the individual substances being mixed. The freezing point of a beer is about $-2°C$. The freezing points of the two main constituents of beer – ethanol and water – are respectively $-114°C$ and $0°C$. Since there is only a small amount of ethanol in beer it only shifts the collective freezing point slightly towards that of ethanol. The freezing point of n-alcohols increases with increasing chain length and at some point the freezing point of the pure alcohol is above biological temperatures. If this is the case the alcohol cannot shift the freezing point downwards but might even instead shift it upwards [25]. The soliton model also explains why some substances that are highly soluble in the membrane and therefore should be potent anaesthetics are in fact not. The downwards shift in temperature caused by adding a substance is in the above derivation caused by the fact that the substance is soluble in the fluid phase but not in the gel phase. If the substance is equally soluble in both phases it might not alter the transition temperature significantly. There are however still several issues yet to be addressed. We mentioned the strong effect of certain neurotoxins such as TTX which very efficiently kill nerve signals without being particularly soluble in the membrane. Other drugs that do not fit neatly in to the above presented picture are the so called *nonimmobilisers*. Nonimmobilisers are drugs that only display one side of the expected anaesthetic effect – amnesia but not suppression of movement(hence the name). In the beginning of the 20th century nonimmobilisers were used to induce so-called *twillight-sleep* during labour [18]. Women were given a combination of morphine and scopolamine. The mixture did not block pain sensation nor inhibit movement but it would induce amnesia. After delivery the woman would believe it had been completely pain free as she was told so and could not remember anything.

In the HH-picture the dominating lipid theory today says that the drug dissolves in the membrane inducing a lateral pressure affecting the conformations of the protein ion channels. Through the years there have been a wilderness of suggested mechanisms. Others believe that general anaesthesia works through binding to specific targets. Today this is probably the mainstream believe within the HH-framework. In 1984 Franks and Lieb published a very influential paper presenting a correlation similar to the Meyer-Overton correlation but instead of involving the lipid solubility of the drugs it considers inhibition of the enzyme firefly luciferase [19]. In figure 14 the correlation is shown. Just as the Meyer-Overton relation indicates a mechanism of a general nature and related to the state of the lipid membrane the Franks-Lieb relation indicates an underlying molecular mechanism.

The last couple of decades considerable effort has been spent trying to identify the specific binding targets of general anaesthetics. Receptors for the neurotransmitter gamma-Aminobutyric acid (GABA) is now believed to play a central role, in particular the $GABA_A$ receptor is thought to be of key significance [66][18]. A neurotransmitter is a signal substance used to relay signals across chemical synapses. GABA is the primary neurotransmitter involved in most inhibitory processes in the central nervous system of mammals. It therefore makes sense that it should play a role in the mechanism of general anaesthesia. It is difficult to say precisely which functional form the threshold as a function of increased anaesthetic concentration would take in this picture since it is a specific binding mechanism, but it is likely that it would be exponential or sigmoid rather than linear.
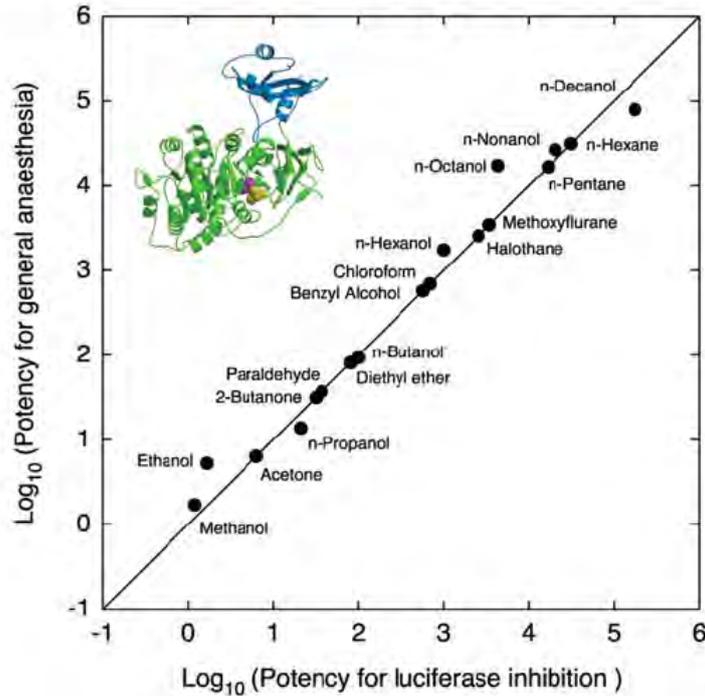
Figure 14: *Potency of general anaesthesia as a function of potency of inhiibition of firefly luciferase. Compare the above graph with the one seen In figure 1. Figure taken from [18].*

3   EXPERIMENTS

In the last chapter we introduced the two models and the background theory underlying them. We will now look at experimental data acquired through a series of different experiments carried out in an attempt to test the applicability of the models in different situations. Three experiments were carried out

- Collision of pulses

- Temperature dependence of threshold

- Dependence of threshold on added anaesthetic

In collision experiments a pulse was initiated in one end of the cord, then from the other end, and lastly from both ends at the same time. The signals were recorded about two thirds of the way between the two stimulation electrodes. The actual, measured signal, when the cord was stimulated at both ends, was then compared to the sum of the individual signals with stimulation only at one end at a time. The signals are expected to meet at about the halfway mark between the stimulation electrodes. The signal from the stimulation electrode nearest the recording electrode will always reach the recording electrode, but the signal from the other end collides with the counter-propagating signal before reaching the recording electrode. This means that if traces of both signals are found in the signal when both ends are stimulated simultaneously, the two pulses have to have passed by each other in some way. This should not be possible according to the Hodgkin Huxley model, but the soliton model allows for such behaviour.

In temperature experiments the threshold dependence on temperature is measured for temperatures between about $\sim 6°C$ and $\sim 26°C$. When cooling the cord we approach the phase transition. This should result in a linear decrease in threshold with decreasing temperature

33

and vice versa for increasing temperatures. If the cord is cooled below the melting/freezing temperature of the membrane, it should not be possible to elicit signals at all. A few worms were kept at higher temperatures ($\sim 35 - 40°$) for about a month, and measurements were recorded from these as well. The idea behind this is that the membranes should acclimatise to the ambient temperature over time thereby shifting the transition temperature towards higher temperatures in this case. This should make it easier to cool the cord below the phase transition of the membrane. Worms were normally kept in the fridge at 5°.

In anaesthetic experiments the threshold dependence on added anaesthetic was measured. In the present case lidocaine and pentobarbital were used. The soliton model predicts a linear increase in threshold as already mentioned through the freezing point depression law. In addition the general anaesthetic pentobarbital and the local anaesthetic lidocaine should show very similar effects on the threshold, as both general and local anaesthetics are believed to function by the same mechanism. From the HH-perspective local and general anaesthetics work in two possibly very different ways. Local anaesthetics are believed to act by binding with ion channel proteins. The threshold response to increasing anaesthetic concentration should probably rather be exponential or sigmoid instead of linear – at least for local anaesthetics. A commonly accepted theory for general anaesthesia is yet to be developed.

3.1 Materials and methods

The earthworm

All three experiments were carried out using earthworm (lumbricus terrestris). Surprisingly extensive research has been made into the anatomy, and physiology of the nervous system of earthworms. See for example [27][39][21][8]. Earthworms were an ideal choice for the experiments presented in the present paper, as they are cheap and easy to get hold of and handle. One could have even just gone and dug them up in the backyard oneself if needed. Earthworms were primarily bought at *Stef's Fluebinding* in Aarhus except for a brief period in winter, where they were out of stock. Worms were then bought at *Tropeland* in Skanderborg. The earthworms bought at Stef's Fluebnding were reared in Germany by the compay Hansa Angelköder. The worms bought at Tropeland were reared in Canada. It was originally planned but dropped due to lack of time that lugworms were to be used as well. The earthworm has myelinated axons, where the lugworm does not [28]. It would be interesting to see, if the nonmyelinated axons of the lugworm would respond differently to the same experiments than the myelinated axons of the earthworm.

The earthworm has a central nerve cord running down the length of the animal on the ventral side – for those of us with slightly rusted latin skills, ventral in layman's terms is the belly. In this cord there are two (or three depending on how you count them) giant axons on the dorsal side (the back) of the cord as well as a two smaller ones on the ventral side of the cord. The two giant axons are the ones of interest. In figure 15 a cross section of the ventral cord is seen. For better pictures see [27].

Three giant axons are clearly seen. A central one – the medial giant axon or medial giant fibre (MGF) – flanked by two slightly smaller ones – the lateral giant axons or fibres (LGF). The two lateral axons are connected, and they effectively function as a single axon. This is what was meant when mentioned that whether there are two or three giant axons in the ventral cord depends on how you count them. A hint of the connection (or anastomosis with a southern European term) between the two lateral axons can also be seen In figure 15 – sticking out of the
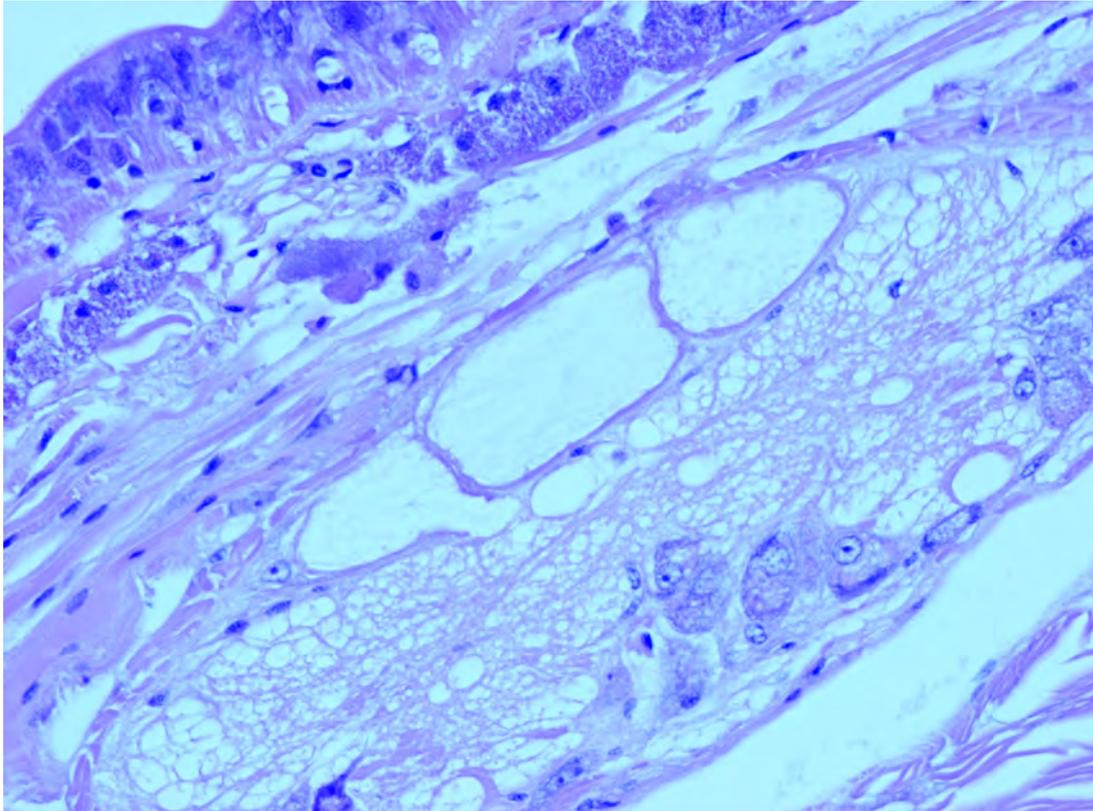
Figure 15: *Histological image using a hematoxylin and eosin stain of a cross section of the ventral cord in lumbricus terrestris. The medial giant axon and the two lateral giant axons are clearly seen (top center). A hint of an anastomosis is seen sprouting out from the bottom of the left lateral giant axon. A bunch of glial cells are seen to fill the center of the cord.*
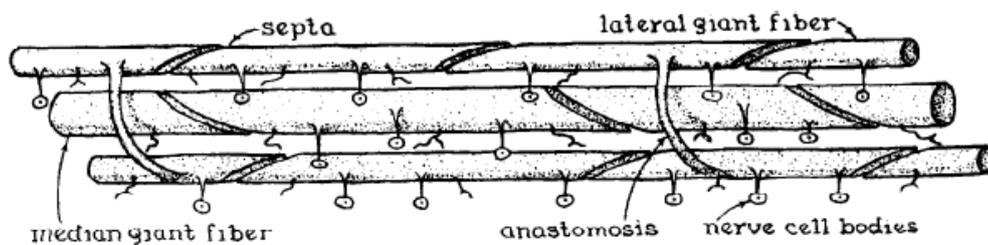

Figure 16: *Sketch of the MGF and LGF. The anastomoses connecting the two LGFs are shown. They connect the two axons at regular intervals. Figure taken from [39].*

bottom right of the left lateral axon. In figure 16 a sketch is shown of the giant fibres in the ventral cord, where the anastomoses are seen.

As can be seen when comparing figure 15 with figure 17 the lateral fibres change diameter quite dramatically from the posterior *tale end* to the anterior *head end* of the animal. The MGF, on the other hand, is relatively constant in diameter. It is also seen In figure 15 that the two fibres are of almost the same size in the posterior end (see figure 18). According to [8] the diameter of the MGF is $100\mu m$ throughout the length of the worm, where the diameter of the LGF ranges from $4\mu m$ in the anterior end of the beast to $50\mu m$ in the posterior end.

In figure 18 the sizes of the three axons are clearly seen to be very similar.

The axons are loosely myelinated increasing the conduction velocity in cooperation with their
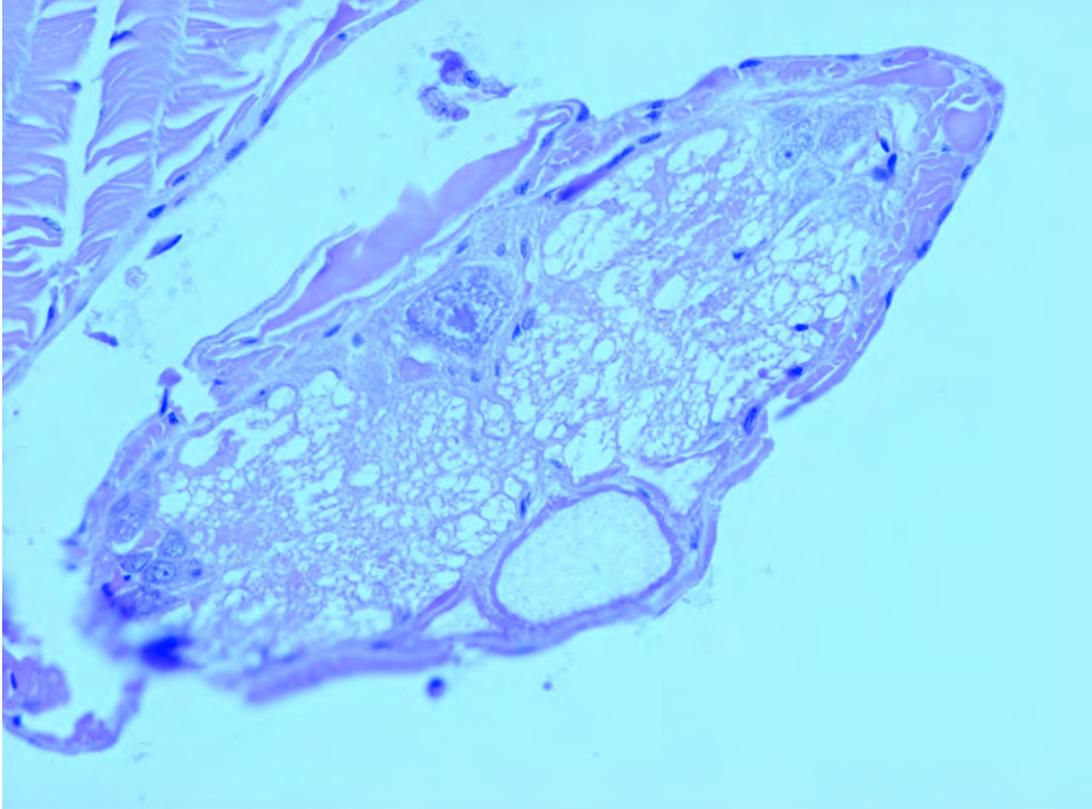
Figure 17: *Histological image of cross section of the ventral cord in the anterior end of the cord near the brain. The LGFs are seen to be significantly smaller than the MGF. Compare to figure 15. Here a hint of an anastomosis is seen as well in the right LGF.*

large diameters. Since the length constant (see *Cable theory* page 13) depends on the square root of the radius, the propagation velocity increases as the square root of the radius. Enlarging axons is one way of achieving faster propagation speeds critical for fast reflexes for example, but it is not nearly as efficient as myelination [28]. The myelin of earthworm giant axons is not as tightly wrapped around the axons as it is in for instance human myelinated nerves, where conduction speeds of up to $100m/s$ are achieved. The conduction velocities of earthworm axons are around $20m/s$ [8][21]. From measurements made for the present paper, conduction velocities were found to lie in the range $10 - 20m/s$ for the MGF and $5 - 10m/s$ for the LGF. Compare to results for conduction velocities found in [22]. In figure 19 an electron microscopic image of the myelin sheath of the MGF of the earthworm can be seen. Here it is clearly seen that the myelin is not wrapped as tightly as it is around human myelinated nerves.

Several projections sprout out from both the medial and the lateral fibres. Side nerves and unmyelinated collaterals sprout out from the sides and from the ventral side of the axons respectively. On the dorsal side of the MGF are also found regular spaced circular openings in the myelin sheath – like small chimneys [27]. These *dorsal nodes* are similar to the nodes of Ranvier found in for example human myelinated nerves, but they do not wrap all the way around the axon. These dorsal nodes are not found on the LGF, only on the MGF. In figure 20 a sketch of a segment of nerve cord is seen with typical locations of all the projections marked. In [27] it is argued based on electrophysiological data that the dorsal nodes play a role in excitation and propagation similar to that of the nodes of Ranvier. That is active spots with significantly higher ionic transmembrane currents during action potential propagation.
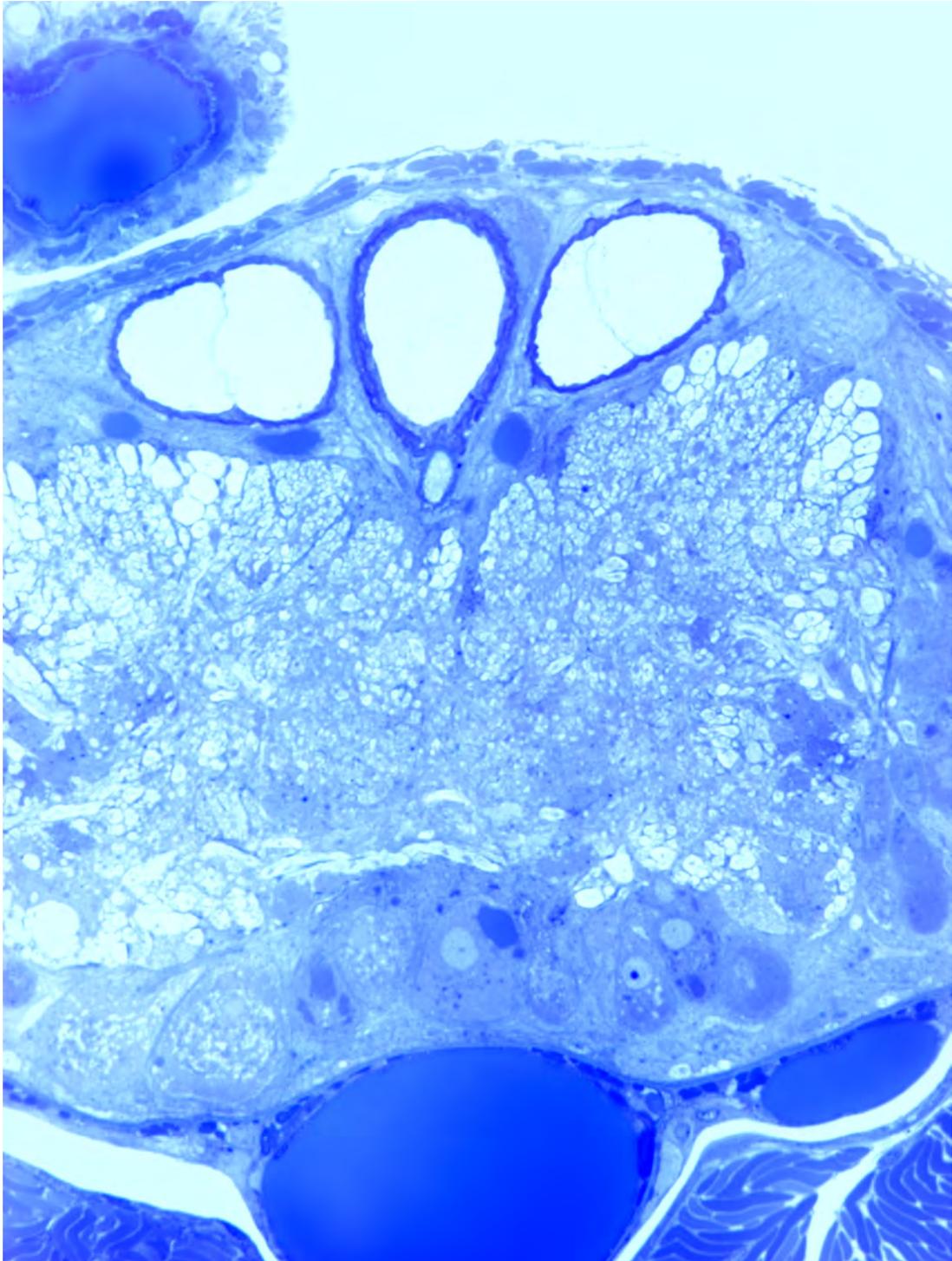
Figure 18: *Hstological image of cross section of the ventral cord. All three axon are clearly seen to be of very similar size.*
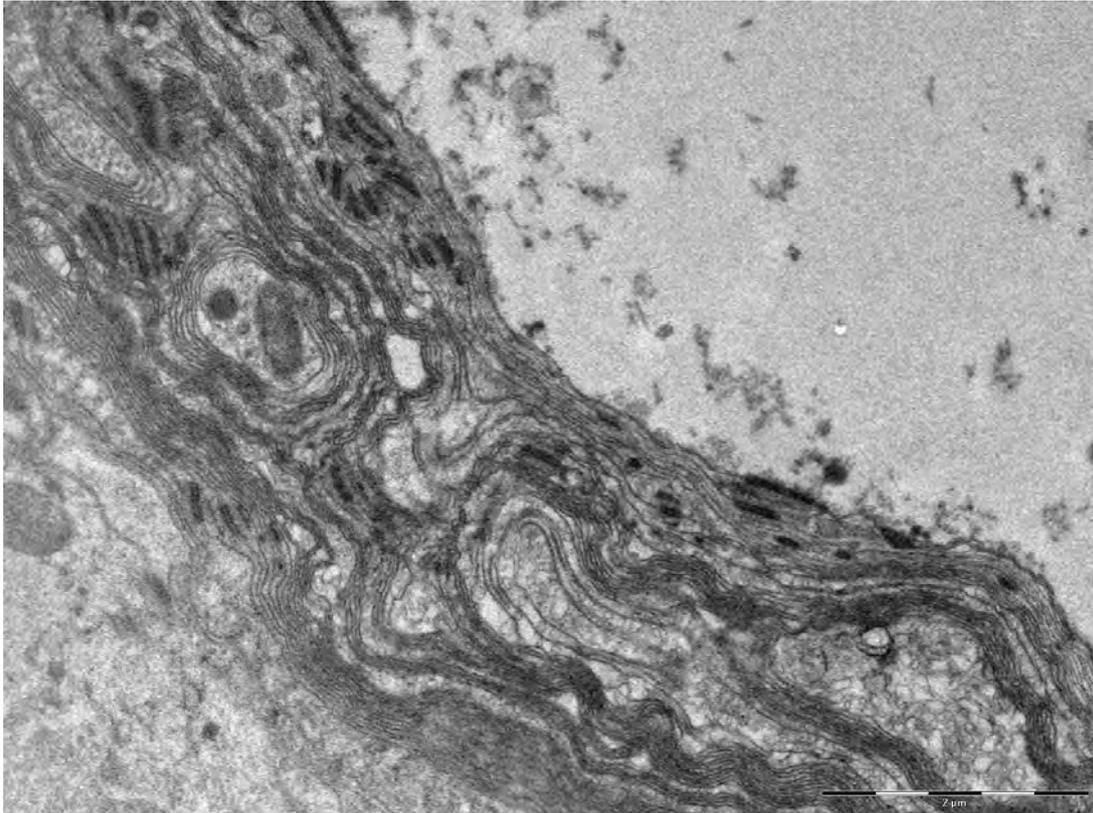
Figure 19: *Electron microscopic image showing the myelin sheath of the MGF in 11000 times magnification.*

The preparation

Earthworm weighing about 5g on average, but ranging from 1.5g to 9g, were used for the experiments. The worms were sedated by leaving them in a 10% alcohol solution in tap water for 8-15 min depending on size and vigor. After sedation the worms were washed in tap water. The worm was then pinned down both longitudinally and laterally lying on its belly to a piece of styrofoam using needles. The worm was cut open using a pair of scissors down the entire length of the animal except at the ends, where it was pinned down. The body wall was then pulled out to the sides and pinned down exposing the gut. The lateral ligaments holding the gut in place were then cut using a scalpel, and the gut was removed. Here the preparation procedures diverge depending on whether the preparation was for a collision experiment or a temperature/anaesthetic experiment.

Collision experiments For a collision experiment the ventral cord was then liberated from the underlying muscle tissue with a pair of micro-scissors. Preferably the whole nerve cord without the brain was liberated. The cord was then left to rest in a saline solution (recipe is found below) for around half an hour, and the preparation was then ready for use.

Temperature/anaesthetic experiments For a temperature/anaesthetic experiment the nerve cord had to be prepared in a slightly different way due to the fact that it would be submerged into a flowing liquid. Lateral incisions were made using a scalpel cutting the body wall from both sides in to the nerve cord with a longitudinal distance of about a centimetre – then a couple of millimetres (just enough for a pin to hold on to) – then about a centimetre again. The nerve cord was then liberated in the centimetre long segments, but not in the short
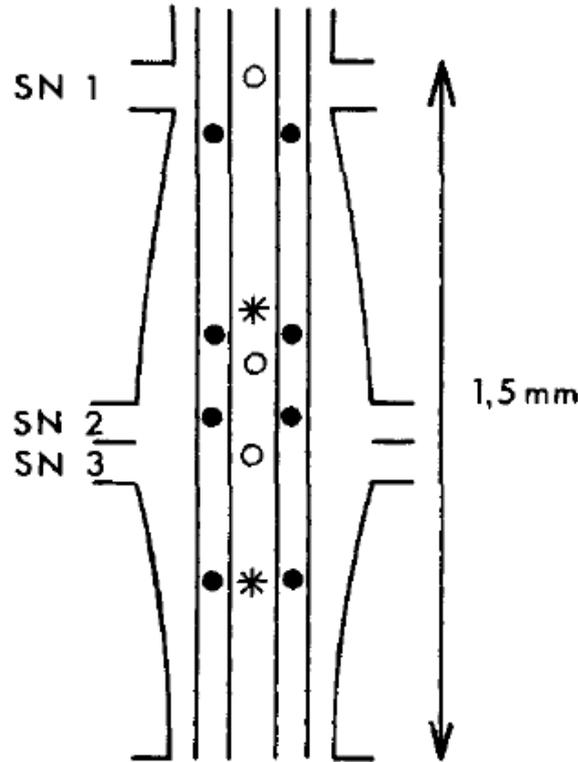
Figure 20: *Sketch of a segment of nerve from the ventral cord of lumbricus terrestris. The MGF and LGF of the dorsal giant fibres are shown. The side nerves are indicated (SN 1,2 and 3). The filled out circles show the collaterals of the LGF, and the open circles indicate collaterals of the MGF. The stars indicate locations of the dorsal nodes found in the MGF. Figure taken from [27].*

segments. The body wall in the centimetre long segments was then removed exposing the nerve cord. The millimetre long segments were left in order to be able to pin the cord down during experiments. Usually the cord would be pinned down four places during experiments.

The saline

The saline used was made following the below recipe adapted from [12] and [22]

Substance	Concentration [mM]
NaCl	75
KCl	4
Tris	10
Glucose	23
$MgSO_4$	1
$CaCl_2$	2

The saline was adjusted with NaOH to a pH of 7.4.

Collision experiments

Following the dissection the nerve cord was typically left to rest in the chamber used for measurements (seen In figure 21) in plenty of the above described saline solution. When the cord had rested, the saline was sucked out of the chamber with a pipette, so the cord was lowered

39

Figure 21: *Picture of the recording chamber used in the collision experiments. The chamber is carved from a 2 by 7 cm block of acrylic glass. The groove is 6 cm in length, 0.5 cm wide and 1 cm deep. 21 electrode wires are inserted into the chamber in equidistant spacing of about 0.25 cm. The electrodes are made of resistance wire with a resistance of $5.40\Omega/m$ at $20°C$.*

onto the array of electrodes. A little bit of saline solution was left in the bottom of the chamber, and a lid was placed on top of the chamber in order to keep the atmosphere humid. The cord dries out quickly and must be kept moist for the entire duration of the experiment.

The array of resistance wires were used both for stimulation and recording. For stimulation two WPI A365 Stimulus Isolators were used. Stimulation duration was set to $50\mu s$, and typical stimulation strengths ranged from $20\mu A$ to $200\mu A$. For recording a couple of simple pre-amplifiers were built. A circuit diagram is shown In figure 22.

With a value of 500Ω for R_G a gain of about 100 was achieved

$$G = 1 + \frac{50k\Omega}{500\Omega} \approx 100. \tag{3.1}$$

The pre-amplifiers were connected to an Axon Instruments Cyberamp 380 and through an Axon Instruments Digidata 1440 analog to digital converter to a computer. Recordings were made in the program Clampex 10.2 also from Axon Instruments. All recordings were made at room temperature ($\sim 21.5°C$).

TEMPERATURE AND ANEASTHETIC EXPERIMENTS

For the temperature and anaesthetic experiments a slightly more advanced chamber was necessary. It can be seen In figure 23. The reservoir where the nerve cord is placed and pinned down is 1.5 cm wide, 8 cm long, and 1 cm deep. The bottom 0.5 cm are filled with Sylgard silicone elastomer, so the cord can easily be pinned down. This *reservoir* will be called the nerve chamber from now on, where the greater surrounding reservoir will be referred to as the surrounding chamber. There is an inlet for liquid in one end of the nerve chamber (bottom In figure 23). And in the other end there is a small circular reservoir connected to the main reservoir by a small groove. From the circular reservoir the liquid is pumped out of the chamber again. It is thus possible to maintain a
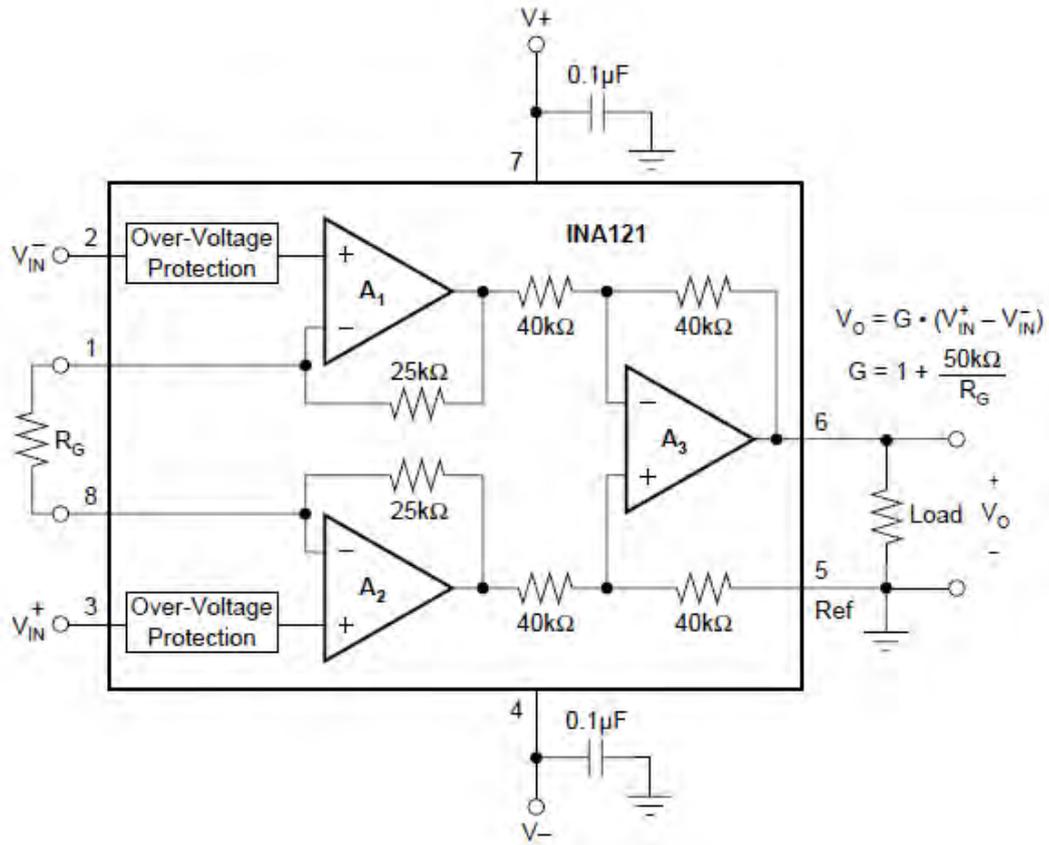
Figure 22: *Circuit diagram for the operational amplifiers built using the INA121 integrated circuit. Diagram found in the datasheet for the INA121 chip [68].*

stable water level without disturbing the water to much when pumping it out either. Perfusion happens at an approximate speed of $1.6ml/min$. With a chamber with a volume of $4ml$ this means that the chamber is filled in around $2.5min$. A Gilson Minipuls 3 peristaltic pump is used for the perfusion. The actual nerve chamber described above is mounted on an elevation in the middle of the surrounding chamber. Room is left around the elevation for water (and ice to lower the temperature). An air pump of the kind normally used for aquariums (Marina 50 in the present case) bought from a local pet shop is used to maintain some circulation in the cooling water providing as homogeneous a temperature in the water as possible. A polyimide thermofoil heating element from Minco was placed in the cooling water and connected to a power supply. Temperature was measured in both ends of the nerve chamber using a Physitemp BAT-10.

Monopolar recordings were made using a silver electrode enclosed in a fine glass pipette of about a couple of micrometres in tip diameter. The signals were measured in reference to the surrounding liquid. The grounding electrodes can be seen In figure 23 as the black wires in both ends of the nerve chamber. The recording electrode was connected to a head stage amplifier from Axon Instruments (HS-2A) with a gain of 0.1LU. The head stage and electrode were mounted on a micromanipulator from Sutter Instrument Co (MP-285) allowing precise spatial control of the electrode. The head stage was connected to an Axon Instruments Axoclamp 2B amplifier, which was then connected to the Cyberamp 380, and through the Digidata 1440 AD converter to the computer. Recordings were again made using the software Clampex 10.2, while signals were simultaneously monitored on an oscilloscope. All data from all experiments were analysed using Matlab R2015b numerical programming software.

Stimulation electrodes were made using two glass tubes normally used for pulling pipettes for recording electrodes. A piece of the same wire used for the electrode array in the small chamber used in collision experiments was inserted into and glued in place in the glass tubes. The two tubes were placed immediately next to each other making for a distance between the two poles of a couple of millimetres. The stimulation electrode was then connected to a WPI Stimulus Isolator A 365. Bipolar stimulation was used. Two pulses of opposite polarity of $100\mu s$ each in duration were sent with an interval of $300\mu s$. This was done in order minimise leak from stimulation electrode to ground of the recording electrode thus shifting the signal, as well as minimising effects of the capacitive coupling between stimulation and recording electrodes resulting in a large *capacitive tale* on the stimulus artefact. Stimulation procedures and programs were programmed using a Master-8 stimulator from A.M.P.I. Stimulation frequency in all experiments was $1Hz$.

In temperature experiments the whole nerve cord was placed on top of a small piece of acrylic glass, which was placed in the middle of the nerve chamber. The cord was then pinned down in the Sylgard using needles in the small pieces of muscle tissue left under preparation. That the cord was elevated slightly, made it easier to control the water level around it. The water level was kept so that the cord was just bathed in liquid, but only just. This significantly decreased noise in recordings in comparison to measurements, where the electrode was submerged deeper in the liquid, but still allowed for the liquid to cool the cord. The cord was then lid from below using an Olympus Highlight 2000 cold light source. This made it possible to actually see the axons under a regular microscope.

In anaesthetic experiments the cord was submerged completely in the liquid in the end, where it was stimulated, for better uptake of the added anaesthetics. The other end of the cord was elevated on a short piece of acrylic glass in a similar way as described above. Recordings were made from the cord immediately after it emerged from the liquid. This was done in order to minimize noise. Again the cord was lid from below. In both temperature and anaesthetic experiments the cord was stretched somewhat both laterally and longitudinally, and a bit of pressure was applied with the stimulation electrode in order to minimize movement of the cord. Movement could not completely be avoided, but it was significantly decreased by stretching the cord. In [21] a study of the effect of stretch on various parameters among others threshold is presented, and the threshold is found to be constant under stretching of the cord. In addition we are only interested in the *relative* threshold increase or decrease.

3.2 Results

Collision experiments

When everything was set up as described above, the cord was stimulated in one end, and the thresholds for both the MGF and the LGF were found. The measurements were made using stimulation well above the threshold, to make sure that APs were evoked each time. For measurements of the MGF alone there was obviously an upper limit to the stimulation strength, because APs in the LGF would then also be evoked at stronger stimulation. Preferably experiments were made with both the MGF and the LGF excited. This removes any doubt that the potentials could be excited in different axons – one in the MGF and one in the LGF – and thus merely pass by each other each, just driving along in their own respective lanes instead of colliding and penetrating. In figures 24 and 25 a typical result can be seen. Measurements were recorded from 7 worms in Aarhus plus 2 worms at the Niels Bohr Institute in Copenhagen. In [22] a similar but more extensive study of colliding pulses in earthworm is presented. The
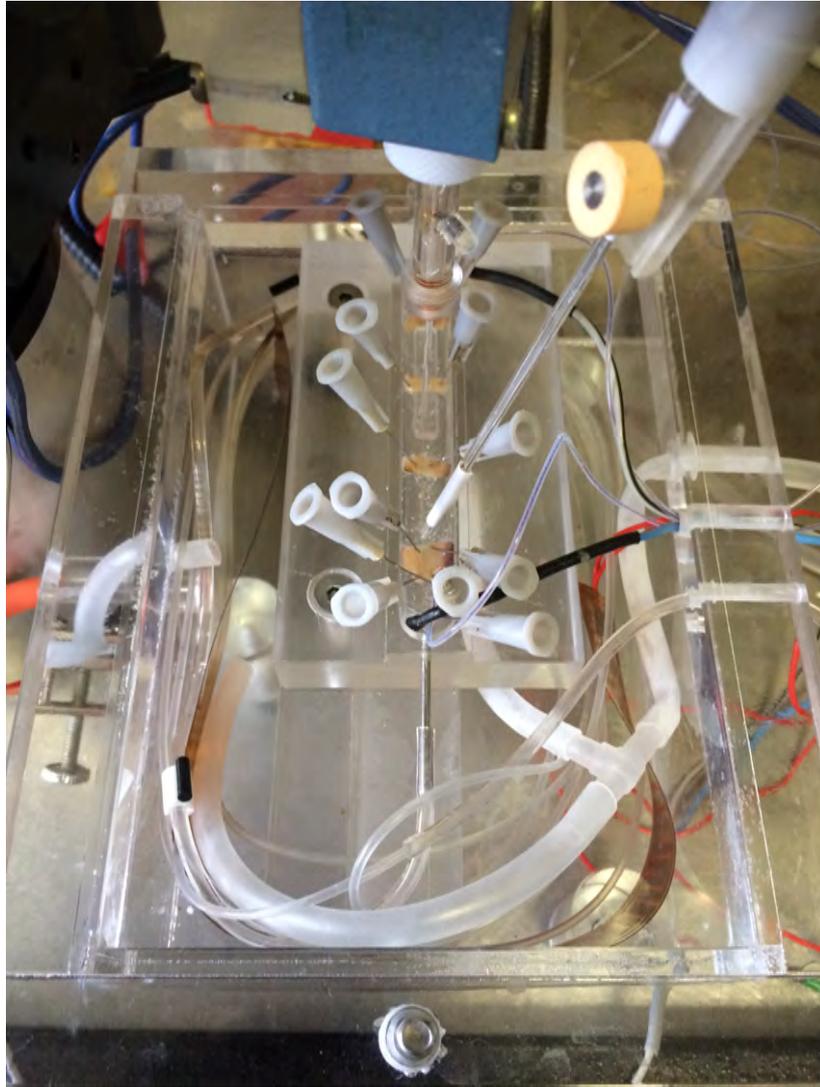
Figure 23: *The chamber used for temperature and anaesthetic experiments. The nerve chamber itself is mounted on a pedestal allowing water to be poured into the surrounding chamber. The plastic tubing through which the perfusion liquid is led is curled up in the surrounding chamber allowing the liquid to be cooled down or heated up by the water before entering the nerve chamber. A nerve is in the chamber and both stimulation (bottom) and recording (top) electrodes are seen. The specific set-up seen is for an anaesthetic experiment.*
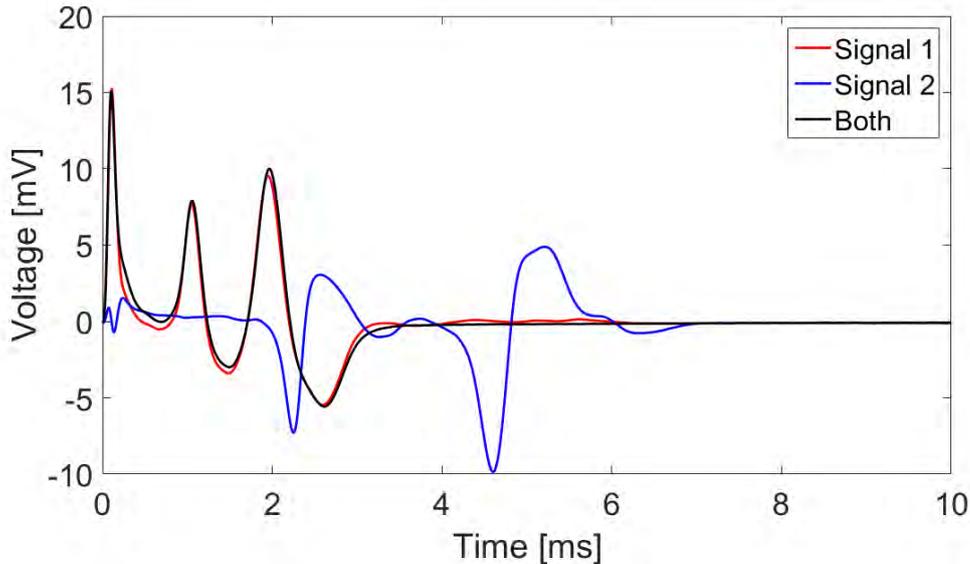
Figure 24: *Superposition of three recordings. Red line: signal elicited by stimulating in just one end. Blue line: signal evoked by stimulation in the opposite end. Black line: signal recorded when stimulating simultaneously in both ends. On all three recordings APs in both the MGF and the LGF are clearly seen. The black and red lines are almost identical, as would be expected, if the pulses annihilated on collision. The peak at 0 ms is a stimulation artefact and not part of the active response of the nerve. The distance from the red stimulator and the recording electrodes was 1 cm. The distance between the blue stimulator and the recording electrodes was 2.75 cm.*

authors found penetration in all samples consistent with the predictions of the soliton model. In some cases annihilation was found at first, but after adjusting the worm's position in relation to the electrodes, penetration was obtained. In all of the samples used in the present study several collision experiments were conducted for different electrode configurations. The recording electrode was always placed about two thirds of the way between the stimulation electrodes. Because of the fairly drastic diameter changes of the LGF as mentioned earlier, the conduction velocity in the LGF depends on position. This has to be kept in mind when arranging the electrodes, as (for the case of the LGF at least) the recording electrodes could thus in fact be at the effective halfway mark even though not being placed at the actual halfway mark. In total 20 collision experiments were conducted in the lab in Aarhus. In three of these 20 penetration or possible penetration was observed. In figures 26 and 27 examples of this are shown. In figures 24 and 26 the individual recordings from stimulation in each end separately are shown as the red and blue lines. The black lines are the recordings of simultaneous stimulation in both ends. In figures 25 and 27 the recordings of simultaneous stimulation are shown as the red lines corresponding to the black lines In figures 24 and 26. The blue lines show the sum of the two individual recordings, and thus what would be expected, if the pulses were to penetrate each other perfectly. The lines shown on all these four figures as well as figures showing examples of raw data from temperature and anaesthetics experiments are averages of 10 individual traces taken immediately after one another.

Despite the simplicity of this experiment it is difficult to find articles describing collision studies. Tasaki published a paper in 1949, in which he claims that colliding pulses penetrate each other [61]. The article is, however, not very transparent, and the results not very clear. The lack of studies of this phenomenon is a bit surprising. The collision experiment is a very simple and
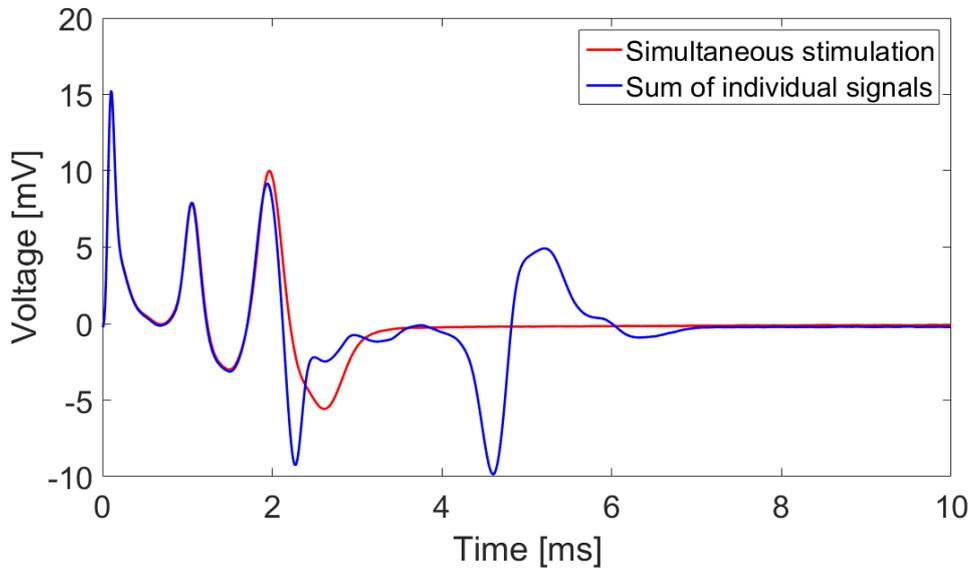
Figure 25: *Superposition of the signal recorded when the cord was stimulated in both ends simultaneously (black line In figure 24) and the sum of the two individual signals (red and blue line In figure 24 added together. The blue line is what one would expect to see, had the pulses penetrated each other. It is clearly seen that the slower of the two individual signals is missing.*
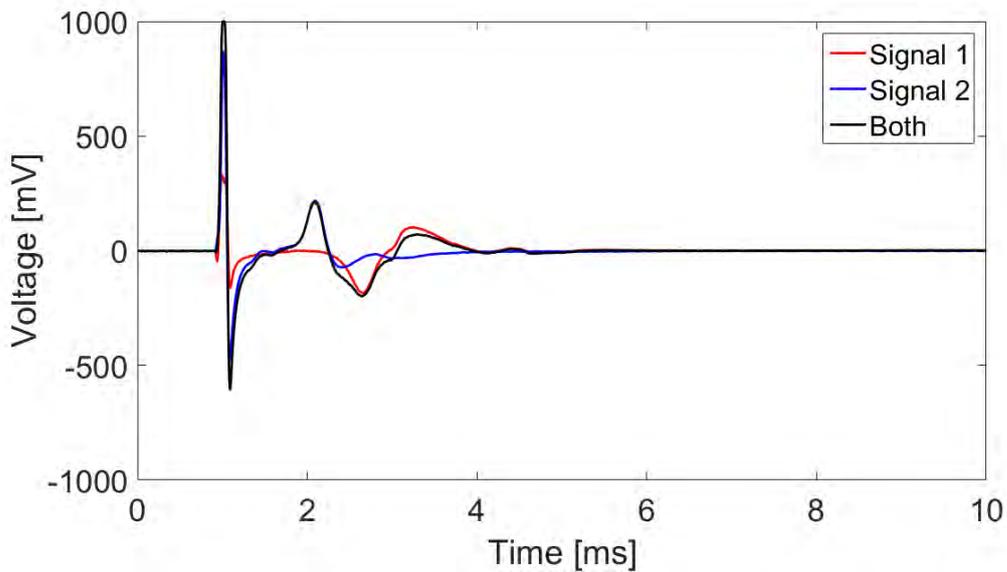

Figure 26: *Superposition of three recordings as In figure 24. The distance between the blue stimulator and the recording electrodes was 1 cm, and the distance between the red stimulator and the recording electrodes was 2.5 cm. Only response from the MGF is seen.*
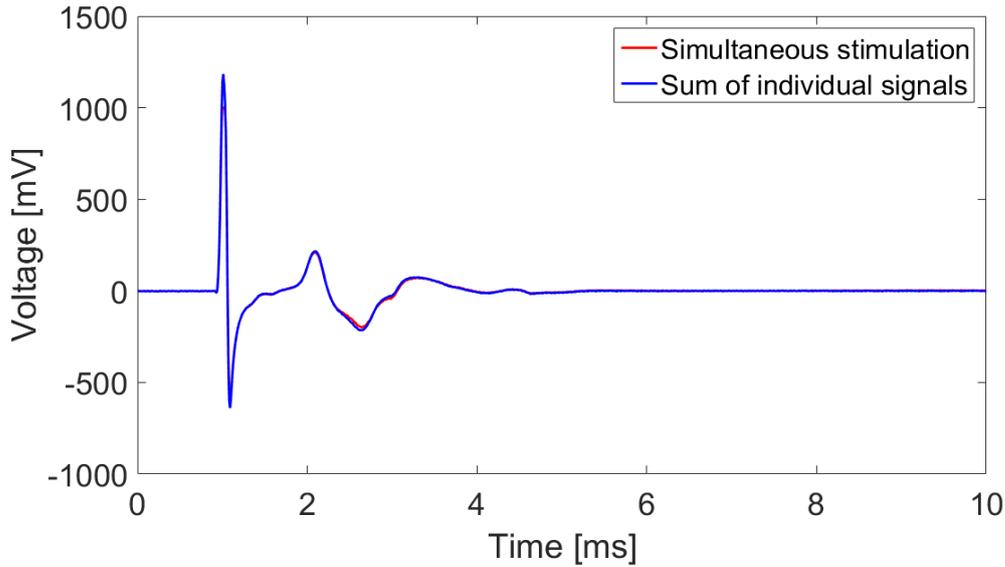
Figure 27: *Actual recorded signal for simultaneous stimulation in both ends of the cord (red line) and the sum of the two individual recordings (blue line) is shown. They are seen to be almost identical.*

efficient test of the HH-model versus the soliton model. The refractory period in the HH-model means that the AP is followed around by a wake of inexcitable membrane. When the pulses collide the APs would have to travel into the inexcitable wake of the other counterpropagating AP. This leads to annihilation of both pulses. In the soliton model the AP is essentially an acoustic wave travelling in the membrane. Mechanical waves, as we know, can simply pass by each other as they like, in most cases at least. Some solitary pulses may be reflected or annihilate on collision [14].

The results of the present study predominantly show annihilation of pulses, but in some cases penetration or indications of penetration was also observed as shown above. In all of the three recordings, where penetration (or signs of it) was seen, only one axon was excited. This leads to the suspicion that maybe the signal from one end was evoked in say the MGF and from the other end in the LGF. The pulses could thereby pass by each other without any problems and perfect penetration would be obtained. As the diameter of the LGF approaches that of the MGF towards the posterior region of the animal (see figure 18), the respective thresholds should also approach each other. Typically excitation thresholds decrease with increasing diameter. It is in fact seen that the thresholds can be very similar in the posterior end of the animal. For the case presented above In figures 26 and 27 it was not possible to evoke more than one potential in each direction. The cord could have been damaged during dissection. One could therefore imagine that only the MGF was intact in one end, and that only the LGF was intact in the other end thereby circumventing the problems of excitation thresholds and again leading to perfect penetration.

TEMPERATURE EXPERIMENTS

The temperature dependence of the stimulation threshold presents another easy test of the soliton model versus the HH-model. The prediction in the soliton model due to its thermodynamic origin is very clear. The picture is a little bit more cloudy in the HH-model. As mentioned earlier in the theory chapter, the HH-model is not thermodynamically based, and therefore explicit dependences on for example temperature for the excitation parameters have had to be inserted

into the theory later on. Several studies have been conducted on the temperature dependence of the excitation threshold. See for example [2][26][67]. The results are not exactly conclusive. Even though it seems to be the case more often than not, that the threshold increases with decreasing temperature, the studies do not agree upon how much or indeed just even *how* – the functional form that is. In some cases the threshold was found to be an increasing function of temperature, which at frst glance seems a fairly counterintuitive result. We will get back to a more detailed and stricter analysis of the thermal behaviour of excitation mechanisms in nerves, after we have presented the data from the present study. For now we can make a few notes based on an every-day, common sense kind of reasoning. One always has to wary of one's steps, however, when relying on intuition and common sense. A decrease in temperature should make it more difficult to overcome the free energy barrier needed for a conformational change of the ion channel proteins. This is not necessarily so since the free energy barrier depends on temperature as $\Delta G = \Delta H - T\Delta S$, but is not unreasonable to suggest that a decrease in temperature would make it more difficult to overcome the free energy barrier. In the extreme case at a low enough temperature the cytoplasm freezes, and in that case obviously no APs are possible, since the phenomenon relies on the diffusion of ions through the cytoplasm. While moving towards this extreme from a higher temperature, diffusion gets slower thus also slowing the ionic currents. It has been observed that the the temporal width of the AP increases with decreasing temperature as a result of this [38]. In our naivety we might also expect this to inhibit pulse excitation. Therefore based on these simple considerations, the most intuitive temperature dependence of the threshold in the HH-model seems to be a decreasing function that goes to infinity at the freezing point of the cytoplasm.

In figure 28 the results from the present study is presented. When the threshold had been measured for room temperature ($\sim 21.5°C$), ice and water were added to the surrounding chamber. Once the temperature had reached about $6°C$ and settled (or as low as it could be driven), the threshold was measured again. The heating element was then turned on, and the temperature raised slowly. The threshold was measured at intervals of approximately $2°C$. The temperature was measured in both ends of the nerve chamber. A temperature gradient down the length of the chamber could not be avoided, and as seen on the graph the difference from one end to the other was most pronounced at lower temperatures quite naturally. The two temperatures were then averaged. The temperature is that of the liquid perfusing through the nerve chamber and over the cord, but since the cord is very thin (a couple of millimetres in diameter), it is fair to assume that the cord equilibrates to the ambient temperature of the liquid fairly quickly. The absolute threshold value differs from sample to sample. It depends sensitively on a lot of low-practice parameters such as the exact placement of the stimulation electrode. The measurements were therefore not directly comparable and had to be normalised to room temperature meaning that threshold at room temperature is one. Measurements were recorded from 6 worms. Plotted In figure 28 is the measurements from both the MGF and the LGF from all 6 worms. In figure 29 raw data from a temperature experiment is seen for measurements at three different temperatures (columns). Top row is subthreshold stimulation. Middle row is above MGF threshold, and the bottom is above both MGF and LGF thresholds.

A decreasing exponential function is found to fit data well. This fits well with the arguments presented a couple of paragraphs above. We will now briefly revisit the theory in order to better understand the thermal behaviour of the threshold.

The rate constants α and β in the HH-model were by Hodgkin and Huxley simply fitted to experimental data. They were not derived from some fundamental law of nature or underlying theoretical foundation. The expressions in equations 2.11,2.13, and 2.12 are purely empirical.
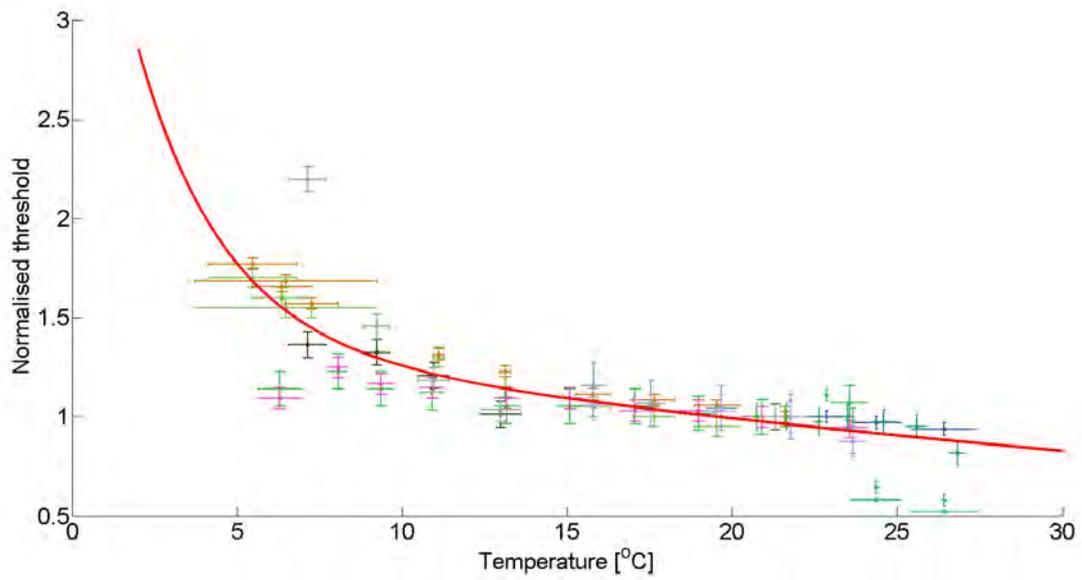
Figure 28: *Temperature dependence of the excitation threshold. The uncertainty on the temperature – directly related to the temperature gradient from one end of the nerve chamber to the other – is seen to be largest at very low temperatures. The vertical errorbars are based on the assessment that the threshold could be determined within $5\mu A$. The red line is an exponential function fitted to the data ($a = 1.773(1.639, 1.907)$, $b = -0.02903(-0.03407, -0.02399)$ with 95% confidence intervals).*
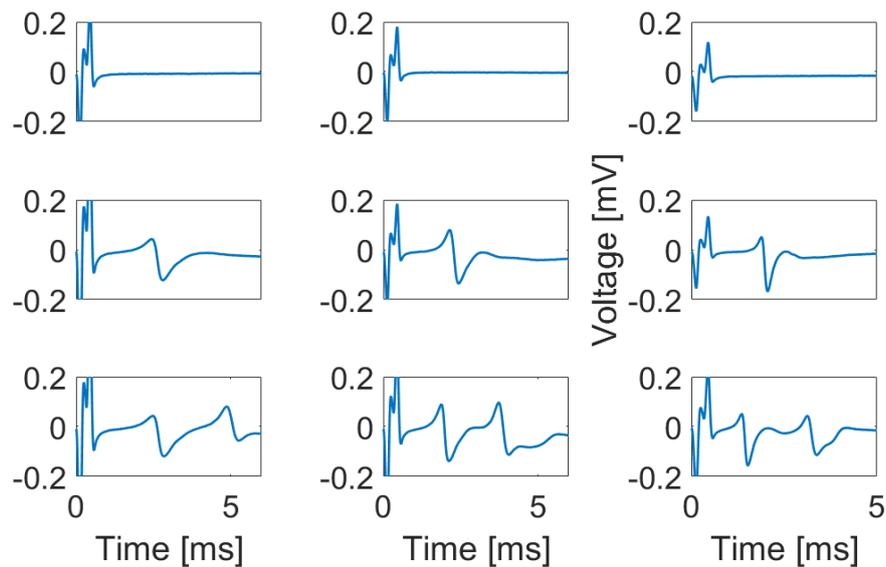

Figure 29: *Raw data from temperature experiment. Left column measured at 6.5°C. Top: $150\mu A$, middle: $290\mu A$, bottom: $300\mu A$. Middle column measured at 13.1°C. Top: $110\mu A$, middle: $210\mu A$, bottom: $215\mu A$. Right column measured at room temperature 21.6°C. Top: $95\mu A$, middle: $150\mu A$, bottom: $180\mu A$.*

This has to do with the fact that the idea of ion channel proteins, that today is generally accepted, was not clearly developed at that time. Hodgkin and Huxley said themselves [38] (see section *Strengths and shortcomings*) that

"...the success of the equations is no evidence in favour of the mechanism of permeability change that we tentatively had in mind when formulating them."

Hodgkin and Huxley performed voltage clamp experiments and measured the currents resulting from changes of the transmembrane potential. The idea of ion channel proteins was then formulated on that basis. Therefore a deductive argument about the functional form of the expressions for the transition rates α and β given in equations 2.11, 2.13, and **??** could not be expected until a welldefined idea of the actual mechanism itself had been formulated. Given the idea of ion channel proteins it makes sense to try to derive expressions for α and β from a thermodynamic jumping off point. This has been done, and the result has quite aptly been named *the thermodynamic Hodgkin Huxley model*. See for example [36][10][64][9][11].

The idea is that the channels are either open or closed, and the transition between the closed and the open state is associated with overcoming a free energy barrier. This is the simplest picture of an ion channel – either it is open, or it is closed. The picture can be refined by inserting more states in between the closed and open states in a Markov chain manner. But for now let us consider the simple case of just two states.

$$\alpha(V) = \alpha_0 \exp\left(\frac{-\Delta G(V)}{RT}\right),$$
$$\beta(V) = \beta_0 \exp\left(\frac{-\Delta G(V)}{RT}\right). \tag{3.2}$$

The free energy is assumed to be a function of voltage and expanded into a Taylor series. Protein structure and protein folding is immensely complicated and not at all understood yet, so the exact form of the free energy difference might be difficult to predict, and therefore a series expansion is applied. The free energy for the state i is thus

$$G_i = A_i + B_i V + C_i V^2 + ..., \tag{3.3}$$

where A_i, B_i, C_i, and so forth are constants defining the specific free energy for the given state. We insert this into equations 3.2, rewrite it slightly, and get

$$\alpha(V) = \alpha_0 \exp\left(\frac{-\left(a_1 + b_1 V + c_1 V^2 + ...\right)}{RT}\right), \tag{3.4}$$
$$\beta(V) = \beta_0 \exp\left(\frac{-\left(a_2 + b_2 V + c_2 V^2 + ...\right)}{RT}\right),$$

where $a_i, b_i, c_i, ...$ are constants describing the difference in free energy between the two states for each term. If we only keep terms up to first order in the Taylor expansion of the free energy, we call the above equations the linear thermodynamic model, and if we include higher order terms as well, we call it the non-linear model. In figure 30 a comparison of the standard HH-model, the linear thermodynamic model, and the non-linear thermodynamic model is shown.

Even better fit to data can be achieved if a Markov chain is employed instead the binary *open-closed* description of the channels used above and throughout this paper. Now this is all very
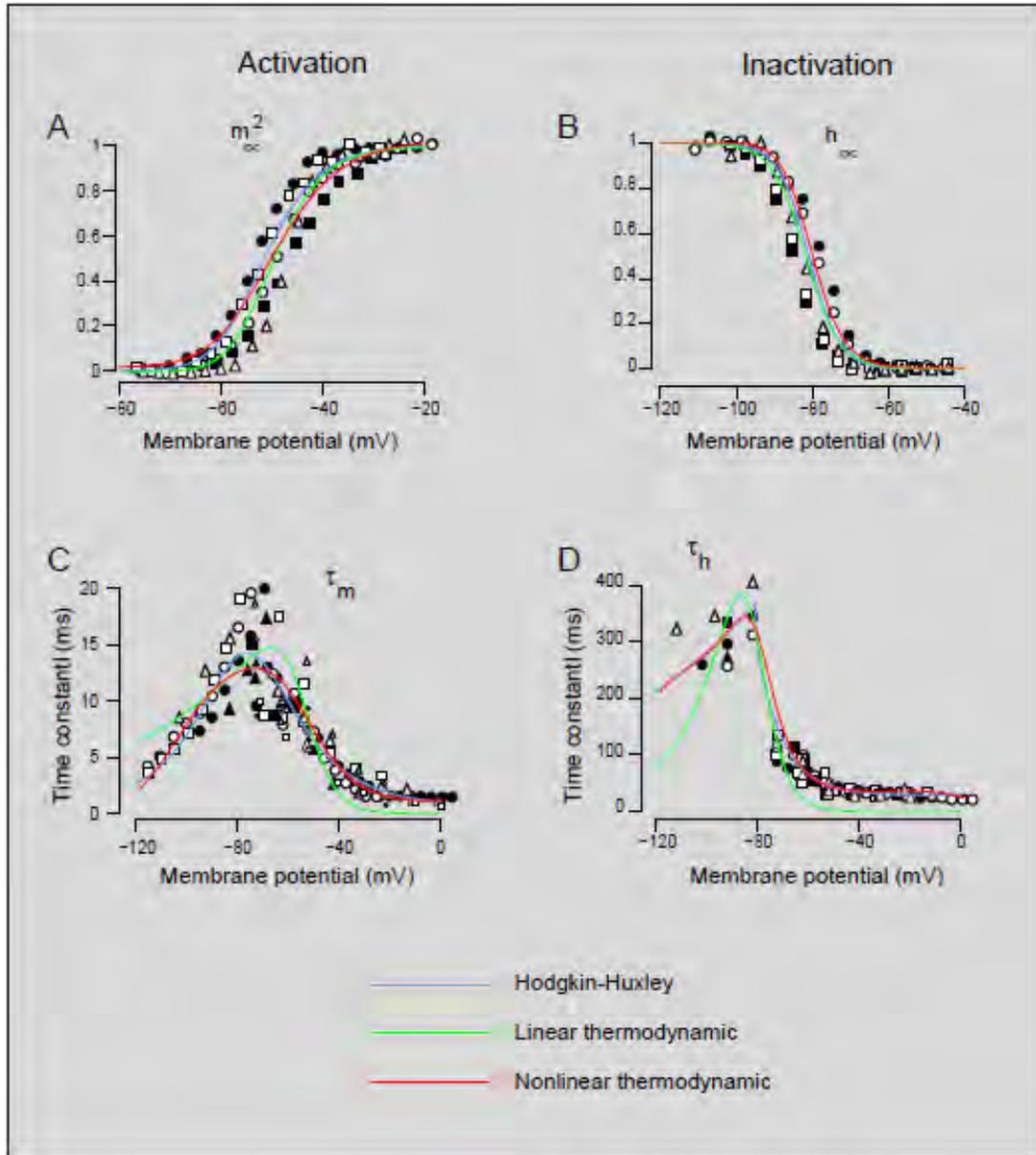
Figure 30: *Comparison of the HH-model, the linear thermodynamic model, and the non-linear thermodynamic model with experimental data for the T-current in thalamic relay neurons. Blue line: HH-model, green line: linear model, red line: non-linear model. Top left: steady state activation. Top right: steady state inactivation. Bottom left: activation time constant, and bottom right: inactivation time constant. Figure taken from [10].*

convincing at first glance, but the actual test of the thermodynamic HH-model is whether it can describe data that is not used for determining the parameters. If one for a given temperature finds values for the constants in the free energy expressions above can one then reproduce behaviour at another temperature using those same values for the parameters. In [17] this has been tested and it is found that it cannot. Despite that the thermodynamic HH-model is able to reproduce data very well it does not solve the problem it set out to solve. It does not tell us anything useful about the thermodynamics at play in the situation.

The threshold dependence on temperature must obviously be closely related to the temperature dependence of the conductances – and in particular the sodium conductance (through the rate constants). However it is not obvious in what way temperature changes the threshold in the above thermodynamic HH-models. In [16] theoretical calculations of the temperature dependence has been made in the HH-picture. The calculations are done by numerically solving an adapted version of equation 2.6 with modified versions of the equations 2.7.

$$C\frac{dV}{dt} = I - \eta I_i, \tag{3.5}$$
$$\frac{dm}{dt} = \phi\left((1-m)\,\alpha_m - m\beta_m\right), etc.$$

where I_i simply indicates the ionic current. The temperature dependence is hidden in the two new Greek letters η and ϕ introduced in the above equations. It is reasonable to assume that temperature might affect how the conductances change. This assumption is the same as made in deriving the thermodynamic HH-models above. We will only now implement it mathematically in a slightly different manner by simply multiplying the rates of change of the gating variables m, n, h with a factor of

$$\phi = 3^{(T-6.3)/10}. \tag{3.6}$$

Here 6.3 is the temperature at which Hodgkin and Huxley performed their voltage clamp experiments. The exact form of the expression above means that the gating varibles m, h, and n each have a Q_{10}-factor of 3. The Q_{10}-factor measures how much a parameter is changed by raising the temperature by 10 degrees. It was found experimentally that the conductances of sodium and potassium change linearly with temperature with about 15% of their value at $15°C$ per degree [16]. In the same study significantly larger conductances than those found by Hodgkin and Huxley were found (about 4 times greater) at the same temperature. These two effects are included in the HH-equations by multiplying all of the conductances, or equivalently the total ionic current, by

$$\eta = A\left(1 + B\left(T - 6.3\right)\right). \tag{3.7}$$

Here A represents the degree to which the conductances differ from those measured by Hodgkin and Huxley at the same temperatures. B determines the rate of change of conductances with temperature. In figure 31 numerical solutions of these equations can be seen. The apparent U-shape that the threshold takes as a function of temperature might seem a bit surprising.

The interpretation is all to do with the interplay between, and relative sizes of, the time constants for the processes involved in evoking an AP. At low temperatures the time constants τ_m, τ_h, and τ_n are all large. They decrease with temperature. This makes intuitive sense, but we also see that in the thermodynamic HH-model α and β depend on temperature as $\exp(-1/T)$. Inserting this into τ gives us a decreasing function of temperature. At low temperatures τ_m, τ_h,

20

14

I
$(\mu\,amp/cm^2)$

10

A = 4

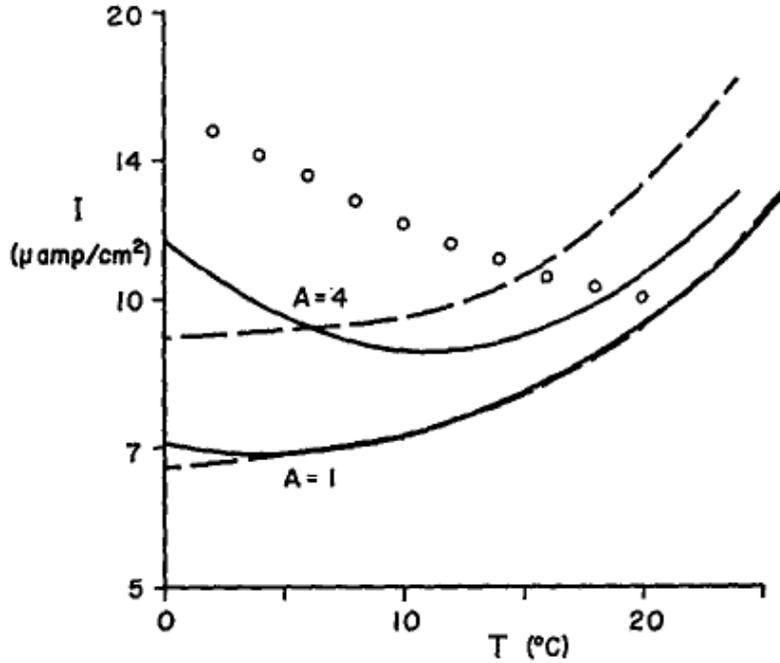7

A = 1

5

0   10   20

T (°C)

Figure 31: *Threshold-temperature relation for stimulus of duration 1 ms. The solid lines are solutions for $B = 0$ and broken lines are solution for $B = 0.061$ corresponding the change of 15% of the value at $15°C$ as mentioned in the text. The two uppermost lines (dashed and fulldrawn) are for $A = 4$ and the two below are for $A = 1$. The dots are experimental results found by Sjodin and Mullins 1958. Figure taken from [16].*

and τ_h are all large compared to the membrane capacitor time constant τ_{RC}. The time constant τ_m for sodium channel activation is smaller than τ_h and τ_n. This means that as temperature increases, the effect of the decrease of the time constants will appear first for τ_m, as it becomes comparable to τ_{RC} before the other two. τ_m controls the temporal length scale of sodium channel activation – uptroke of an action potential. The faster the activation of sodium channels the less stimulus necessary to evoke APs. This explains half of the U-shape curve – the left half with negative slope. For larger temperatures τ_h and τ_n for sodium channel inactivation and potassium channel activation respectively become so small that these processes begin to play a role in excitation as well. Additionally for larger temperatures τ_m becomes so small in comparison to τ_{RC} that the effect of increasing temperature saturates, and the decrease in τ_h and τ_n become more significant than the further decrease in τ_m. This leads to the right half of the U with positive slope.

The effect is also found to be a function of stimulus duration [16]. It is known that the threshold value generally depends of duration. For shorter stimulus duration the threshold is high and there is a minimum duration, below which you can stimulate as furiously as you want, all to no effect, and inversely there is a minimum threshold, you need to surpass, no matter how long the duration of the stimulus. This minimum threshold for infinite stimulation duration – step function stimulus – is called the rheobase. The rheobase is found theoretically to be a monotonically increasing function of temperature. This is the same behaviour as predicted by the soliton model. The U-shape found for stimulus of limited duration and the dependence on stimulus duration of the curve could explain the seemingly contradictory results found in the literature for threshold-temperature experiments.

The modified HH-equations could in principle be solved for the present case to see how well

they would describe the data. Values for α, β, A, and B would, however, be necessary for the earthworm axons. Alternatively these parameters could be found through numerically and iteratively solving the modified HH-equations for different values. This would probably be quite time consuming and has not been done for the present paper. Preliminary computations indicate that a very high value of A would be necessary to account for the present data. As illustrated In figure 31 the effect of increasing A is to shift the minimum of the curve upwards and to the right. The turning point for Sjodin and Mullins data (dots on the graph) is to be found (if it exists) far to the right of the theoretical curves. The preliminary computations were made with the expressions for α and β found by Hodgkin and Huxley for the squid giant axon (equations 2.11, 2.12, and 2.13). The above discussion of the threshold-temperature relation in the HH-model tells us that a qualitative agreement between the data and the predictions from the HH-model is possible – neither a qualitative nor quantitative agreement has concretely been demonstrated for the present data though. The observed behaviour is however in direct conflict with the predictions made by the soliton model. The *threshold* in the soliton model is related to how far we are from the melting/freezing temperature of the membrane. By lowering the temperature we approach this transition, and therefore the threshold should be lowered. Furthermore when we have ventured below the phase transition, it should be impossible to evoke APs. Measurements were also made from a worm which had been kept at about $35 - 40°C$ for about a month, but it showed no differences in the temperature dependence of the threshold. The threshold-temperature relation in the soliton model is thus a linearly increasing function.

ANAESTHETICS EXPERIMENTS

As mentioned the mechanism of anaesthetic drugs is still up for debate, at least for the case of general anaesthesia. Local anaesthetic action is generally agreed to be linked to binding of the anaesthetic drug to specific targets on the sodium channel proteins. Below results are shown and discussed for the dependence of threshold on anaesthetic concentration for both a local anaesthetic drug – lidocaine – and a general anaesthetic drug – pentobarbital.

First the threshold was determined in the absence of anaesthetics. Then anaesthetic was added to the Ringer's solution flowing through the nerve chamber. After addition the drug was given time to take effect – 15 minutes. The perfusion speed of the set-up was $1.6ml/min$. Given the volume of the nerve chamber of $4ml$ the liquid in the chamber is completely replaced after about $2.5min$. It takes just under 3 minutes for the liquid to reach the chamber. This means that the effective equilibration period is 12 minutes, and during those 12 minutes the liquid is completely replaced just under 5 times. After the equilibration period the threshold was measured again, and more anaesthetic was subsequently added. The concentration was raised in equidistant steps of 0.1mM for lidocaine and 0.2mM for pentobarbital (in some cases measurements were recorded at concentrations in increments of 0.1mM). The threshold increase was measured for ranges of concentrations (in the Ringer's solution) of 0.1 mM to 0.6 mM for lidocaine and 0.2 mM to 0.8 mM for pentobarbital. No higher concentrations were used in part due to loss of signals and in part due to time considerations. With 15 minutes in between measurements plus time for dissection and miscellaneous preparations it was not always practically possible to reach higher concentrations.

LIDOCAINE

In figure 32 results for lidocaine are seen. Measurements were recorded from 7 worms. As in the temperature experiments the thresholds were not the same in the different worms, since it depends
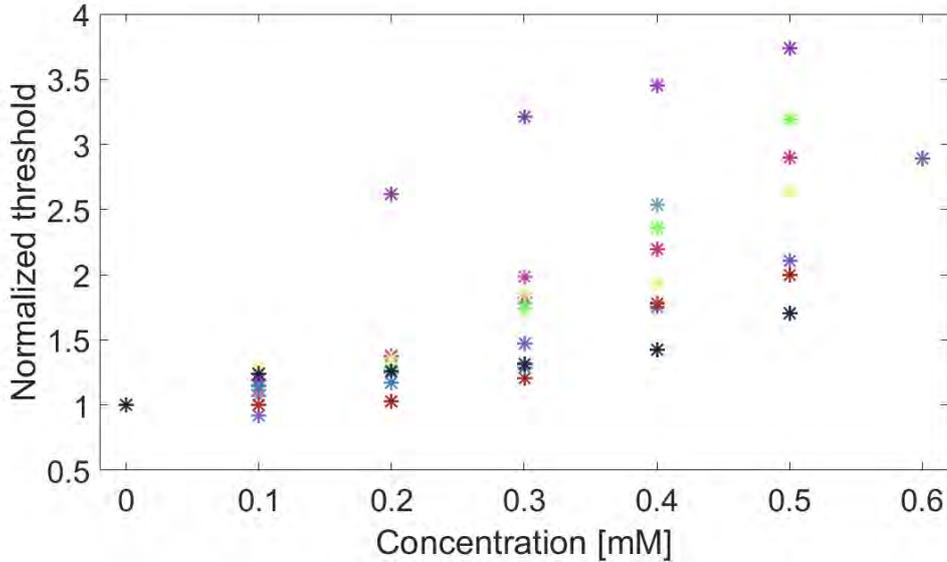
Figure 32: *Measurements of the excitation threshold as a function of the concentration of lidocaine in the Ringer's solution. Thresholds are normalized to the value measured in the absence of anaesthetic. The colors indicate recordings from different axons. Both results for the LGF and the MGF are plotted.*

strongly on where the stimulation electrode is placed in relation to the cord. The thresholds were therefore normalized such that the threshold measured in the absence of anaesthetic in the Ringer's solution is 1. The increase in threshold in the different worms can then be compared. It was assessed that the threshold could generally be determined within $5\mu A$. This uncertainty is not plotted as errorbars, since they would only add confusion. The concentration in figure 32 is the concentration in the Ringer's solution and not in the nerve cord itself.

In figure 33 examples of raw data for the lidocaine experiment is shown. It is seen that the pulses do not exactly line up. There was a slight jitter in position of the pulses just around the threshold, but already just above the threshold the signals would settle at a from there on fixed position. A possible explanation for this could be linked to the existence of the dorsal nodes. If these play a central role in the excitation of the signal stimulus just at the threshold could be enough to excite a node closer to the center of the stimulation electrode. When the stimulus is increased it could then maybe be strong enough to excite a node just at the edge of the electric field of the stimulation electrode thus reducing the latency in jumps corresponding to the distance between nodes. As the distances between the nodes are of the order of a few hundred micrometres the jumps in temporal position would with the conduction speeds found here (and reported in other studies) be quite small – tens or hundreds of microseconds. Another probably more reasonable explanation is that the cord could have moved slightly between measurements. It was found that movement could not be completely avoided but was greatly minimised by stretching the cord. The cord would at times move due to contractions in the still attached muscle tissue, but after the muscle tissue relaxed the cord would approximately return to where it was before.

Other parameters could have been interesting to measure as well such as the amplitude of the action potential, the latency and thereby the conduction velocity. Due to the fact that not all of the cord between stimulation and recording electrodes was submerged (as described in the materials and methods section), this was not possible. In [43] the amplitude of the compound action potential in the sciatic nerve of frogs before and after application of anaesthetics was
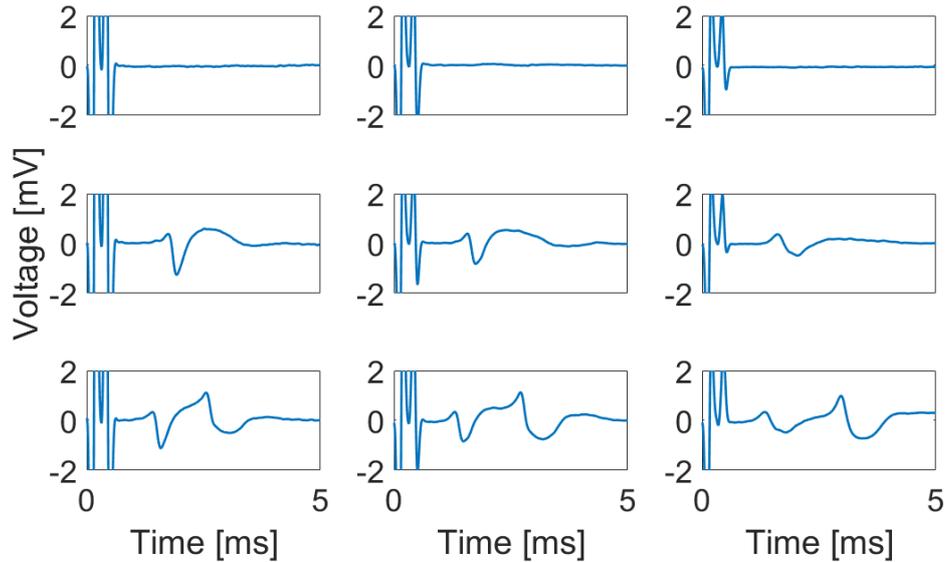
Figure 33: *Examples of raw data for experiments with lidocaine. Left column: without lidocaine. Top: $65\mu A$, middle: $69\mu A$, bottom: $103\mu A$. Middle column: $0.1mM$ lidocaine. Top: $65\mu A$, middle: $69\mu A$, bottom: $119\mu A$. Right column: $0.2mM$ lidocaine. Top: $69\mu A$, middle: $71\mu A$, bottom $133\mu A$. A slight jitter in the position of the AP was seen at stimulus just around the threshold. If the stimulus was increased only a few μA the signal would settle at a fixed position. To the left in all nine examples is seen the stimulus artefact from the biphasic stimulus.*

studied. With the experimental set-up used in [43], it was not possible to control the concentration of the substances used. This was a key concern when designing the set-up for the experiments presented in the present paper. It is difficult to measure the amplitude reliably using the chamber seen In figure 23. In [43] a chamber similar to the one seen In figure 21 (used for the collision experiments) was used. In [48] a similar study as [43] is presented, but conducted on humans. The amplitude-stimulus curves found in the two articles are qualitatively similar, but the interpretation of the data is quite different in the two cases. In the latter a great increase in threshold is observed as well, which cannot fully be explained by the HH-model. The thing of primary interest in the present study was therefore the threshold increase.

In figure 34 the measurements seen In figure 32 have been averaged and plotted as a function of the concentration. This time the concentrations have been multiplied by the n-octanol:water partition coefficient for lidocaine of 43 [25]. In the ideal case this should then be the concentration in the membrane. Things in the real world are obviously not as in the ideal case, however. The drug has to diffuse through the surrounding cord and into the membrane, and obviously the membrane is not pure n-alcohol nor the Ringer's solution pure water so the membrane:Ringer's solution partition coefficient might deviate somewhat from the value of 43 used here.

Lidocaine is a local anaesthetic. Local anaesthetics are generally believed to act primarily via binding with sodium channel proteins thereby disabling them or at least inhibiting their action. Local anaesthetics are not as diverse chemically speaking as general anaesthetics are. General anaesthetics comprise all sorts of different types of substances, but local anaesthetic drugs fit neatly into a particular chemical template. They consist of an aromatic ring linked to a terminal amine via an ester or amide chain as shown In figure 35. The first local anaesthetic substance to be discovered was cocaine. Cocaine is extracted from the leafs of the coca plant found predominantly in South America. It was commonplace among the Incas to chew coca leafs for refreshment while
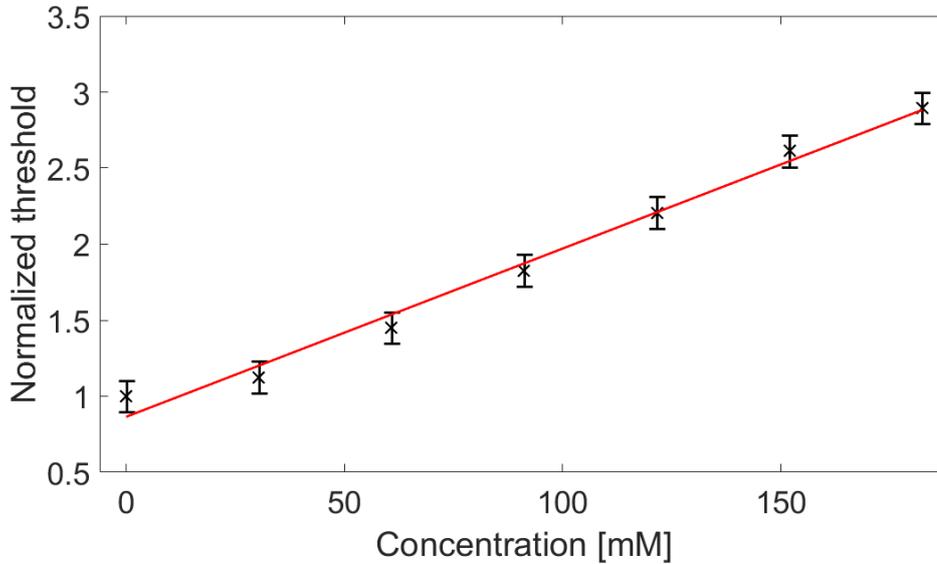
Figure 34: *Averaged results for measurements from 7 worms. The individual measurements are shown In figure 32. The concentration is the bulk concentration in the Ringer's solution multiplied by a factor of 43 – the n-octanol:water partition coefficient for lidocaine [25]. This is done to get an estimate of the concentration in the membrane.*

working. The drug was extracted in the 19th century, and it was then put to use in medicine among other places. Sigmund Freud famous for his psychoanalysis was an avid proponent for the use of cocaine in medical practice. Him and his colleagues performed experiments on the corneas of both frogs and themselves numbing the cornea with cocaine and poking at it with needles to see when reflex reactions to the touch ceased. He wrote thus in a letter to his sister-in-law

"The cocaine business has indeed brought me much honor, but the lion's share to others."

Cocaine is still very much in use today, but not in the medical services. Modern local anaesthetics are however predominantly cocaine derivatives for example lidocaine, which was synthesised in the mid 20th century. The cocaine inheritance can be found in many substances in the *-caine* ending of their names. The chemical homogeneity found in the family of local anaesthetics makes it easier to believe that the underlying mechanism of action is to do with binding to specific targets.

The results seen In figure 34 show a nice linear dependence on the anaesthetic concentration. The soliton model predicts a linear increase in excitation threshold. It has long been known that general anaesthetics affect the membrane, and lipid theories of general anaesthetic action has been proposed, and for a long time it was the mainstream view as has been discussed already. In [25] local anaesthetics (for example lidocaine) are seen to shift the phase transition of the membrane in the same manner as general anaesthetics, and it is proposed that the two types of drugs share a common underlying mechanism. The affect of anaesthesia in the soliton model is due to the depression of the freezing point. This is a linear function of the concentration. In addition the signals should never disappear either. No matter how anaesthetised a nerve might be, stronger stimulus should restore the signal, since the transition is just shifted. A slight distortion of the transition profile is however also observed [25]. This will obviously also affect how the signal behaves, but still it should be possible to restore the signal with sufficient stimulus.
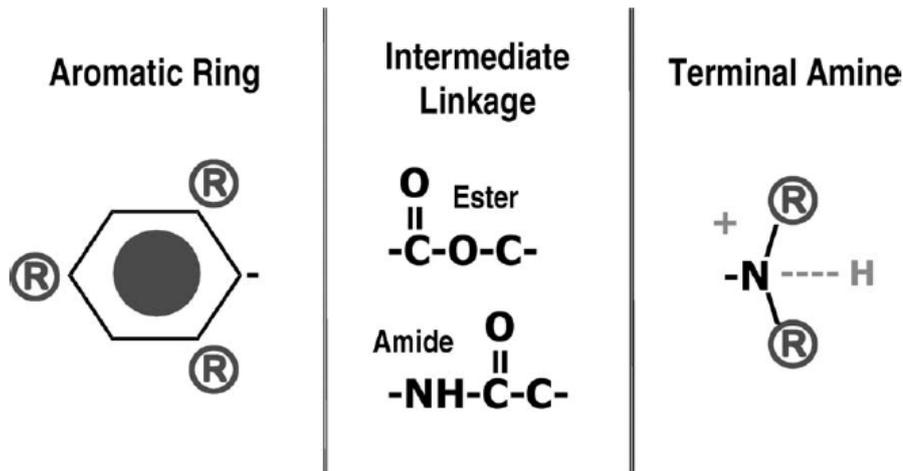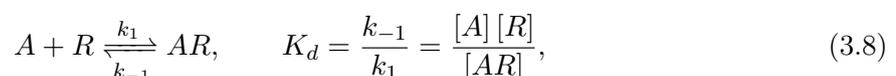
Figure 35: *The chemical structure of local anaesthetics. An aromatic ring and a terminal amine linked by either an ester or an amine chain. Figure taken from [7]*

Again the predictions of the HH-model are a little more confuse. In the soliton model the drug affects the nerve in a very general manner, but if the drugs bind to specific targets thereby disabling or altering the response of individual ion channels, the overall response is a little more complicated to predict. In myelinated axons the density of sodium channels at the active spots on the axons – the nodes of Ranvier in for example human nerves and the dorsal nodes in the earthworm MGF – is very high and significantly higher than necessary for eliciting action potentials. Again proceeding with caution we apply our intuition and make a rough sketch of the possible behaviour of the threshold increase as a function of concentration. When anaesthetising the axon the drug can crudely be said to slowly *take out* sodium channels, but for low concentrations there are still many channels still working, so the threshold is probably not affected that much. This picture of the drug *taking out* or *closing* channels is obviously hugely simplified. In none of the different theories for local anaesthetic action are the anaesthetics thought to act simply by closing channels. They influence gating kinetics in more subtle and sophisticated ways. They also affect various channels and do not bind solely to sodium channels. Local anaesthetics are just one class of channel-blocking chemicals. We encountered TTX earlier in this paper for instance. TTX is not an anaesthetic, but it does affect sodium channels. There is a range of different *channel-blockers*, and they all work in slightly different ways. Local anaesthetics do tend to favour the closing of gates however, so for illustrative purposes we will for now imagine the anaesthetic action being thus. For higher and higher concentrations the fraction of channels being *taken out* out of the total number of channels still working with each step-increase in concentration is also higher and higher. In other words the loss of each individual channel becomes more and more severe, when there are fewer and fewer ones left. One would therefore naively expect an increasing function with a positive curvature. The above hadwaving *argument* assumes a linear relationship between the concentration of the drug and the number of disabled sodium channels. This is not the case (see figure 36).

We can describe the reaction of an anaesthetic drug (A) binding to a receptor (R) by the rate constants for binding (k_1) and unbinding (k_{-1})

$$A + R \underset{k_{-1}}{\overset{k_1}{\rightleftharpoons}} AR, \qquad K_d = \frac{k_{-1}}{k_1} = \frac{[A]\,[R]}{[AR]}, \tag{3.8}$$
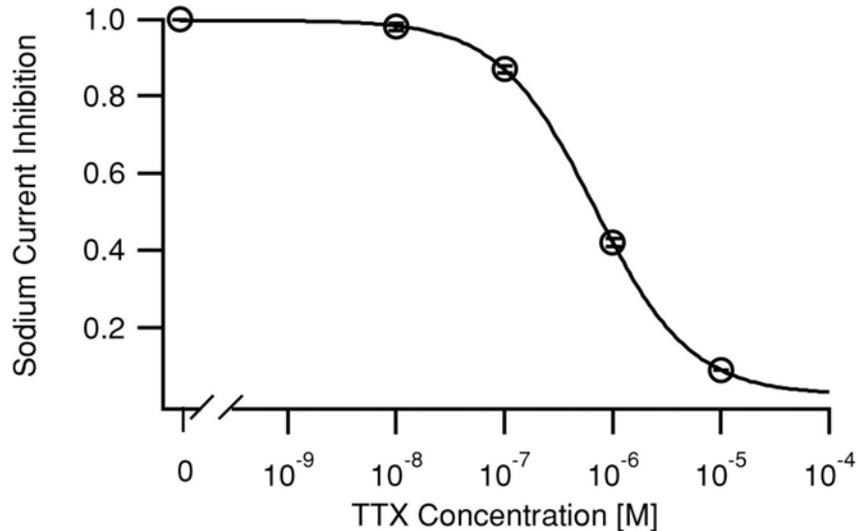
57

Figure 36: *Fraction of maximal sodium conductance as a function of concentration of TTX. Figure taken from [47].*

where K_d is the dissociation constant. The fraction of receptors blocked by anaesthetics out of all the receptors is

$$y = \frac{[AR]}{[AR] + [R]} = \frac{[A]}{[A] + K_d} = \frac{1}{1 + K_d/[A]}.$$ (3.9)

The above equation is known as the Langmuir adsorption isotherm. It immediately leads to the following expression for the fraction of free receptors

$$1 - y = \frac{1}{1 + [A]/K_d}.$$ (3.10)

The fraction of receptors not closed by the anaesthetic drug directly translates into a fraction of the maximal sodium conductance. This can be seen In figure 36. Here the above equation is plotted along with actual measurements of the sodium conductance expressed as a fraction of the maximum conductance plotted as a function of concentration of TTX. This is a typical result from pharmacological studies of channel blockers. This behaviour is obviously not linear as in the handwaving argument above. As we see it is difficult to predict the behaviour of the threshold as a function of concentration. In principle if one assumes that the *only* effect of the anaesthetic drug is to *completely* close sodium channels one could solve the HH-equation for varying values of the maximal sodium conductance and find the concentration dependence by applying the above formula (3.10). Local anaesthetics do, however, not work in this simplified way and such an approach would be better suited for describing the effect of neurotoxins such as TTX which binds much more specifically to sodium channels, and even then it would probably still be a rough simplification.

The threshold is in general difficult to predict in the HH-model due to the fact that it does not explicitly appear in the model. In order to find it one has to solve the differential equations for varying stimulus and look for a sudden increase in response. The fact that the threshold does not explicitly appear in the equations is obviously intimately linked with the fact that it has only a somewhat opaque physiological explanation in the model. A certain potential has to be reached for the ion channel proteins to change their conformation but what extracellular stimulus

is necessary for this depends subtly on the conductances for various ions and the opening and closing dynamics of the gates.

Naturally there are only a finite number of sodium channels in a given node. This means that there is a natural upper limit for when action potentials can be evoked. When all channels are affected and incapable of opening, no APs are possible, since no sodium can enter the cell. Well before this situation arises, signals are lost, since less positive charge enters the cell over the duration of the stimulus. The amount of charge is not necessarily enough to charge the membrane to the threshold. This can be understood using a simplified model based on current-voltage curves as proposed by Denis Noble [53] [41].

In figure 37 is shown the two major components (sodium and potassium) of the total membrane current together with the combined current all as functions of membrane potential. This graph is based on the assumption that m (activation of sodium channels) changes with time much faster than both h and n (sodium inactivation and potassium activation respectively). If this assumption is made one can at each membrane potential equate m to its steady state value $m = m_\infty$, while h and n are held constant resulting in a linear current-voltage relation for the potassium current. This is what is plotted In figure 37. At the resting potential no net currents are running across the membrane – this is the leftmost intersection with the x-axis. As the membrane is depolarised by a stimulus, a positive current is generated driving charge out of the cell thus repolarising it. This happens until the second intersection with the x-axis – the threshold – is reached. There the slope of the curve is negative. This means that for depolarisations larger than the threshold, a negative current (into the cell) will be generated further depolarising the cell. This is the self-re-enforcing phenomenon that leads to the all-or-none behaviour of APs. When the third and rightmost intersection with the x-axis – the peak amplitude – is reached, the cell cannot be depolarised further (actually rather positively polarised). A higher membrane potential only leads to positive currents driving the potential down. Obviously h and n also change with time, and at higher voltages potassium channels are opened, and sodium channels are closed again. This raises the I-V curve for potassium, and decreases the sodium current, thus forcing the rightmost intersection towards the left. This time development of the I-V curve can be seen In figure 38.

When the potassium channels open, and the sodium channels close, the amplitude is forced down (towards the left), and the threshold is forced up (towards the right). At some point (as seen on the curve C In figure 38) there is no threshold anymore – that is no intersection with the x-axis besides at the resting potential. This illustrates the refractory period very elegantly. This, albeit simplified, model serves as a great, intuitive illustration of some of the defining traits of the AP. When anaesthetics enter the fray, the sodium conductance is changed, since fewer channels are able to contribute. This in a way corresponds to what happens when the channels start deactivating again after firing. The C curve In figure 38 is the combination of the sodium and potassium currents. Thus there can be a non-zero sodium conductance even if it is impossible to evoke APs – not all channels have to be blocked before the signals disappear. When the sodium conductance is decreased by the anaesthetic drug, the peak amplitude decreases, and the threshold increases. They thus move towards each other and typically meet at around the halfway mark. If still more anaesthetic is added, the threshold disappears, and no signals are found. For a typical neuron the resting potential is $-70mV$, the threshold potential is $-50mV$, and the peak of the overshoot is $30mV$. If the threshold and peak meet exactly half way, this results in a maximum threshold increase of a factor of 3. In [21] the resting potential, threshold potential, and the peak of the overshoot of the action potential in the earthworm medial giant axon were investigated. The found values are approximately $-71mV$, $-48mV$, and $22mV$ respectively. Applying the arguments above on this case gives us a maximal increase in threshold of about a
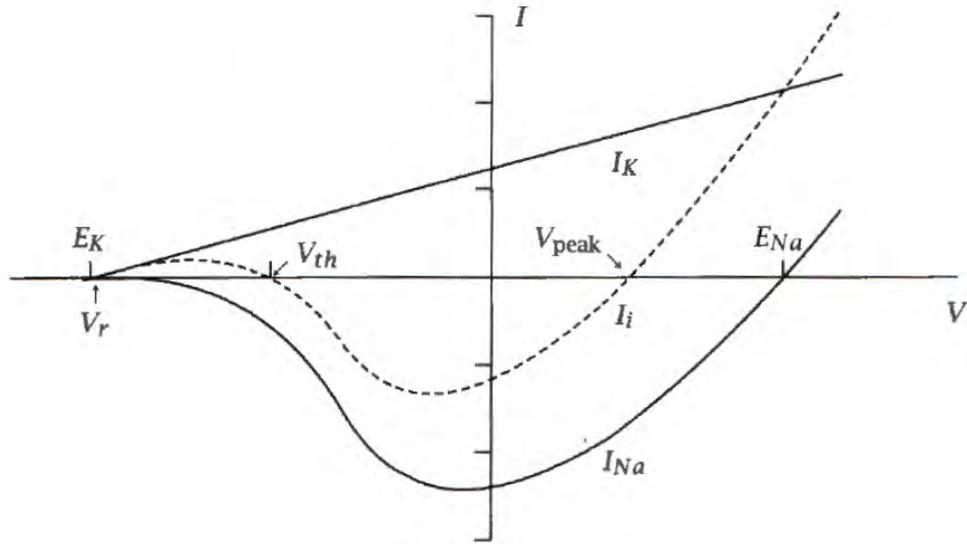
Figure 37: *I-V curves for the sodium and potassium components (full drawn lines) of the total current (dashed line). The three intersections of the dashed line with the x-axis indicate the resting potential, the threshold potential and the peak amplitude respectively from the left. Figure taken from [41]*
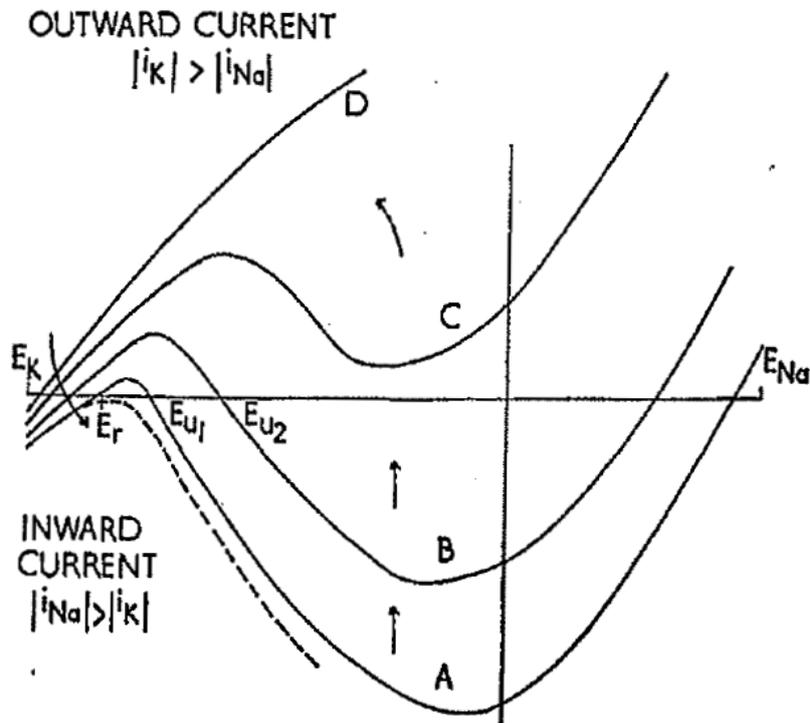

Figure 38: *I-V curves for the net membrane current of a neuron (as the dashed line In figure 37). The lines A,B,C, and D represent current-voltage relations at different times in the firing process. A represents the starting situation. When the membrane is depolarised the effects of potassium channel opening and sodium channel closing become important resulting in the upwards deflection of the I-V curve. At C and D the current is always positive (outwards) and thus no APs are possible. Figure taken from [53].*
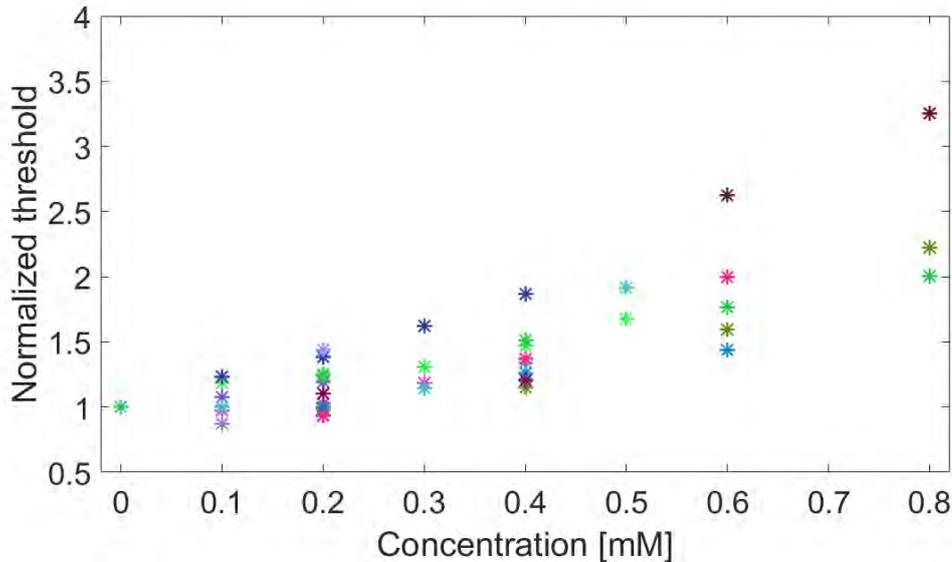
Figure 39: *Measurements of threshold for increasing concentration of pentobarbital in the Ringer's solution. Measurements have been normalised so that the starting threshold in the absence of any pentobarbital is set to one. Different colors indicate measurements from different axons. Measurements from both the MGF and the LGF are shown. The concentrations are in the Ringer's solution.*

factor 2.5.

PENTOBARBITAL

In the last section results for experiments with the local anaesthetic lidocaine were presented. In this section we will take a look at results for the general anaesthetic pentobarbital. We have referred to pentobarbital as a general anaesthetic up until now, but this is not completely true. Chemically speaking pentobarbtal belongs to the family of substances known as barbiturates. Barbiturates are derivatives of barbturic acid. Barbituric acid was synthesised by Adolf von Baeyer in 1864. There is a cute story attached to the name. Again as is the case with many of these stories the truth value of the story is probably questionable. The synthesis process involves condensation of the substance urea which is found in urine. The story goes that barbituric acid is called thus because it was synthesised from the urine of a local waitress called Barbara. Barbiturates such as pentobarbital affect the central nervous system. They have been used for a wide variety of purposes. They are *depressants*, or what might in more colloquial terms be known as *downers*, depressing stimulation in the central nervous system. The antonym for depressant is stimulant, or *upper*. An example of a stimulant is cocaine – the first known local anaesthetic. Barbiturates are today mainly used as anti-epileptics, though they have been used for other things such as sleeping pills or for anxiety treatment. Today they have been replaced by benzodiazepines for those purposes. We will discuss this link in a minute when discussing the mechanisms of barbiturates. In some American states pentobarbital is further used for both capital punishment and euthanasia of both humans and animals.

In figure 39 results are shown from experiments with pentobarbital. Again the thresholds are determined with $5\mu A$ uncertainties, and again these uncertainties are left out in the interest of clarity. The experiments were conducted in the exact same manner as the experments using lidocaine – the only difference being the drug. Measurements were recorded from 7 worms.
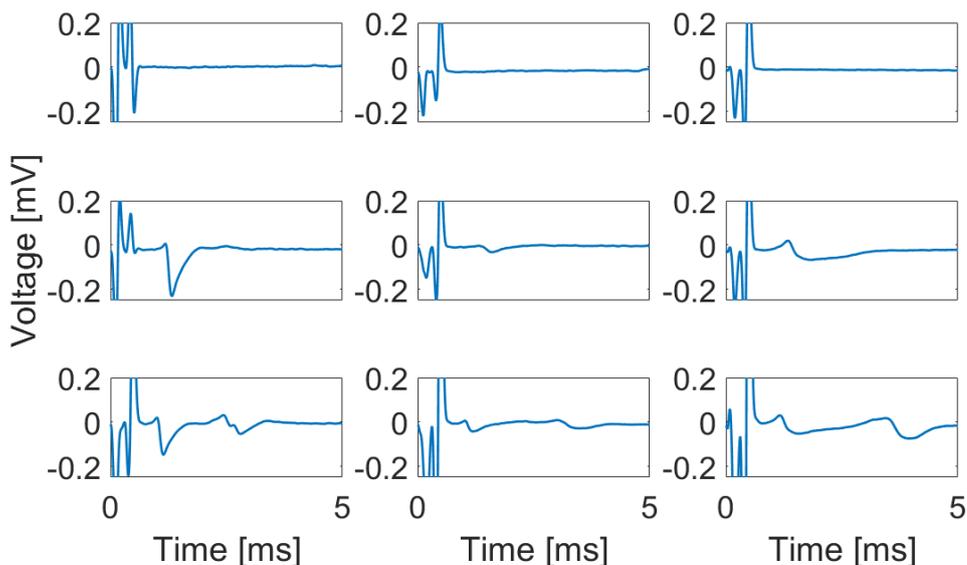
Figure 40: *Examples of raw data from an experiment with pentobarbital. Left column: no pentobarbital added to the Ringer's solution. Top: $55\mu A$, middle: $59\mu A$, bottom: $150\mu A$. Middle column: $0.2mM$. Top: $70\mu A$, middle: $74\mu A$, bottom: $208\mu A$. Right column: $0.4mM$. Top: $85\mu A$, middle: $87\mu A$, bottom: $280\mu A$. All curves are averages of 10 individual traces recorded back to back.*

A slightly slower increase in threshold is seen and slightly higher concentrations were used. Concentration was increased in steps of 0.2 mM (in most cases). In figure 40 is shown examples of raw data from an experiment.

Again the signals do not exactly line up. As was discussed in the last section this is probably due to movement of the cord. This fits with the observation that the signals line up increasingly better with decreasing temperature (confer figure 29).

In figure 41 the averages of the individual results shown In figure 39 is shown with respective uncertainties plotted as errorbars. A straight line is fitted to the data and is seen to agree well with the results. The concentrations In figure 41 have, as in the section above, been multiplied with the n-octanol:water partition coefficient of pentobarbital of 117 [25].

In [25] the mechanism of action of local anaesthetics and general anaesthetics including barbiturates is proposed to be the same. We have already touched upon arguments for and against this view and it will be further discussed later on. Before that discussion it is interesting to compare the results from the lidocaine experiments with the results from the pentopbarbital experiments. In figure 42 the results shown separately In figures 34 and 41 are shown together. The two substances show not completely identical but similar behaviour.

The mechanism of action of barbiturates on the nervous system is as the mechanism of general anaesthetics and many other things in neuroscience still not completely understood. As mentioned barbiturates exhibit many different effects on the nervous system – anticonvulsant and anxiolytic activity, sedation, hypnosis, general anaesthesia and in the end at too high dosages death. All barbiturates exhibit these effects. Furthermore they all show them in phases related to increasing doses [46]. This indicates that they act in a number of different ways. Several interactions have been suggested. Especially their effect on GABA-receptors has been of particular interest to researchers. Binding to GABA-receptors is believed to be one the major ways of interaction with the nervous system of barbiturates much like it has been theorised for the case
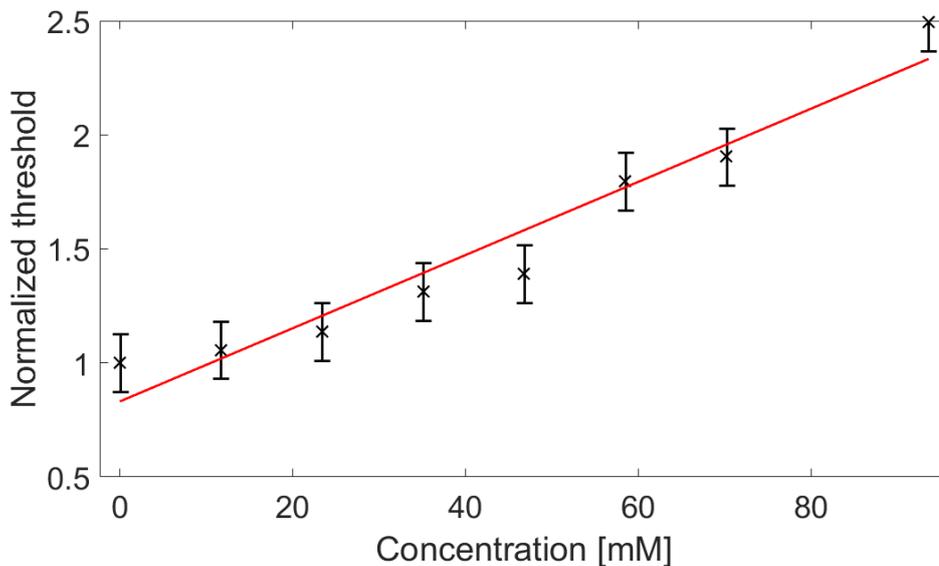
Figure 41: *Averages of results shown In figure 39. Concentrations have been multiplied by 117 – the n-octanol:water partition coefficient for pentobarbital.*

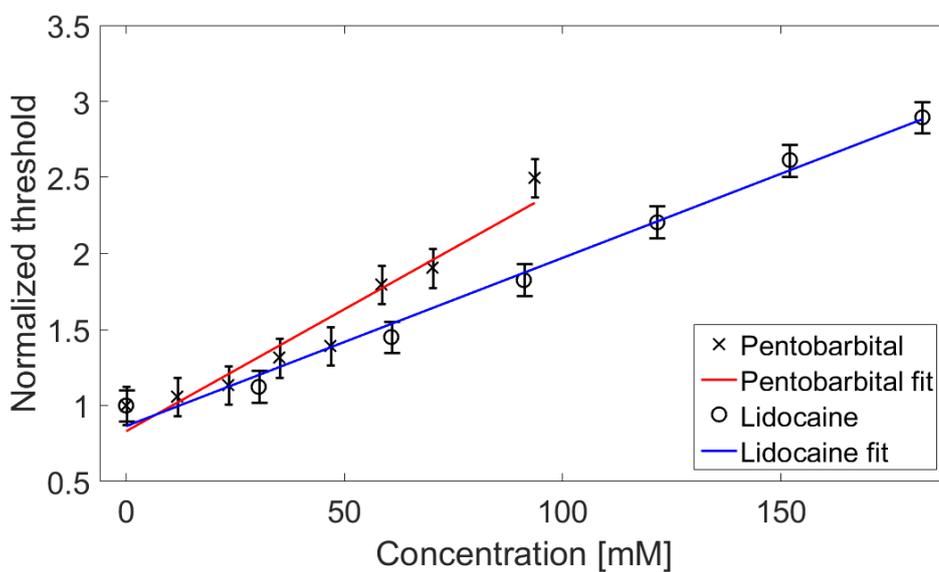Figure 42: *Results from lidocaine experiments and pentobarbital experiments plotted together. The results are the same that have been shown separately In figures 34 and 41. The concentration is thus both that of lidocaine (multiplied by the partition coefficient for lidocaine) for the blue line and that of pentobarbital (multiplied by the partition coefficient of pentobarbital) for the red line.*

of general anaesthetics. Another class of drugs that is believed to act as GABA receptor agonists are benzodiazepines. As mentioned above benzodiazepines have replaced barbiturates in most clinical treatments. Their similar effect makes sense if both classes of drugs act primarily by influencing GABA-receptors. The effect on GABA-receptors of barbiturates and bezondiazepines are not exactly similar and benzodiazepines have been found to be safer in clinical use hence the replacement. Barbiturates are also thought to influence glutamate receptors and a number of other ion channel proteins such as sodium, potassium, and calcium channels.

In figure 42 the two substances – lidocaine and pentobarbital – are seen to behave in a fairly similar manner, but these are just two substances. Barbiturates have been found to have a wide variety of psychoactive effects, but different barbiturates can also behave quite differently from each other. In the present case pentobarbital and lidocaine are found to behave in a similar manner on the earthworm giant axons for the range of concentrations used. It would be interesting to test other substances on the same preparation with the same experiments. Originally it was planned to use the local anaesthetic drug bupivacaine as well, but due to time constraints this was dropped.

These measurements of the threshold increase should be compared with calorimetric measurements of the heat capacity profiles for the concentrations used for a complete picture. In figure 43 this is shown.

The figure shows measurements of the heat capacity at constant pressure as a function of temperature for samples of the concentrations used in the anaesthetics experiments described above. It is clearly seen that the anaesthetics when added to the lipid membrane (in this case an artificial DPPC pure lipid membrane) alters the phase transition. The lidocaine sample shifted the transition temperature downwards with about $0.26°C$, while the pentobarbital sample broadened the transition (a small downwards shift is also seen in the pretransition and apparently a small upwards shift in the maintransition). It would obviously be ideal to measure the effect of the samples on the actual earthworm nerve membrane. Though it has been done [54], it is considerably difficult to extract samples of the actual membrane from the earthworm in quantities sufficient for performing calorimetric measurements. As seen in figure 42 0.4 mM lidocaine and 0.6 mM pentobarbital both resulted in a threshold increase of approximately a factor 2. We would therefore from the soliton model expect the two samples to affect the phase transition in approximately the same way. As is seen In figure 43 this is not exactly the case. It would be very interesting to see the effect of samples of other concentrations as well, but due to limited time this was not possible.

4   DISCUSSION

In the last two chapters first the background theory was presented, and the two models were discussed in a more general sense in the section *Strengths and shortcomings*, then data from a series of experiments conducted on the large earthworm (lumbricus terrestris) was presented. The results are not as conclusive, as one could have hoped, but they show clear indications.

The majority of measurements recorded during the collision experiments showed annihilation of pulses upon collision. This is in conflict with the predictions from the soliton model. In a couple of cases seemingly penetration of pulses was observed. As explained in the section concerning the collision experiment in the last chapter there are possible explanations for this, and it could in fact be an artefact. In all the cases where penetration was observed, only signals in one of the axons were evoked. This allows for the possibility that the signals were in fact not travelling in the same axon – thus they would not collide. In one of the cases where apparent penetration was
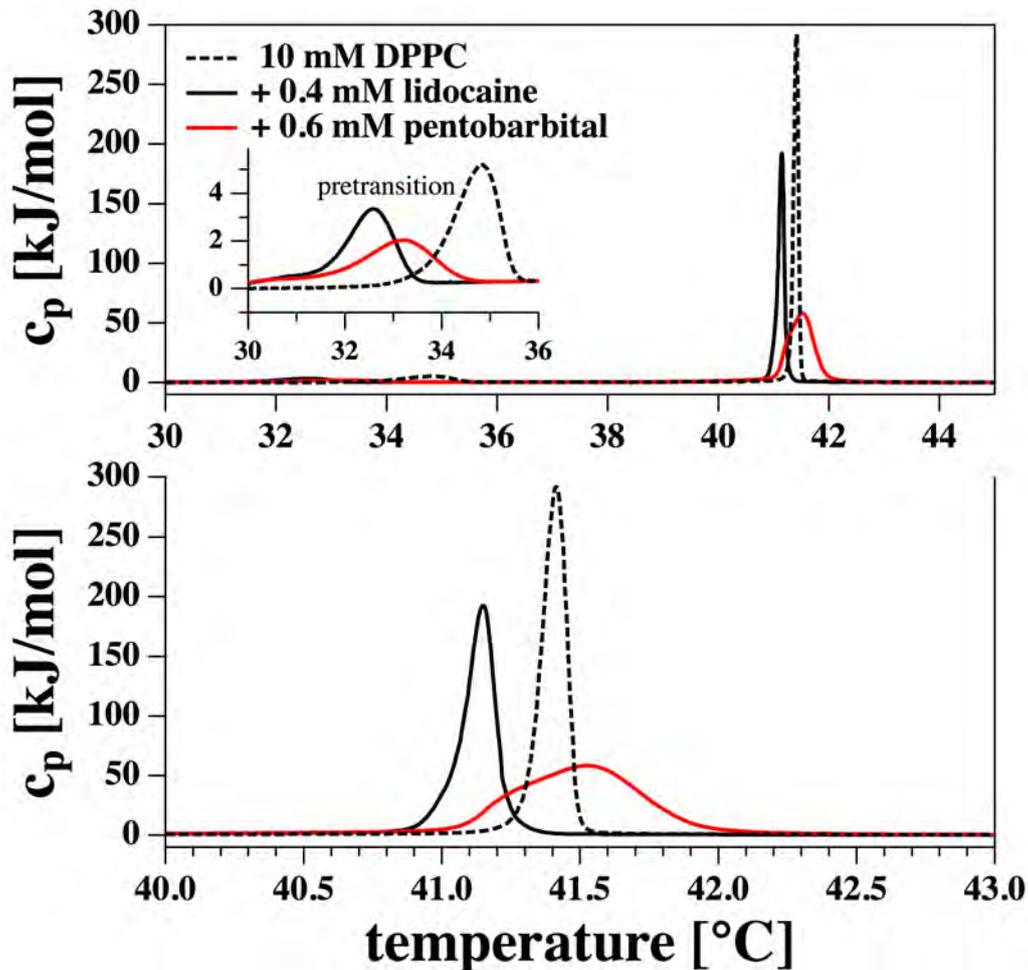
Figure 43: *Top: Heat capacity profile at constant pressure for DPPC multilamellar pure lipid membrane in the absence of anaesthetic (dashed line) and with added anaesthetics – 0.4 mM lidocaine (black line) and 0.6 mM pentobarbital (red line). The pretransition is shown magnified in the insert. Bottom: Main transition magnified. Results courtesy of Thomas Heimburg, University of Copenhagen.*

observed it was in fact only *possible* to evoke one signal in each direction. This is most likely because the nerve cord had been damaged during dissection. The nerve cord is fairly robust and can withstand a fair amount of stretching and twisting, but it is very possible that it could have been damaged, such that one of the axons did not work. If one axon had been intact in one end but not the other end and inversely for the other axon, the signals could have been travelling in each their own axon. Whether or not this is in fact the case is, however, impossible to say. In the other cases where both axons could be excited, it could possibly be due to the thresholds of the two axons having been very close to each other. It was found from time to time that at certain places on the cord, the thresholds would be within a few μA of each other or indeed indistinguishable. There are thus possible explanations for the results found in the present study, but the actual penetration of pulses in the three cases, where it was found, cannot be ruled out. In the article [22] the authors present results from similar studies also on lumbricus terrestris giant axons as well as lobster abdominal ventral cords. They found penetration of pulses in all of their measurements. Even though there might be possible explanations for the anomalous observations made in this study, it has still been observed in a more extensive study elsewhere. This has

to be explained. The HH-model cannot explain this. The differences between the experiment described in [22] and the experiment in the present study are hard to find. Obviously these contradicting results have to have some explanation, but that explanation has yet to be found. The experiment is very simple. The set-up and procedure were exactly identical – same stimulus durations, frequencies and all other parameters were identical, and still contradicting results were found. This is obviously somewhat unsatisfying, but the discrepancy in results indicates that neither the HH-model nor the soliton model in their current forms tell the whole truth about these phenomena in earthworms. Further studies would have to be conducted to shed light on this.

Some authors have suggested theories similar to the soliton model describing solitary mechanical pulses based on the non-linear nature lent to the membrane by the fluid-/gel-membrane phase transition – solitary wave pulses, but not solitons [59][58]. As discussed in the theory chapter a true soliton is left unchanged by collisions with other solitons. This is why it is possible for the signals to pass through each other in the soliton model. Solitary wave pulses do not necessarily have to possess this property [14]. The authors also claim that their model explains the all-or-none behaviour so characteristic of APs.

In the literature one finds surprisingly few studies on the behaviour of colliding pulses, and especially now in the light of the new alternative theories being proposed predicting different behaviour of colliding pulses, it is a particularly interesting experiment.

The temperature experiments showed temperature dependence of the excitation threshold in apparent qualitative agreement with predictions from the HH-model and in direct disagreement with predictions from the soliton model. There were several challenges with the experimental set-up. More exact temperature control would obviously have been preferable, but the uncertainties on the temperature of the measurements are in total acceptable. The uncertainties on the temperature tend to increase at lower temperatures, where temperatures were more difficult to keep at a steady level, and the temperature gradient from one end of the nerve chamber to the other was larger. The data show a clear tendency, and it is found that an exponential function describes the data well. The temperature was decreased by pouring ice into the chamber surrounding the actual nerve chamber, and it was increased using an electric heating element. A feedback temperature control system would have been a fairly easy improvement. The temperature gradient down the length of the nerve chamber could probably not have been avoided but could have been minimised by adding more inlets down the length of the nerve chamber. These improvements would grant better quantitative data, but the qualitative behaviour of the data is quite clear and seems unlikely to change significantly with such modifications. For a more complete temperature study the exact quantitative behaviour predicted by the HH-model would have to be computed by solving the modified HH-equations presented in the experiments chapter. Even though the data seems in apparent agreement with the HH-model, the predictions from the modified HH-equations vary greatly with varying stimulus duration for instance. These equations should probably not be taken too literally though. The ways in which temperature is assumed to affect the threshold in the derivation of the equations are somewhat simplified, and other effects should probably be taken into account as well and/or the effects considered implemented in a more sophisticated manner. The rates of change of conductance for all the different ions are assumed to change with temperature in the same way, likewise for the change in ionic conductance. In other words all channels are assumed to behave identically as a function of temperature. Based on the predictions of the modified HH-equations it would be interesting to look at a wider temperature range – both lower but also, and in particular, higher temperatures. The threshold should begin to increase again around some temperature T_0. It would be interesting to look for this temperature. The

temperature range of the present study was determined downwards by the minimum temperature reached (within a reasonable amount of time) after adding ice to the chamber and upwards in part by the maximum temperature the heating element could produce (again within a reasonable time) and in part by the maximum temperature reached before signals became too unreliable. Signals were found to be significantly more stable at lower temperatures than at higher ones.

The results from the anaesthetic experiments are probably the least conclusive ones. The exact functional form of the dependence on concentration is not readily deducible from theoretical foundations in the HH-picture. There are more clear (and generally acknowledged) hypotheses for the mechanism of action for local anaesthetics than for general anaesthetics, but still due to the subtleties of the exact binding mechanism a threshold-concentration function is not readily obtainable. The soliton model predicts a linear increase in both cases. The results found in the present study are linear over the range of concentrations studied. For the case of general anaesthetics it is particularly difficult to say how the threshold increase should go in the HH-model due to the lack of a consensus on what the underlying mechanism is. The behaviour for the two drugs lidocaine and pentobarbital was found to be approximately identical after multiplication with their respective n-octanol:water partition coefficients. This is in agreement with predictions from the soliton model, but is not in anyway in contradiction with predictions from the HH-model. Further studies should be made, and the threshold increase compared between several other drugs from both categories. If similar behaviour is found, this indicates that it is not unreasonable to assume similarities in the mechanisms of action. The range of concentrations used was decided in part by when reliable signals were lost. This does not necessarily mean no signals could be evoked, but merely that they were deemed too unreliable for use. At times it was found at higher concentrations that the threshold value would vary wildly, and that after stimulation at a certain strength for a period of time signals would be lost, and higher stimulation was needed. If the nerve was left to relax for a while without stimulation the threshold would then drop. Lidocaine has been found to be sensitive to the frequency of stimulation – use dependent block. This could possibly be an effect here. Reliable measurements under such conditions were not possible. It has to be noted that in order to measure a signal, the signal first has to be evoked, and then it has to travel down the length of axon between the stimulation and recording electrodes. This means that signal loss could just as well be an expression of the loss of longitudinal conductance, as an expression of the impossibility to evoke signals locally at the location of the stimulus electrode. The loss of signals at sufficiently high concentrations seem in apparent conflict with the soliton model. It should always be possible to restore signals, no matter how anaesthetised the nerve is, by applying strong enough stimulus. On the other hand a threshold increase of up to a factor of about 3 in average for lidocaine and slightly lower for pentobarbital was observed and in individual cases increases of up to a factor of almost 4 was observed (confer figures 32 and 39). This is in apparent conflict with the HH-model which expects signals to disappear at a threshold increase of about 2-2.5. In [48] threshold increases of a factor of 7 were observed. Such high increases in threshold fit with the soliton model, but the HH-model struggles to explain them. There are thus observations pointing in both directions.

4.1 Concluding remarks

Different theories incorporating the mechanical changes associated with action potentials have been proposed. We have dealt with the soliton model in detail, and we have also encountered a theory describing non-linear mechanical pulses different from the soliton model [59]. Last year an article was published describing what the authors call *action waves*. These action waves are

mechanical responses to a propagating electrical signal. This model tries to explain the mechanical changes as a function of the electrical changes. The exact nature of the mechanism producing the electrical pulse is not considered. It might be a HH-type mechanism, but this does not matter for the proposed model. It only considers what happens when an electrical signal has already been produced. In the soliton model, on the other hand, the electrical pulse is driven by the mechanical pulse.

Mechanical changes in the membrane and the heat profile associated with the AP have to be explained somehow. Research into this might lead to a fundamental change in the way we understand nerve signals, but it might also lead to a refinement of current theories. Under all circumstances it will grant us a better understanding of nerve signals, which obviously are the foundation for all neuroscience. To me it seems that the central question is to what degree the electrical pulse drives the mechanical pulse or the other way around. One might be a result of the other, but the two might also be part of an intricate feedback mechanism and thus coexist in a symbiotic relationship. This is a question for future investigations to answer.

This thesis has tried to outline some of the challenges facing neuroscience at its most basic level. Results from experiments carried out in earthworm axons have been compared with two fundamentally different models on the subject – the Hodgkin Huxley model and the soliton model. The results in this present study fit better with the predictions from the HH-model than of the soliton model, but the results are not conclusively in favour of the HH-model, and there are observations that are better explained by the soliton model. In addition, as pointed out throughout the thesis, there are still several unanswered questions left by the HH-model that need to answered. As these questions are of thermal and mechanical nature, the answers should naturally be found in thermodynamics.

Bibliography

[1] Abbott, B. C.; Hill; A. V., Howarth, F. R. S. & Howarth, J. V. *The positive and negative heat production associated with a nerve impulse*, 1958 Proc. R. Soc. London B, volume **148**, 149-187

[2] Abrams, Thomas & Pearson, Keir G. *Effects of temperature on identified central neurons that control jumping in the grasshopper*, November 1982 The Journal of Neuroscience, volume **2**, number 11, 1538-1533

[3] Alle, Henrik & Geiger, Jörg R. P. *Combined Analog and Action Potential Coding in Hippocampal Mossy Fibers*, 3 March 2006 Science, volume **311**

[4] Andersen, Søren S.L.; Jackson, Andrew & Heimburg, Thomas *Towards a thermodynamic theory of nerve pulse propagation*, 2009 Progress in Neurobiology, volume **88**, 104-113

[5] Antonov, Valerij F.; Anosov, Andrej A.; Norik, Vladimir P. & Smirnova, Elena Yu. *Soft perforation of planar bilayer lipid membranes of dipalmtoylphosphatidylcholine at the temperature of the phase transition from liquid crystalline to the gel state*, 2005 Biophysical Journal, volume **34**, 155-162

[6] Appali, Revathi; Lautrup, Benny; Heimburg, Thomas & Van Rienen, Ursula *Soliton collision in biomembranes and nerves- A stability study* in *Scientific Computing in Electrical Engineering*, 2010 B. Michielsen and J.-R. Poirier (eds.)

[7] Becker, Daniel E. & Reed, Kenneth L. *Essentials of local anesthetic pharmacology*, 2006 Anesth Prog, volume **53**, 98-109

[8] Coggeshall, Richard E. *A fine structural analysis of the ventral nerve cord and associated sheath of lumbricus terrestris L.*, December 1965 Journal of Comparative Neurology, volume **125**, issue 3, 393-437

[9] Dayan, Peter & Abbott, L. F. *Theoretcal neuroscience computational and mathematical modeling of neural systems*, The MIT Press, Cambridge Massachusetts 2001

[10] Destexhe, Alain & Huguenard, John *Which formalism to use fr modeling voltage-dependent conductances*, in *Computational Neuroscience: Realistic Modeling for Experimentalists*, editor De Schutter, Erik

[11] Destexhe, Alain & Huguenard, John *Nonlinear thermodynamic models of voltage-dependent currents*, 2000 Journal of Computational Neuroscience, volume **9**, 259-270

[12] Drewes, C. D. & Pax, R. A. *Neuromuscular physiology of the longitudinal muscle of the earthworm lumbricus terrestris. I. Effects of different physiological salines*, 1974 J. Exp. Biol., volume **60**, 445-452

[13] Ebel, Holger; Grabitz, Peter & Heimburg, Thomas *Enthalpy and Volume Changes in Lipid Membranes. I. The Proportionality of Heat and Volume Changes in the Lipid Melting Transition and Its Implication for the Elastic Constants*, 2001 J. Phys. Chem. B, volume **105**, 7353-7360

[14] Eckl, C.; Mayer, A. P. & Kovalev, A. S. *Du surface acoustic solitons exist?*, 1998 Physical Review Letters, volume **81**, number 5

[15] Emerson, Ralph Waldo *Nature*, 1995 The Oxford Companion to American Literature, Ed. Hart, James D., Rev. Leininger, Philip W., Oxford University Press, Web.

[16] Fitzhugh, Richard *Theoretical effect of temperature on threshold in the Hodgkin-Huxley nerve model*, 1966 The Journal of General Physiology, volume **49**, 989-1005

[17] Forrest, Michael D. Can the termodynamic Hodgkin-Huxley model of voltage-dependent conductance extrapolate for temperature, 2014 Computation, volume **2**, 47-60

[18] Franks, Nicholas *The unfolding story of how general anesthetics act*, from *The wondrous story of anesthesia*, E. I. Eger II et al. MD 2014

[19] Franks, N. P. & Lieb, W. R. *Do general anaesthetics act by competitive binding to specific receptors*, 16 august 1984 Nature, volume **310**

[20] Glaser, Ralf W.; Leikin, Sergei L.; Chernomordik, Leond V.; Patushenko, Vasili F. & Sokirko, Artjom I. *Reversible electrical breakdown of lipid blayers: formation and evolution of pores*, 1988 Biochim. Biophys. Acta, volume **940**, 275-287

[21] Goldman, L. *The effects of stretch on cable and spike parameters of single nerve fibres; some implications for the theory of impulse propagation*, 1964 J. Physiol., volume **175**, 425-444

[22] Gonzalez-Perez, Alfredo; Budvytyte, Rima; Mosgaard, Lars D. & Heimburg, Thomas *Penetration of Action Potentials During Collision in the Median and Lateral Giant Axons of Invertebrates*, 2014 Physical Review X, volume **4**

[23] Greene, Richard F. & Callen, Herbert B. *On the formalism of thermodynamic fluctuation theory*, september 15 1951 Physical Review, volume **83**, number 6

[24] Gross, David; Williams, Wendell S. & Connor, John A. *Theory of Electromechanical Effects in Nerve*, 1983 Cellular and Molecular Neurobiology, volume **3**, number 2, 89-111

[25] Græsbøll, Kaare; Sasse-Middelhoff, Henrike & Heimburg, Thomas. *The Thermodynamics of General and Local Anaesthesia*, may 2014 Biophysical Journal, volume **106**, 2143-2156

[26] Guttman, Rita *Temperature characteristics of excitation in space-clamped squid axons*, 1966 The Journal of General Physiology, volume **49**, 1007-1018

[27] Günther, Jorge *Impulse conduction in the myelinated giant fibers of the earthworm. Structure and function of the dorsal nodes in the median giant fiber*, 15 august 1976 Journal of Comparative Neurology, volume **168**, issue 4, 505-531

[28] Hartline, D. K. & Colman, D. R. *Rapid conduction and the evolution of giant axons and myelinated fibers*, 9 January 2007 Current Biology, volume **17**

[29] Heimburg, Thomas *Mechanical aspects of membrane thermodynamics. Estimation of the mechanical properties of lipid membranes close to the chain melting transition from calorimetry*, 1998 Biochim. Biophys. Acta, volume **1415**, 147-162

[30] Heimburg, Thomas *Thermal Biophysics of Membranes*, 2007 Wiley, Weinheim

[31] Heimburg, Thomas. *Die Physik von Nerven*, 2009 Physik J., volume **3**, number 3 33-39

[32] Heimburg, Thomas. *Lipid ion channels*, 2010 Biophysical Chemistry, volume **150**, 2-22

[33] Heimburg, Thomas *The Capacitance and Electromechanical Coupling of Lipid Membranes Close to Transitions: The Effect of Electrostriction*, September 2012 Biophysical Journal, volume **103**, 918-929

[34] Heimburg, Thomas & Jackson, Andrew *On soliton propagation in biomembranes and nerves*, july 12 2005 Proceedings of the National Academy of Sciences, volume **102**, number 8

[35] Heimburg, Thomas & Jackson, Andrew *On the action potential as a propagating densty pulse and the role of anaesthetics*, 2007 Biophys. Rev. Lett., volume **2**, 57-78

[36] Hill, Terrell L. & Chen, Yi-Der *On the theory of ion transport across the nerve membrane, VI. Free energy and activation free energies of conformational change*, July 1972 Proc. Nat. Acad. Sci. USA, volume **69**, number 7, 1723-1726

[37] Hille, Bertil *Ion channels of excitable membranes*, 2001 third edition, Sinauer Associates, Sunderland Massachusetts

[38] Hodgkin, Alan & Huxley, Andrew. *A quantitative description of membrane current and its application to conduction and excitation in nerve*, 1952 J. Physiol., volume **117**, 500-544

[39] Holmes Bullock, Theodore *Functional organization of the giant fiber system of lumbricus*, 1945 J Neurophysiol, volume **8**, 55-71

[40] Howarth, J. V. *Heat production in non-myelinated nerves*, 1975, Phil. Trans. R. Soc. Lond. B, volume **270**, 425-432

[41] Johnston, Daniel & Wu, Samuel Miao-Sin *Foundations of cellular neurophysiology*, 1995 MIT Press

[42] Kandel, Eric R.; Schwartz, James H.; Jessell, Thomas M.; Siegelbaum, Steven A. & Hudspeth, A. J. *Prnciples of neural science* 2013 fifth edition, McGraw Hill Medical

[43] Kassahun, Binyam T.; Murashov, Alexander K. & Bier, Martin *A thermodynamic mechanism behind an action potential and behind anaesthesia*, 2010 Biophysical Reviews and Letters, volume **5**, number 1, 35-41

[44] Kaufmann, K.; Hanke, W. & Corcia, A. *Ion Channel Fluctuations in Pure Lipid Bilayer Membranes: Control by voltage*, available at: `http://membranes.nbi.dk/Kaufmann/pdf/1989_Kaufmann_book3_ed.pdf`, Caruaru (1989)

[45] Lautrup, B.; Appali, R.; Jackson, A. D. & Heimburg, Thomas *The stability of solitons in biomembranes and nerves*, 2011 European Physical Journal E, volume **34**

[46] Löscher, Wolfgang & Rogawski, Michael A. *How theories evolved concerning the mechanism of action of barbiturates*, 2012 Epilepsia, volume **53**, number 8, 12-25

[47] Maier, Sebastian K.G.; Westembroek, Ruth E.; Schenkman, Kenneth A.; Feigl, Eric O.; Scheuer, Todd & Caterall, William A. *An unexpected role for brain-type sodium channels in coupling of cell surface depolarization to contraction in the heart*, 2002 Proceeding of the National Academy of Sciences of the United States of America, volume **99**, number 6, 4073-4078

[48] Moldovan, Mihai; Lange, Kai Henrik Wiborg; Aachmann-Andersen, Niels Jacob; Kjær, Troels Wesenberg; Olsen, Niels Vidiendal & Krarup, Christian *Transient impairment of the axolemma following regional anaesthesia by lidocaine in humans*, 2014 Journal of Physiology, volume **592**, number 13, 2735-2750

[49] Mosgaard, Lars D. & Heimburg, Thomas *Lipid ion channels and the role of proteins*, 2013 Accounts of Chemical Research, volume **46**, number 12, 2966-2976

[50] Mosgaard, Lars D.; Zecchi, Karis A. & Heimburg, Thomas *Mechano-capacitive properties of polarized membranes*, 2015 Soft Matter, volume **11**, 7899-7910

[51] Nagle, J. F. & Scott, H. L. *Lateral compressibility of lipid mono- and bilayers theory of membrane permeability*, 1978 Biochim. Biophys. Acta, volume **513**, 236-243

[52] Neher, Erwin & Sakmann, Bert. *Single-channel currents recorded from membrane of denervated frog muscle fibres*, april 29 1976 Nature, volume **260**, 799-802

[53] Noble, Denis *Applications of Hodgkin-Huxley equations to excitable tissues*, 1966 Physiological Reviews, volume **46**, number 1, 1–50

[54] Okamura, Nobuyyuki; Stoskopf, Michael; Yamaguchi, Hisao & Kishimoto, Yasuo *Lipid composition of the nervous system of earthworms*, 1985 Journal of Neurochemistry, volume **45**, number 6

[55] Papahadjopoulos, D.; Jacobsen, K.; Nir, S. & Isac, T. *Phase transitions in phospholipid vesicles. Flouresence polarization and permeability measurements concerning the effect of temperature and cholesterol*, 1973 Biochim. Biophys. Acta, volume **311**, 330-340

[56] Schuetze, Stephen M. *Perspectives the discovery of the action potential*, 1983 Trends in Neurosciences, volume **6**, 164-168

[57] Scott-Russell, John *Report on waves*, Rep. Fourteenth Meeting of the British Association for the Advancement of Science, John Murray, london, 1844, 311-390 + 57 plates

[58] Shrivastava, Shamit; Kang, Kevin Heeyong & Schneider, Matthias F. *Solitary shock waves and adiabatic phase transition in lipid interfaces and nerves*, 2015 Physical Review E, volume **91**

[59] Shrivastava, Shamit & Schneider, Matthias F. *Evidence for two-dimensional solitary sound waves in a lipid controlled interface and its implications for biological signalling*, 2014 Journal of the royal society interface, volume **11**

[60] Shu, Yousheng; Hasenstaub, Andrea; Duque, Alvaro; Yu, Yuguo & McCormick, David A. *Modulation of intracortical synaptic potentials by presynaptic somatic membrane potential*, 2006 Nature, volume **441**

[61] Tasaki, Ichiji *Collision of two nerve impulses in the nerve fibre*, 1949 Biochimica et Biophysica Acta, volume **3**, 494-497

[62] Tasaki, Ichiji & Byrne, P. M. *Volume expansion of nonmyelinated nerve fibers during impulse conduction*, 1990 Biophys. J., volume **57**, 633-635

[63] Tasaki, Ichiji & Iwasa, Kunihiko *Rapid mechanical changes in crab nerve and squid axon during action potential*, 1981 J. Physiol., volume **77**, 1055-1059

[64] Tsien, R. W. & Noble, D. *A transition state theory approach to the kinetics of conductance changes in excitable membranes*, 1969 J. Membrane Biol., volume **1**, 248-273

[65] Villagran Vargas, Edgar; Ludu, Andrei; Hustert, Reinhold; Gumrich, Peter; Jackson, Andrew D. & Heimburg, Thomas *Periodic solutions and refractory periods in the soliton theory for nerves and the locust femoral nerve*, 2011 Biophysical Chemistry, volume **153**, 159-167

[66] Weir, Cameron J. *The molecular mechanisms of general anaesthesia: dissecting the $GABA_A$ receptor*, 2006 Continuing Education in Anaesthesia, Critical Care & Pain, volume **6**, number 2

[67] Zecevic, Dejan & Paw, Mira *Temperature compensation of the threshold potential for excitation of the snail bursting neuron*, 1983 Comp. Biochim. Physiol., volume **76A**, number 1, 173-176

[68] INA121 Datasheet, Burr-Brown

[69] `http://32f7sg2by83y1dtg9mdxf11m.wpengine.netdna-cdn.com/wp-content/uploads/2012/04/canstockphoto6235139-906x1024.jpg`

[70] `http://biomedicalengineering.yolasite.com/resources/neuron_structure.jpg`

[71] `http://www.historylearningsite.co.uk/a-history-of-medicine/`

[72] `https://upload.wikimedia.org/wikipedia/commons/4/46/The_Meyer-Overton_correlation.png`

[73] `https://en.wikipedia.org/wiki/Cell_membrane#/media/File:Cell_membrane_detailed_diagram_en.svg`

[74] `https://en.wikipedia.org/wiki/Cell_membrane#/media/File:Cell_membrane_detailed_diagram_en.svg`

[75] `http://www.ebi.ac.uk/biomodels/ModelMonth/2006-09/Hodgkin1.png`